8-2010

Temporal and spatial assessment of evaporation, transpiration, and soil moisture redistribution

Brian M. Bird
University of Nevada, Las Vegas

TEMPORAL AND SPATIAL ASSESSMENT OF EVAPORATION, TRANSPIRATION, AND SOIL MOISTURE REDISTRIBUTION

by

Brian M. Bird

Bachelor of Science in Computer Science
College of Engineering
University of Nevada, Las Vegas, 2004

A thesis submitted in partial fulfillment
of the requirements for the

Master of Science in Water Resources Management
Department of Water Resources Management
College of Science

Graduate College
University of Nevada, Las Vegas
August 2010

UNLV
UNIVERSITY OF NEVADA LAS VEGAS

THE GRADUATE COLLEGE

We recommend the thesis prepared under our supervision by

Brian Michael Bird

entitled

Temporal and Spatial Assessment of Evaporation, Transpiration, and Soil Moisture Redistribution

be accepted in partial fulfillment of the requirements for the degree of

Master of Science in Water Resource Management

Dale Devitt, Committee Co-chair

Michael Young, Committee Co-chair

David Kreamer, Committee Member

Paul Schulte, Graduate Faculty Representative

Ronald Smith, Ph. D., Vice President for Research and Graduate Studies
and Dean of the Graduate College

August 2010

ABSTRACT

Temporal and Spatial Assessment of Evaporation, Transpiration, and Soil Moisture Redistribution

by

Brian M. Bird

Dr. Dale Devitt, Examination Committee Chair
Professor of Soil and Water Science
University of Nevada, Las Vegas

At a native stand of creosote bush (*Larrea tridentata*) in North Las Vegas, a rainfall simulation study was conducted over a 12 month period from October 2005 to October 2006. Simulated rainfall occurred during the winter, spring, summer, and fall periods. Rainfall simulation systems were positioned on each of 12 plots, each containing a single creosote bush. Simulated rainfall events occurred at night with multiple short pulses designed to maximize infiltration while minimizing ponding. Yearly simulated rainfall amounts were set at 0, 15, 30 and 60 cm (replicated three times) and were approximately 0, 1.5, 3.0 and 6.0 times the natural rainfall. The cumulative reference evapotranspiration (ET_{ref}) was 156.7 cm and cumulative ambient precipitation was 7.9 cm. Soil and plant canopy surface to air temperature differentials (T_s-T_a and T_c-T_a) were assessed using an infrared thermometer (IRT). Significant differences were based on simulated rainfall treatment ($P<0.001$) and over time ($P<0.001$). Soil evaporation (E) measurements were obtained using a custom hemispherical chamber, results showed that 87% of the variability in chamber measurements could be explained by ET_{ref}, simulated rainfall amount, and the soil area ($P<0.001$). Transpiration measurements of individual plants were estimated using stem flow gauges and were normalized to a canopy leaf area basis. Soil surface volumetric water content was assessed using a hand held probe. Soil

moisture with depth was assessed using both portable and permanently installed time domain reflectometry (TDR) sensors. TDR waveforms recorded were analyzed via custom post-processing algorithms written in the C++ programming language and based on the methods of Topp et al. (1980) and Herkelrath et al. (1991). Results showed that for the Mojave Desert with sparse, open vegetation of creosote bush under elevated precipitation, evaporation dominated, whereas transpiration was a minimal component of the soil-plant system. The level of soil moisture redistribution was greater under lower environmental demand, creating a seasonal change in water holding storage. Based on the water holding capacity of the soil profile, plant water uptake, and environmental demand, the recurrence interval for deep percolation can be predicted and used for long-term performance assessment studies of soil covers.

ACKNOWLEDGEMENTS

It is with great honor and gratitude to give recognition to the people who have directly shaped my life and work.

I would like to thank the Department of Energy for funding of this project. With great admiration and respect, I would like to thank my Principal and Technical Assistant Advisors, Dr. Dale Devitt and Dr. Michael Young for their never-ending support and confidence. My personal thanks to my committee members: Dr. Michael Young, Dr. David Kreamer and Dr. Paul Schulte, for giving me this honor.

I would also like to thank Mr. Jeff Anderson (field technician), Miss Polly Conrad, Ms. Janey Balvin, Ms. Lena Wright, Ms. Amanda Wagner, Mr. Don Clark, Ms. Brittany Holtzman, Mr. Joseph Poliquin and 'Tino' for their immeasurable assistance in the lab and field. Thanks to all my fellow graduate students in Dr. Devitt's Lab and the Department of Water Resources Management. I would like to thank my parents Melody Bird and Mike Bird for their loving support and for always pushing me to succeed. I would like to thank my wife Nicole and kids Brandon and Tyler for their support especially during long field events. I would also like to thank my grandparents, Mr. Larry and Mrs. Kathleen Weber for their lifelong encouragement and support to whom this thesis is dedicated to.

TABLE OF CONTENTS

LIST OF TABLES

LIST OF FIGURES

CHAPTER I

INTRODUCTION

The safe containment and isolation of radioactive waste is important to the United States. According to the U.S. Nuclear Waste Technical Review Board (2004), research is needed to better understand how aspects of natural systems affect waste containment, including the role of vegetative covers. Therefore, the objectives of this work are: (1) to impose different precipitation regimes on soil plant systems; (2) to monitor soil evaporation, plant transpiration and soil water storage after natural and simulated precipitation events; and, (3) to examine how precipitation treatments alter the partitioning of water into water balance components.

The expected benefit from the study will be a better understanding of the dynamics involved with soil water movement with respect to evaporation, transpiration and soil moisture redistribution critical to both the design and management of vegetative covers. The results from this study will improve upon the current fundamental understanding of evapotranspiration (ET) related to its effects on water movement and spatial distribution within the unsaturated zone of arid regions. Current scientific literature shows a limited number of studies have investigated the effects of different quantities of simulated rainfall amounts on the change in magnitude of evaporation, transpiration, and moisture redistribution in an arid climate. Additionally, results of the temporal changes of water loss and water storage from the plant soil system from this research will assist the Department of Energy (DOE) in their performance assessment modeling activities of radioactive waste covers.

CHAPTER II

LITERATURE REVIEW

Stored Waste Covers in Arid Environments

Storage of wastes at sites in arid desert environments has become attractive due to their high ET rates, deep unsaturated soils, and isolation from populated areas (Reith and Thomson, 1992). The safe containment and isolation of radioactive waste is now a leading concern in the United States and is quickly becoming a challenging policy issue for the DOE. The U.S. Nuclear Waste Technical Review Board in March of 2004 identified aspects of natural systems where additional research is needed to improve DOE's radioactive waste containment program. Specifically, the board identified that both the spatial distribution and composition of the unsaturated alluvium serve critical roles in the design and maintenance of better vegetation covers for radioactive waste disposal sites. In particular, a better understanding of the spatial and temporal variability of the climatic and hydraulic processes associated with these covers is needed. Vegetation covers actively move water out of natural systems. In the absence of such covers, the possibility of deep percolation down to stored waste is enhanced (Gee et al. 1993). Compounding this problem, some high level radioactive waste needs thousands of years to decay to safe levels near back ground levels (U.S.NRC, 2007) which is globally now at 5 microsievert [$\mu Sv\ yr^{-1}$], (U.S.NRC, 2007) as determined by the nuclear regulatory commission. This has increased the need for a cover designed to withstand extreme climatic conditions that can occur over time.

The water balance status of these hydrologic systems ultimately determines the magnitude and direction (upward as evaporation and transpiration, or downward as deep

drainage) of water flux after storm events. Arid environments typically contain plant covers of less than 50% (Wythers et al., 1999) resulting in the potential for bare soil evaporation to play a large role in the water balance of these desert ecosystems. The relationship between plant cover and bare soil distribution is expected to change over large biogeographic regions of the world due to global climate change (Schwinning et al. 2005a). This is especially true for arid ecosystems due to their tight coupling between soil moisture and vegetative growth and diversity (Schwinning and Ehleringer, 2001; Knapp et al., 2002).

Global mean surface temperature and atmospheric CO_2 concentrations have been increasing and are predicted to continue increasing at greater rates (Brohan et al., 2006). The atmospheric mixing ratio of CO_2 has increased globally by ~100 ppm (36%) over the last 250 years (Keeling and Whorf, 2005) to the current rate of 379 ppm (±0.04 ppm) as of August 2008 (Van der Laan et al, 2009). Due to observable increases in atmospheric constituents and radiative forcing, regional precipitation patterns are predicted to dramatically change with a larger occurrence of heavy precipitation events (Figure 2-1) (IPCC, 2007; Karl et al., 2008). Figure 2-1, shows an example of the probability of extremes in a warmer climate. Many currently rare extreme events will become more common place in a warmer climate. The exact threshold for classified extreme values will normally fall within the top or bottom 10% of all occurrences. Relatively small shifts in the mean produce greater occurrences in both temperature and precipitation extremes as shown in the top right and bottom right sections of Figure 2-1. Currently, the global climate change models (GCCM's), such as HadCRUT3, which incorporates a land surface and vegetation component, are unable to agree on the exact location and

magnitude of these changes. However, these current models converge on two new climate conclusions: seasonally specific trends of mean precipitation timing and duration will differ among the seasons (i.e., winter trends may not follow for summer), and inter-annual variability of precipitation will increase. Thus, as variability of precipitation increases, the occurrence of long droughts and intense rainfall events will also increase. Furthermore, as the probability of rain events of significantly greater magnitude increases (Figure 2-1), the magnitude of water partitioned within surface vegetative cover systems during these events will also increase.

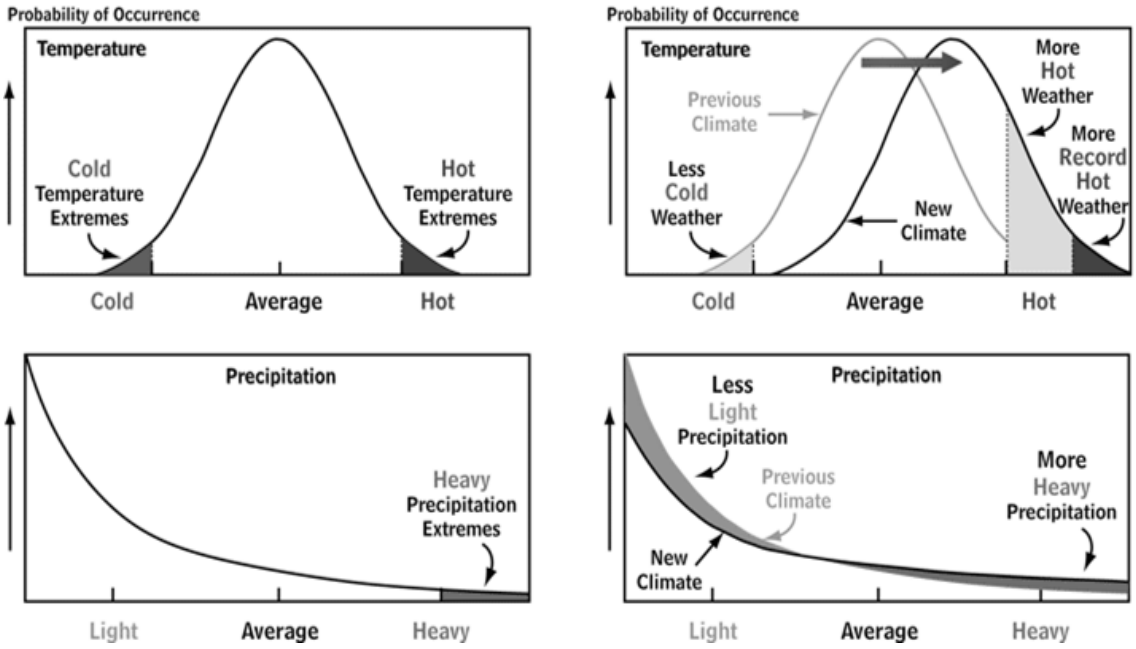

Figure 2-1. Example of probability of extremes in a warmer climate. Results based on observations from the National Climate Date Center, National Oceanic and Atmospheric Administration. Source: Karl, et al. 2008, from Fig. ES-1.

Partitioning Evapotranspiration

Only a limited number of ecological studies examining the partitioning of evaporation from transpiration have been conducted in arid environments. According to the work of Lascano et al. (1987), soil evaporation accounted for 30% of the total water loss in a semi-arid environment. Whereas, with irrigated grassland, estimated daily evaporation was shown to be 45% of the total daily ET (Suleiman and Crago, 2004). Ham et al. (1990) showed estimated evaporation to represent 45% of total ET over an eight-day period during the early stages of cotton development. For a sparse mixed-species (creosote, desert zinnia, and tar bush) shrub canopy in the southeastern Arizona desert, transpiration accounted for 84% of landscape ET whereas bare soil evaporation only accounted for 13% when measured with a portable chamber (Stannard and Weltz, 2006). A summary of studies in the western US listed in (Huxman et al., 2005) show ET/Precipitation to vary from a high of 100% for a low woody plant (*Prosopis gladulosa*) in a small watershed study near Beaver Creek, AZ to a low of 68% for another low woody plant (*Juniperus ashei)* in a Bowen ratio study near Seco Creek, TX. Additionally, Liu et al. (1995) found the average reported ratio of transpiration to evapotranspiration (T/ET) of 80.0 for *Larrea tridentata* within a Sonoran desert community (mean annual precipitation [MAP] of 230 mm) was similar to Schlesinger et al's (1987) T/ET estimate of 72.0 in the Chihuanhan desert (MAP of 250 mm). However Sammis and Gay (1979) found a T/ET ratio of 7.0 for *Larrea tridentata* within the Sonora desert (MAP of 280 mm).

In a desert shrub land study of the unsaturated zone at the burial site for low-level radioactive waste near Beatty, Nye County, Nevada, the cumulative and mean yearly

actual evaporation was estimated to account for 97% of the cumulative precipitation over a 16 year period (Nichols, 1987). Water use by plants is known to vary based upon rainfall amounts and time of year. Ehleringer et al. (1991) investigating differential utilization of summer rains by desert plants, found that herbaceous perennial species used summer precipitation more than woody perennials. Devitt et al. (1997) identified a six-week sap flow delay in salt cedar (*Tamarix ramosisima*) to weekly summer irrigations. Their studies showed that *Tamarix* roots were highly suberized and that only after six weeks did new roots begin to grow on the older established roots.

Portable Chamber for Evaporation Estimates

When estimating ET rates of mixed vegetation landscapes associated with arid covers, knowledge of the various ET components (transpiration by plant species and bare soil evaporation) are paramount to understanding water use rates within a hydrologic system. Micrometeorological or hydrologic methods used to estimate ET of sparse stands of native vegetation within large basins often makes identifying the individual ET components more difficult (Stannard and Weltz, 2006). Portable chambers help solve this problem by allowing direct measurement of evaporation and/or transpiration. Typical instantaneous daytime ET measurements, when using a portable chamber, can reach 3.5 mm and nighttime ET rates have been found to be near zero in arid regions (Stannard, 1988); but this is not always the case, especially with wet soils where night time ET can be as much as 12% of the 24 hour ET portion with nighttime losses approaching 2 mm (Tolk et al., 2006).

Some studies have found chamber flux measurements to be consistent with other methods for measuring ET. One such study (Pickering et al., 1993) compared lysimeters measuring instantaneous ET with a portable chamber and found maximum errors of less than 0.13 mm h^{-1} with an r^2 of 0.90 (4% chamber overestimate) under clear skies for both wet and dry soils. Similar results for maximum chamber error have been reported at 0.16 mm h^{-1} by Reicosky et al. (1983). Also, Wagner and Reicosky (1992) reported an agreement within 5% between measured ET with a closed chamber system and lysimeter values during a drying period. Others have found an over estimation bias; for example, Grau (1995) found chamber ET measurements to be 25% higher than gravimetric measurements of potted plants. Stannard and Weltz (2006) found instantaneous ET chamber estimates of soils and mixed-species shrub canopy in southeastern Arizona to be highly correlated with simultaneous eddy correlation measurements within the flux tower footprint (Schuepp et al., 1990) but found chamber-derived ET values to be 26% higher. They attributed this over estimation to excessive internal air speed within the chamber. Also, they did not incorporate corrections to their eddy covariance processing techniques besides the Webb et al. (1980) and Tanner and Greene (1989) corrections. ET totals without frequency response corrections to retrieve flux losses due to sensor separation and orientation (Moore 1986; Massman 2000, 2001) have been shown to underestimate latent heat fluxes (i.e., ET) by as much as 10% and possibly to a greater extent in hyper-arid environments. (Moore 1986; Lee et al., 2004).

Portable chambers have been criticized in the past for changing the natural environmental conditions of the plant or soil being measured (Wagner and Reicosky, 1992; Dugas et al., 1997; Denmead and Reicosky, 2003; Heijmans et al., 2004).

Denmead and Reicosky (2003) attributed these unnatural conditions or 'chamber effects' to soil variability, chamber size and placement, and internal wind speed. Whereas, Pickering et al. (1993) reported solar radiation losses from light interception at the chamber surface to have negligible effects on recorded ET rates.

Denmead and Reicosky (2003) found the optimal internal wind speed of 2.27 m s^{-1} was the best fit ratio for 'constant concentration' and the wind speed within their chamber was constant at 2.2 m s^{-1}. Stannard (1988) suggested setting the internal wind speed to the average onsite wind speed or attaching a rheostat to match internal with external wind speeds. Additionally, chamber studies have been specifically designed in the past to compare sites (Pickering et al., 1993; Grau, 1995; Heijmans et al., 2004) and assess measurement bias.

Assessing Transpiration from Stem Flow Measurements

To assess the water balance and deep drainage of sparsely vegetated areas, field methods were chosen to facilitate nondestructive and independent measurements of transpiration rates. Continuous sap flow measurements were made using the heat balance method to estimate transpiration (T) rates from selected plants (Ham et al., 1990; Devitt et al., 1993; Dugas et al., 1994). Other methods for measuring T such as with lysimeters or surface-applied barriers are destructive or alter the surface energy balance and can be difficult to implement due to uncertainties with drainage (Griffin et al., 1966; Ham et al., 1990; Smith and Allen, 1996). Another method for measuring transpirational flow exists and is based on the Granier (1985) method for sap flow from thermal gradients, but can be destructive for smaller stems, due to insertion of heated probes into the conductive

vascular system. Devitt et al. (1993) showed transpiration rates of ornamental trees using stem flow gauges and lysimeters to be highly linear ($r = 0.98$, $P = 0.001$).

Dugas et al. (1994) showed that average daily sap flow rates varied from 442 to 950 g day^{-1} or 4.4 to 9.5 mm day^{-1}, given 1000g ≈10mm (for a plant density of 10 plants m^{-2}) for individual stands of cotton grown in a field. Ham et al. (1990) calculated LAI of 2.09 to 2.74 for cotton using a digital leaf area meter (Delta-T Devices Ltd., Cambridge, U.K.) with stem flow T rates of 3.0 to 4.0 mm day^{-1} normalized by leaf area.

Rainfall Simulation

Natural rainfall can be complex with interactions between drop size, drop velocity, uniformity, intensity, duration, and influence by topography and climate variations. To properly simulate rainfall, several criteria are required (Blanquies, et al., 2003; Bubenzer, 1979). First, drop size distribution should be near natural rainfall and impact velocity should reach near terminal velocity (Laws, 1941; Gunn and Kinzer, 1949). The later is typically important with erosion studies. Second, rainfall intensity should be near uniform and have a random drop size distribution (Laws and Parsons, 1949). Third, the rainfall application should be applied uniformly or near uniform over the entire plot. Finally, storm pattern duration and intensity should be considered when designing field studies (Moore et al., 1983). Drop size distribution can vary in intensity between 1 mm to 7 mm, and for high intensity storms a median drop size of 2.25 mm is typical (Laws and Parsons, 1943).

Nevada's climate and topography can range from arid to semi-arid and with elevation ranges extending from 609 to 3960 meters. Nevada is located in the Basin and

Range physiographic province where elevational changes have a dramatic effect on rainfall distribution and duration. Las Vegas, Nevada, is located in a desert valley nearly surrounded by mountains, including the Sheep and Las Vegas Range to the north, Spring Mountains to the west, and the Muddy Mountains, and the Eldorado Range to the east. The highest mountain peak in Nevada is Boundary Peak (ca. 4,002 m). The closest mountain peak to Las Vegas is Mount Charleston which rises to a height of approximately 3,627 m. The southern part of Las Vegas valley borders Black Mountain and the McCullough Range. Las Vegas currently has an average annual precipitation rate of 10.16 cm per year (Gorelow, 2008). The three largest annual precipitation totals recorded since 1937 for the Las Vegas area were 27.2 cm in 1941, 25.1 cm in 1992, and 20.22 cm in 1965 (Gorelow, 2008). No studies known to the author of rainfall characteristics in Nevada have been conducted to assess drop size or microclimate storm intensity. Parameters can be approximated from other areas, but without specific microclimate data, accurate rainfall simulation for Nevada would be extremely difficult.

CHAPTER III

MATERIAL & METHODS

Field Site and Experimental Design

The research site selected for this study was located on a parcel of land (8,200 m^2 area) just north of the University of Nevada Las Vegas, Center for Urban Horticulture and Water Conservation. The site had an undisturbed stand of creosote bush (*Larrea Tridentata).* The soil type at the site was classified as Las Vegas Loam (loamy, carbonatic, thermic, shallow typic petrocalcid). Twelve individual creosote plants were selected for this study based on size and health status.

Each field plot was treated as a separate experimental unit but was prepared uniformly. For example, a square soil berm was placed around each plant, providing a 3.66 x 3.66 m plot. Berms were constructed of dry surface soil taken from intra-plot areas. The purpose of the berms was to minimize run off of water from the plots after the simulated rainfall and to prevent run on from non-monitored areas. Also, trenches were dug and refilled just outside the soil berms on all sides of each plot to a depth of approximately 60 cm to cut any surface roots that might be leaving or entering each plot. Thus, each plot was designed to contain all water within the plot boundaries, including root water uptake.

Simulated rainfall treatments were replicated three times and were imposed eight times over the course of a year, consisting of a control (rainfall with 0 cm simulated rain, control plus 1.875 cm, control plus 3.75 cm, and control plus 7.5 cm, (15, 30 and 60 cm total simulated rain imposed annually)(Figure 3-1.) Data were collected from October 2005 to September 2006. The low and medium simulated rainfall treatments fell within

the upper quartile (1.5 and 3 times the mean) of historical rainfall data, whereas the highest was over twice the highest rainfall on record or nearly 6 times the mean.

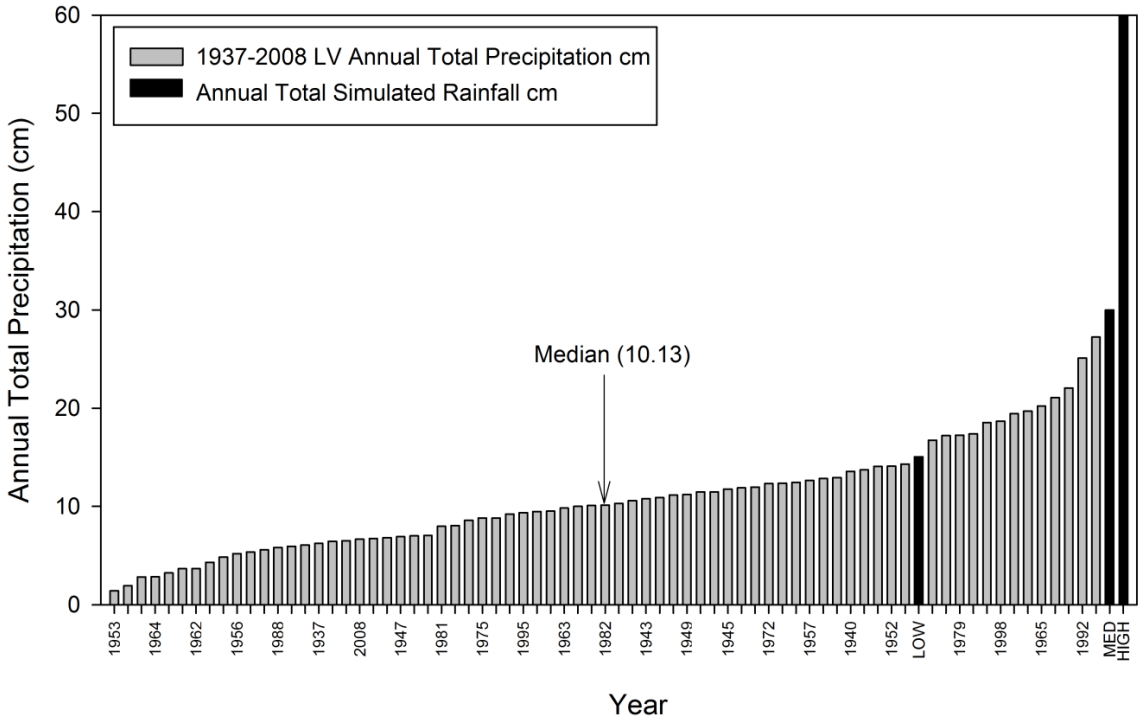

Figure 3-1. Measured yearly rainfall totals from (1937 to 2008) showing precipitation extremes within the local climate, (Gorelow, 2008).

The 3.66 m square plots were located with sufficient buffer area between them (average spacing of 22.2 m, Figure 3-2), to minimize the impact of one treatment on another. Simulated rainfall events occurred throughout the year (winter, spring, summer, and fall). Eight simulated rainfall events occurred on 10/13/05, 12/15/05, 2/21/06, 4/18/06, 6/6/06, 7/5/06, 8/8/06, and 9/14/06. Simulated rainfall was delivered in pulses of 0 mm, 18.75 mm, 37.5 mm or 75 mm to the 12 plots. Subsequent diurnal soil-plant-atmospheric measurements occurred on 10/14/05, 10/16/05, 10/19/05, 12/17/05, 12/19/05, 12/21/05, 2/22//06, 2/23/06, 2/25/06, 4/19/06, 4/20/06, 4/22/06, 6/8/06, 6/9/06,

7/6/06, 7/7/06, 8/9/06, 8/10/06, 9/15/06, and 9/16/06. Diurnal measurements were followed by mid-day soil-plant-atmospheric measurements which occurred on 10/15/05, 10/21/05, 12/16/05, 12/18/05, 12/20/05, 12/22/05, 2/24/06, 2/26/06, 2/27/06, 4/21/06, 4/23/06, 4/24/06, 6/7/06, 6/10/06, 6/12/06, 6/14/06, 7/8/06, 7/10/06, 7/12/06, 8/11/06, 8/13/06, 8/15/06, 9/17/06, 9/19/06, and 9/21/06.

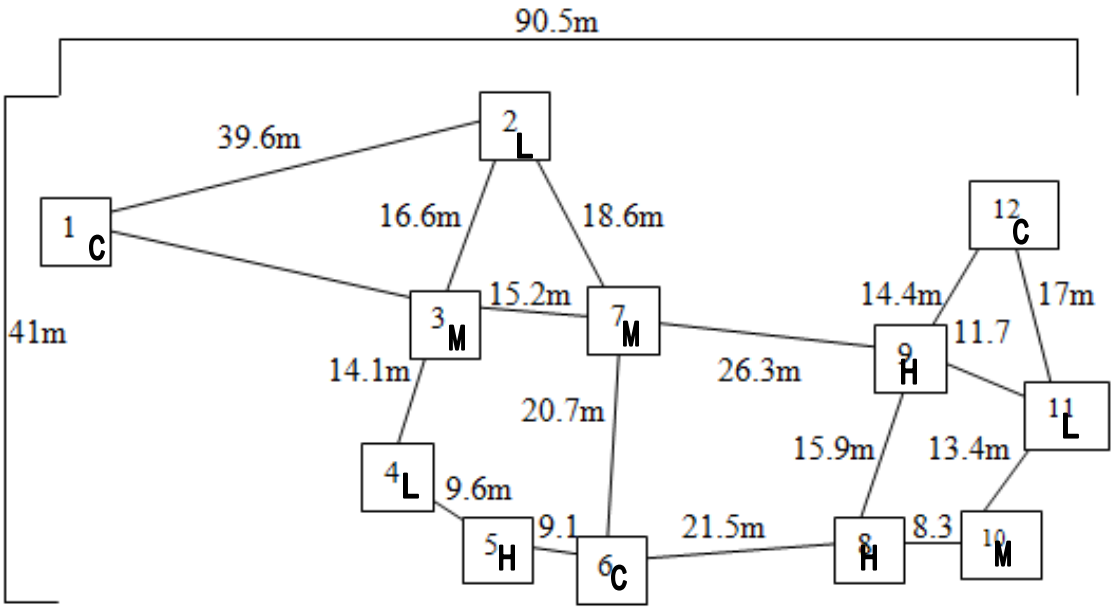

Figure 3-2 Illustration of relative distances between plots with a center positioned creosote bush. Water treatments were randomly selected (L-15cm, M-30cm, H-60cm, & C). Square plots and measured distances are not shown to scale

Rainfall Simulator

Twelve stationary rainfall simulator systems (one per plot) were individually constructed with four spray heads at 1.52 m above ground (12 series VAN, Rainbird©, Las Vegas, NV). Each spray head produced a horizontal 90° arc, 15° trajectory and throw

radius of 3.66 m at 30 psi. Irrigation heads were corner positioned to uniformly distribute water over the 13.4 m^2 plots. A photograph of the rain simulator setup is shown in (Figure 3-3). Preliminary testing showed a combined output from the four sprinkler heads of approximately 13.25 L min^{-1} (5.9 cm hr^{-1}) as measured with an attached water meter. Simulated rainfall application rates were set based on infiltration rates (see calculated hydraulic conductivity rates in Table A-1, Appendix 1). Simulated rainfall uniformity was evaluated by centering 25 cups in a 5x5 grid with a geometric spacing of 0.66 m between nearest cups and 0.51m between outer cup and nearest soil berm under the simulator. Collected water volumes from each cup were used in the calculation of the Christiansen uniformity coefficient (CU) (Christiansen, J.E. 1942, Hart et al. 1965). The CU was calculated using Equation 1:

$$CU = 1 - 0.8\left(\frac{SD}{\overline{X}}\right) \qquad \text{Eq. [1]}$$

where *SD* is the standard deviation and $\overline{X}$ is the population mean associated with the 25 cup volume measurements. The rain simulator produced a CU of 70 percent.

Pumped groundwater was provided for the rainfall treatments using an onsite well. One 5.08 cm main lateral was installed to transport groundwater to each of the above ground rainfall simulators, (Figure 3-4). Each simulator system was equipped with a water meter, ball valve before and after the water meter, a 30 psi pressure regulator, and a pressure meter to monitor system performance.

Figure 3-3 Photograph of a newly constructed rainfall simulator during preliminary testing of precipitation rates.

Before each simulated rainfall treatment, tarps were placed around the perimeter of each simulator to prevent wind induced distortion of the water spray pattern, which was observed when wind speeds exceeded 2.2 m s^{-1}. Additionally, the entire system was pressurized and checked for optimal pressure at 30 psi as previously determined for the best uniformity. Relief valves were opened to remove trapped air from all laterals leading to each simulator spray head loop, eliminating pressurizing startup time and ensuring maximal performance during use.

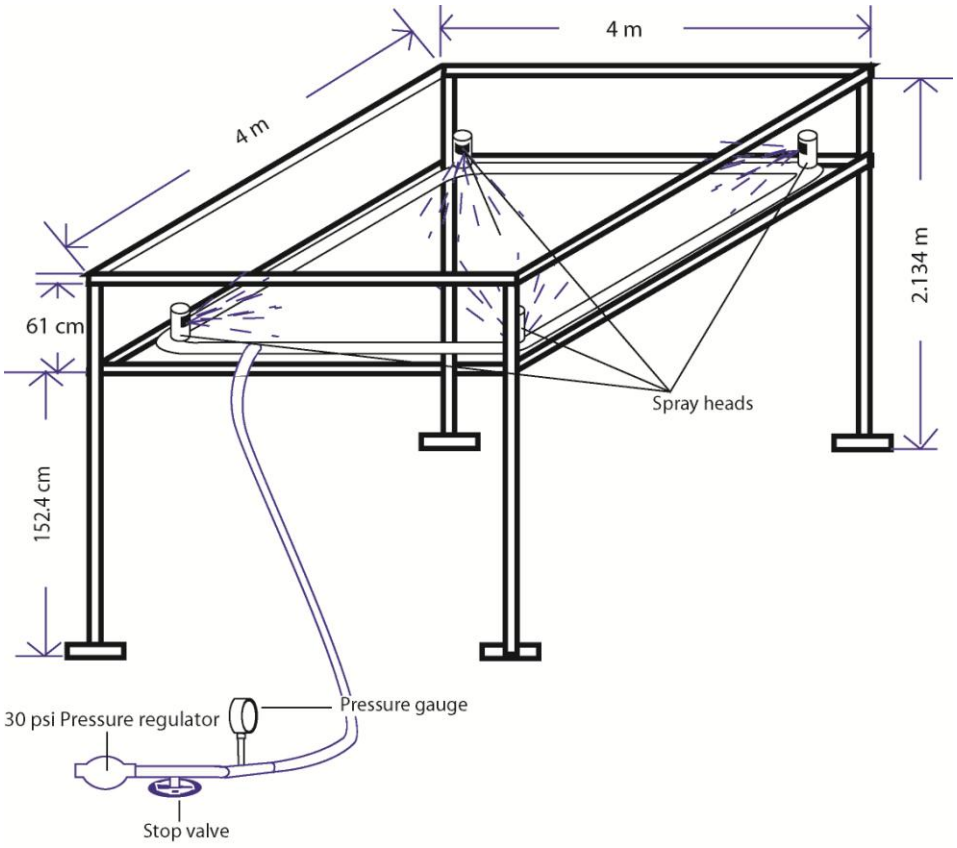

Figure 3-4 Illustration showing the rainfall simulator and individual parts. Measured distances and objects depicted are not shown to scale.

Simulated rainfall treatments were applied at night over a 4 to 8 hour window, depending on the soil infiltration rate and treatment volume. During this window, many short (2-10 minute) pulses (approximately 0.2 cm to 1 cm) of rainfall were applied to minimize ponding and maximize infiltration. The duration of the rainfall application was dictated by field observations of the saturated/unsaturated soil surface conditions. For low and medium treatment plots, rainfall pulses ended as soon as the soil surface began to saturate visibly and subsequent pulses did not begin until the soil surface began to dry. For high treatment plots or medium treatment plots with low hydraulic conductivity, (Table A-1, Appendix 1), to meet treatment volumes before sunrise, rainfall pulses were

applied at a constant duration rather than at increasingly shorter durations, and lasted until water just began to pond (approximately 1 cm). Night time pulses were used to reduce the volume of unrecorded evaporative losses during infiltration, maximizing the consistency of daily evaporative measurements between plots.

Time Domain Reflectometry

Time Domain Reflectometry (TDR) was used to assess soil moisture with depth. Plots were instrumented for both continuous soil water content measurements and for daily measurements. Within all 12 plots, three horizontal and two vertical arrays of 20 cm long stainless steel TDR probes were installed at 15, 45, 75 cm depth within the soil interspace, 190 cm north-east from each shrub (see photo in Figure 3-5a) and at 0-20, 20-40 cm under the outer edge of the canopy (Figure 3-5b). Sensors to be used in continuous mode were networked together through a series of multiplexors. The network consisted of 22 TDR probes with four multiplexors. Of these, five TDR probes each were placed into four separate plots. Two plots (2 and 5) were also equipped with two, 80 cm long probes. Specifically, the probe numbers and respective plot - simulated rain amounts were; probes 1-5 in plot(7)-(37.5 mm), 6-10 in plot (2)-(18.75 mm), 11-15 in plot (5)-(75 mm), and probes 16-20 in plot (12)-(control). TDR probes in all other plots were monitored daily after application of nighttime rain using a portable cable tester and waveform analyzer (Figure 3-6) (TRASE 6050X1 System 1, Soil Moisture Corp., Santa Barbara, CA).

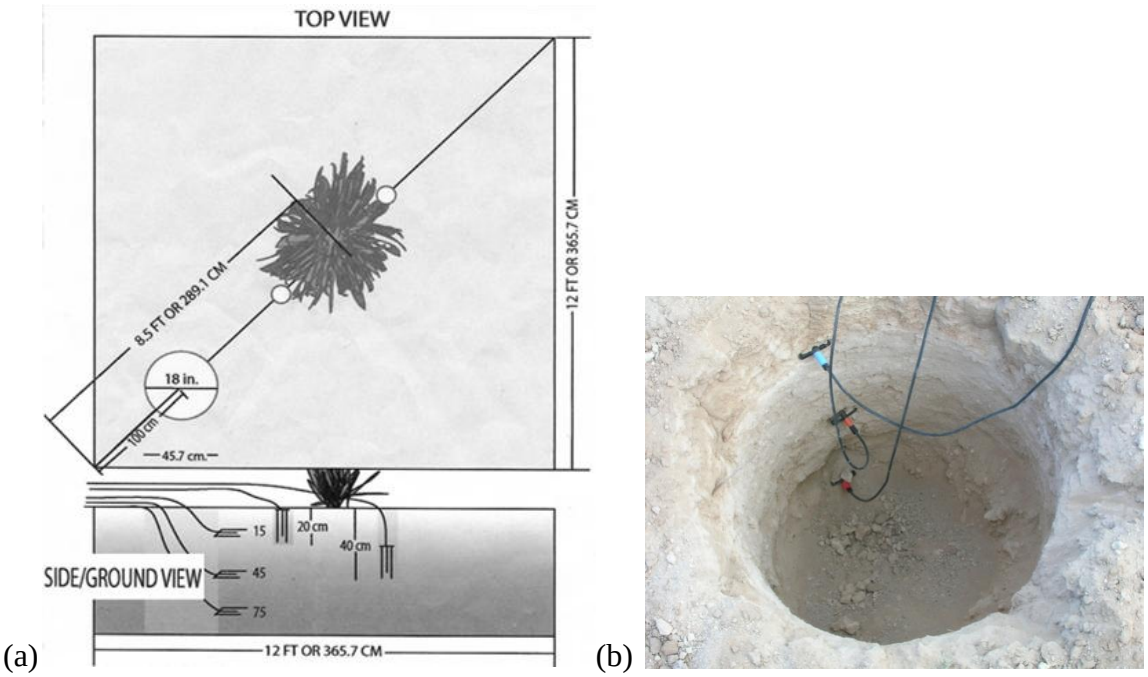

Figure 3-5 **(a) Illustration of typical TDR probes relative to center positioned Creosote bush and corner plot inter-space. (b) Photograph of typical nested TDR 3-rod probe placement within the soil matrix.**

Figure 3-6 **Photograph of the portable TRASE unit for measuring soil moisture.**

The networked TDR probes were connected to 50 Ohm TDR multiplexors (Campbell Scientific Logan, UT) using coaxial cables (RG-58U) ranging in length from 4 to 54 meters (Figure 3-7). Hourly TDR waveforms from the TDR network were collected and analyzed via a customized C++ program that used double tangent algorithms (DTA) based on the methods of Topp et al. (1980) and Herkelrath et al. (1991). An example TDR waveform analysis is shown in (Figure 3-8). T1 and T2 (reflection points labeled in Figure 3-8) are shown as the intersection of the tangent line with the slope of the lines. The T2-T1 difference is used to compute relative permittivity (k) and soil water content (Ɵ) using Topp's equation.

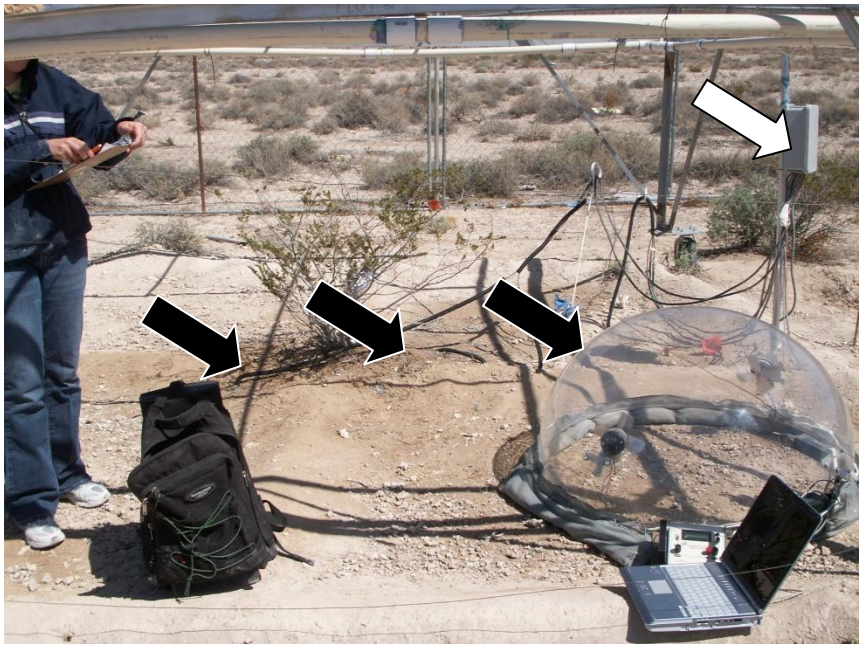

Figure 3-7 Photograph taken on April 4th of fully installed nested TDR probes (black arrows) connected to a 50 ohm multiplexor network (white arrow) at plot 2. The portable evaporation chamber with laptop is also shown.

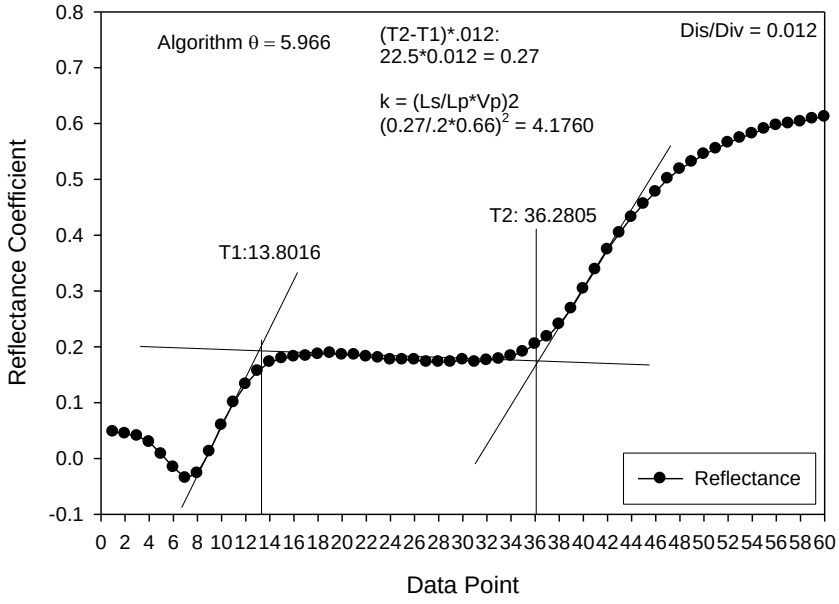

Figure 3-8 TDR waveform analysis via C++ algorithms for a probe placed 75cm in the soil inter-space at plot 5.

TDR Program Methodology

The main steps performed by the double tangent algorithm M1-M5 are outlined below;

M1

Read first waveform and find global minimum, compute the first derivative based on the central difference formula:

$$(F(x_{i+1})\text{-}F(x_i)/\text{deltaX}), \qquad \text{Eq. [2]}$$

where xi is the reflectance at position i and deltaX is the distance x_{i+1}-x_i. The maximum and minimum slopes are found in the n-window slopes (Equation 6 below) to find peak 1 and 2 associated with the probe handle and end of electrodes needed for calculating the apparent length $\mathbf{L_s}$ for M2

M2

Find the apparent length between reflection points. Use 20 data point sliding regression window routine to set tangent lines at peak 1 and 2. If error in setting tangent lines skip to M5. Find the intersection points T1 and T2 at tangent line intersections. Calculate the apparent length $\mathbf{L_s}$ = T2 – T1 (See Figure 3-8)

M3

Calculate the relative permittivity *k'*.

$$k' = (L_k/L_s * V_p), \qquad \text{Eq. [3]}$$

where L_k is the known probe length (20cm), and V_p is the relative propagation velocity of the electro-magnetic (EM) pulse through the probe material (0.66 in this case).

M4

Calculate the volumetric water content θv via Topp's equation.

$$\theta_v = -0.053 + 0.0292\, k' - 0.00055\, k'^2 + 0.0000043\, k'^3 \qquad \text{Eq. [4]}$$

M5

Repeat M1-M4 for each additional waveform.

Before fitting tangent lines to the collected TDR wave-forms, a post-processing filter was used to smooth noise observed with waveforms associated with drier soils, which were observed on control plots and before and several days after simulated rain

events, and longer cable lengths. A 5-point moving average (Equation 5) routine was used on raw TDR waveforms.

For any given TDR data point y_i;

$$y_i = \left(0.2y_{i-2} + 0.2y_{i-1} + 0.2y_i + 0.2y_{i+1} + 0.2y_{i+2}\right), \text{ i} = 2,\ldots, \text{(n-2)}. \qquad \text{Eq. [5]}$$

Waveforms were numerically processed for slopes (Equation 6) and y-intercepts (Equation 7) in the DTA TDR program, as follows:

$$\text{Running Slope } (m): \; m_k = \frac{w\left(\sum_{i=1,\ldots,n} x_i y_i\right) - \left(\sum_{i=1,\ldots,n} x_i\right)\left(\sum_{i=1,\ldots,n} y_i\right)}{w\left(\sum_{i=1,\ldots,n} x_i x_i\right) - \left(\sum_{i=1,\ldots,n} x_i\right)\left(\sum_{i=1,\ldots,n} x_i\right)} \qquad \text{Eq. [6]}$$

$$\text{Running Y-intercept } (y): \; y_k = \frac{\left(\sum_{i=1,\ldots,n} y_i\right) - m_k\left(\sum_{i=1,\ldots,n} y_i\right)}{w} \qquad \text{Eq. [7]}$$

where, window (w) = 5, k = n-w, i = k+w, n= 1,…, (j), j = number of values in a waveform (250 for this study), y = measured reflection coefficient, x = iterator associated with y.

As noted above, the equation from Topp et al. (1980) was used to compute final hourly volumetric water content. All results were stored for calculations of the change in storage (Equation 18) and water balance estimates (Equation 19).

Baseline soil moisture measurements began before simulated rainfall events occurred and continued on a daily basis with consecutive TRASE measurements, continuing typically for one to two weeks until soil moisture measurements returned to baseline values. Periodic water content measurements were taken, using probes in the TDR network, April 4, September 26 and October 3. Accuracy and comparability of the TRASE and DTA methods were assessed by periodically unplugging cables from the

network and measuring soil moisture with the TRASE portable system. A total of 51 comparison measurements were taken and were shown to have an overall good linear agreement, ($r^2 = 0.7866$, $P<0.001$). Selected waveforms were taken at 10:30 am on 10/30/06, 12:30 pm on 9/26/06 and 11:00 am on 4/4/06 from 22 probes. Volumetric water content measurements using the DTA algorithm were well preserved, having a daily average soil water content standard deviation of only 0.0028 $m^3\ m^{-3}$.

Regression analysis showed a significant correlation between the two methods, given that the relative structures of the change in magnitude of soil water content over time was similar for both approaches. Both methods produced water content time series (Figure 3-9) spanning 5 to 10 days with similar key characteristics; increases from base line water content after treatment, followed by an exponential decay that was asymptotic to baseline levels. However, an apparent offset bias was observed when comparing not just the periodic and continuous data sets for the same plot but to all available replicate periodic measurements within the same rain treatment, (Figure 3-9). One simple solution for this systematic bias was to add the offset between the maximum TRASE and computed measurements (0.121 $m^3\ m^{-3}$) for the entire experiment to the computed values, referred to][as the DTA-offset. The new DTA-offset was found to be highly correlated with all available TRASE measurements from replicate plots 3 ($r^2 = 0.90$, $P<0.001$) and 11 ($r^2 = 0.83$, $P<0.001$).

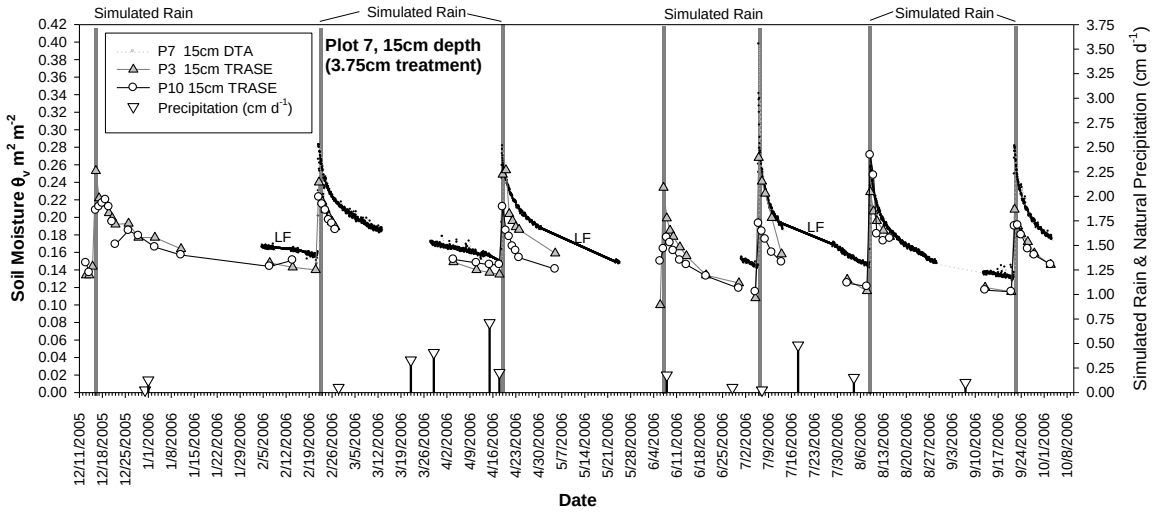

Figure 3-9 Volumetric water content obtained with the TRASE at replicate plots 3 and 11 compared to volumetric water contents obtained with the double tangent algorithm (DTA) at plot 7. All measurements were made at a 15 cm depth, for plots receiving 37.5 mm of rain on 7 occasions.

Soil Surface Volumetric Water Content Measurements

Soil surface volumetric water content (0-6 cm) were measured after simulated rainfall pulses diurnally from approximately 8am to ca. 3:30pm on days 1 and 2 and at mid-day on days 3-7. A Theta Probe (SM-200 Delta-T Devices, Dynamax, Houston Texas) sensor was used to measure soil moisture content (m^3 m^{-3}) at the soil surface. These soil water content measurements were incorporated in the soil water storage estimate for water balance closures.

Environmental Demand

Reference evapotranspiration (ET_{ref}) was assessed via an onsite automated weather station (Campbell Scientific Logan, UT, 2008), located in an adjacent tall fescue (*Festuca arundinacea* Schreb) plot. The weather station collected direct measurements of

air temperature (^{o}C), relative humidity (RH, %), barometric pressure (kPa), incident solar radiation (W m^{-2}), wind speed (m s^{-1}) and direction (degrees). Vapor pressure deficit (VPD), kPa) was calculated from the RH and the saturated VP calculated from temperature. The Penman-Monteith (Monteith, J. L. and M. H. Unsworth. 1990) calculation was based on a grass reference and flux density to provide an assessment of environmental demand.

The Penman-Monteith equation used by the weather station (ASCE, 2005) is defined as the following:

$$ET_{ref} = \frac{\Delta(R_n - G)}{\lambda(\Delta - \gamma^*)} + \frac{\gamma^* M_W (e_a - e_d)}{R\Theta r_v (\Delta - \gamma^*)} \quad \text{Eq. [8]}$$

where;

ET_{ref}	Reference evapotranspiration (kg m^{-2} s^{-1} or mm s^{-1})
R_n	Net radiation (kW m^{-2})
G	Soil heat flux density (kW m^{-2})
M_W	Molecular mass of water (0.018 Kg mol^{-1})
R	Gas constant (8.31 X 10^{-3} KJ mol-1 K^{-1})
Θ	Kelvin temperature (293 K)
$e_a - e_d$	Vapor pressure deficit of the air (kPa)
λ	Latent heat of vaporization of water (2450 kJ kg^{-1})
r_v	Canopy plus boundary layer resistance for vapor (s m^{-1})
Δ	Slope of the saturation vapor pressure function (Pa ^{o}C^{-1})
γ^*	Apparent psychrometer constant (Pa ^{o}C^{-1})
R_n	Net radiation (kW m^{-2}) is approximated via solar radiation from pyranometer sensor, crop absorptivity constant, latitude, date and temperature.

The daily total reference ET results are shown in Figure 4-1 and the raw daily results can be found in Appendix 1 Table A-2.

Radiometric and Light Intensity Measurements

Diurnal and mid-day measurements of soil and plant canopy temperatures were obtained with a portable infrared thermometer (IRT, Model 39800-22, Cole Parmer, Vernon Hills, Illinois). Ambient air temperatures were also assessed daily within minutes of IRT measurements to evaluate soil and plant temperature differentials (Suleiman and Crago, 2004). The IRT was physically held at a 30 degree angle of incidence. Soil surface emissivity (**ϵ**) was set to 0.95 (from Sellers 1965; Conaway, J., C.H.M. Van Bavel, 1967; Idso, and Jackson 1968; Ben-Asher et. al., 1983). As a rule, IRT measurements were taken facing away from the sun, such that early morning measurements pointed westerly and evening measurements pointed easterly. Shaded ambient air temperature and wind speed measurements were taken at roughly 1.0 m height using a hand held anemometer vane probe (Sper Scientific, Scottsdale Arizona). Solar radiation (W m^{-2}) measurements using a quantum flux meter (Model LI- 250 Pyranometer, LI-COR Inc., Lincoln, NE) were used to assess diurnal light intensity driving evaporative flux measurements (Jackson et al., 1973).

Bare Soil Evaporation Measurements

Soil evaporation rates (mm day^{-1}) were assessed for all field plots after each simulated rain pulse was applied using a custom built portable chamber (Stannard, 1988; Reicosky, 1990; Stannard and Weltz, 2006), (Figure 3-10 and 3-11). During soil dry down (Idso et al., 1974), the evaporation chamber was placed within soil plots and vapor measurements were recorded to a field laptop computer. The portable chamber maintained internal wind speed at 2.2 m s^{-1} using a custom DC-motor speed controller,

with adjustments made using a hand-held anemometer set 27 cm above the flange midway between two fans. An average annual ambient wind speed of 2.29 m s^{-1} was recorded using a Wind Sentry cup anemometer (model 03101-5, R.M. Young Co., Logan, UT) set at a height of 3 m above ground level (agl) attached to the automated weather station.

Figure 3-10 Portable vapor pressure dome used for measuring soil water evaporation fluxes.

The entire chamber assembly was developed following the guidelines of Stannard (1988) at a cost of approximately $2,000. The chamber (Plasticrafts, Inc. Denver, Colorado) was made from a sheet of 4.76-mm-thick Plexiglas G that transmits 92 % of all

wavelengths greater than 0.374 μm. Sampled vapor density (µg ml^{-1} s^{-1} or g m^{-3} s^{-1}) within the chamber was obtained with a water vapor analyzer (RH-300 RH/Dew Point Analyzer, Sable Systems, Las Vegas, NV) and was attached internally, 27 cm above the flange, midway between the fans. The vapor analyzer had a vapor density range of 0 to 10 µg mL^{-1}, resolution of 0.0001 µg mL^{-1}, and non-condensing relative humidity range of (0% to 100%).

The zero and span of the vapor analyzer was calibrated and verified using a DG-1 Dew Point Water Vapor Generator, (DG-1 Dew Point Generator, Sable Systems, Las Vegas, NV). Evaporation rates based on this portable chamber technique was computed using Equation 9 (Stannard, 1988).

$$E\ (mm) = 86.4MVC/A \qquad \text{Eq. [9]}$$

where E is the instantaneous evaporation rate for a site in units of mm day^{-1}, 86.4 is a conversion factor to convert grams of water m^{-2} s^{-1} to an hourly rate of mm h^{-1}, M is the maximal slope for the vapor density time series (g m^{-3} $second^{-1}$), V is the volume of the chamber (m^3), C is the calibration factor of the chamber (unitless) and A is the area of the land surface covered by the chamber (m^2). The instantaneous E measurements are later integrated over the course of a day yielding daily total evaporation rates.

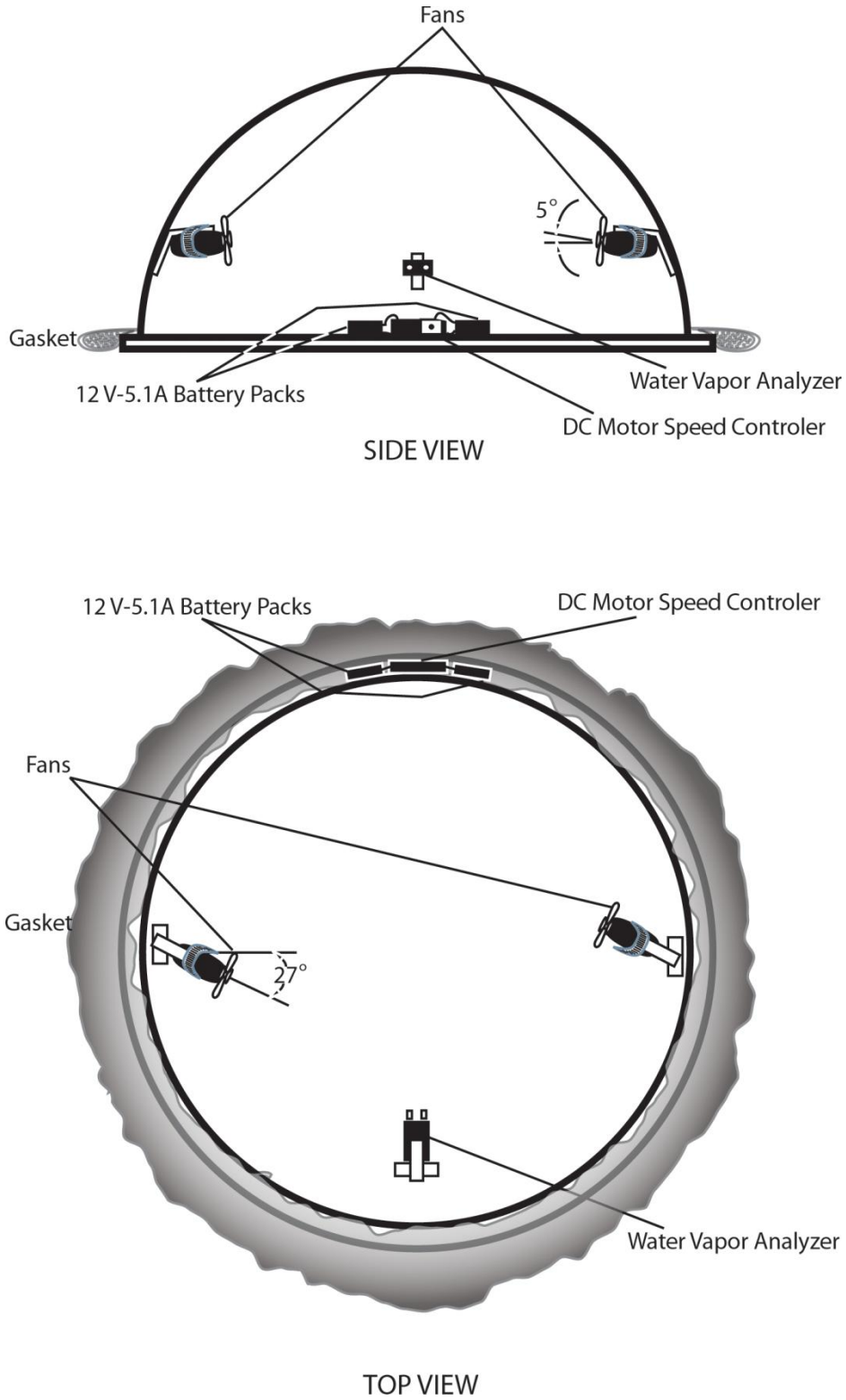

Figure 3-11 Diagram showing locations of fans, water vapor analyzer, DC motor controller, vapor barrier/gasket and battery packs for the portable water evaporation chamber. Measured distances and objects depicted are not shown to scale.

Instantaneous vapor density measurements from the portable chamber were sampled on a 1Hz basis over a typical range of 2 to 5 minutes. For quality control, vapor time series were accepted only if the following three measurement characteristics were satisfied:

1. Increasing vapor density response after dome emplacement (equilibration of vapor air mixing),
2. Constant slope response (rate of vapor flux),
3. Decreasing vapor density response (chamber saturation).

A typical water vapor series measured by the chamber is shown in Figure 3-12 for consecutive mid-day measurements the day after a rain simulation event. To rapidly process all chamber flux data, minimizing the possibility of introducing a bias by hand calculating slopes of vapor fluxes, a post-processing algorithm was implemented in the C++ computer programming language. The algorithm finds the maximum slope (M) by an iterative search-update approach.

The maximum slope always exits within the constant slope region (i.e., the average vapor flux), because the first and third regions have either increasing slopes into this region or decreasing slopes out of the region, respectively. The slope was found by calculating the regression line fitted through a sliding 20 data point window (Equation 6 above) and only updating M when a new maximum was found. The window value of 20 data points was sufficient to find the slope of the evaporative flux for the range of conditions in this study. Over estimation and under estimation errors due to over/under sensitivity of small/large slope changes were avoided by using a slightly modified version of Equation 6.

The only modification to the analysis of TDR waveforms in Equation 6 was the window *w* was set to 20. Also, just as in Equation 6, k = n-w, i = k+w, where n = 1,…, (j), j = number of values in a series (number of measurements), x = iterator associated with y, where y in this case is the given water vapor density (g m^{-3} s^{-1}) and *M* was initialized to zero for each new series. This slight modification of *w* enabled the algorithm to efficiently search for the maximal slope and solve for E using Stannard's (1988) vapor equation, (Equation 9).

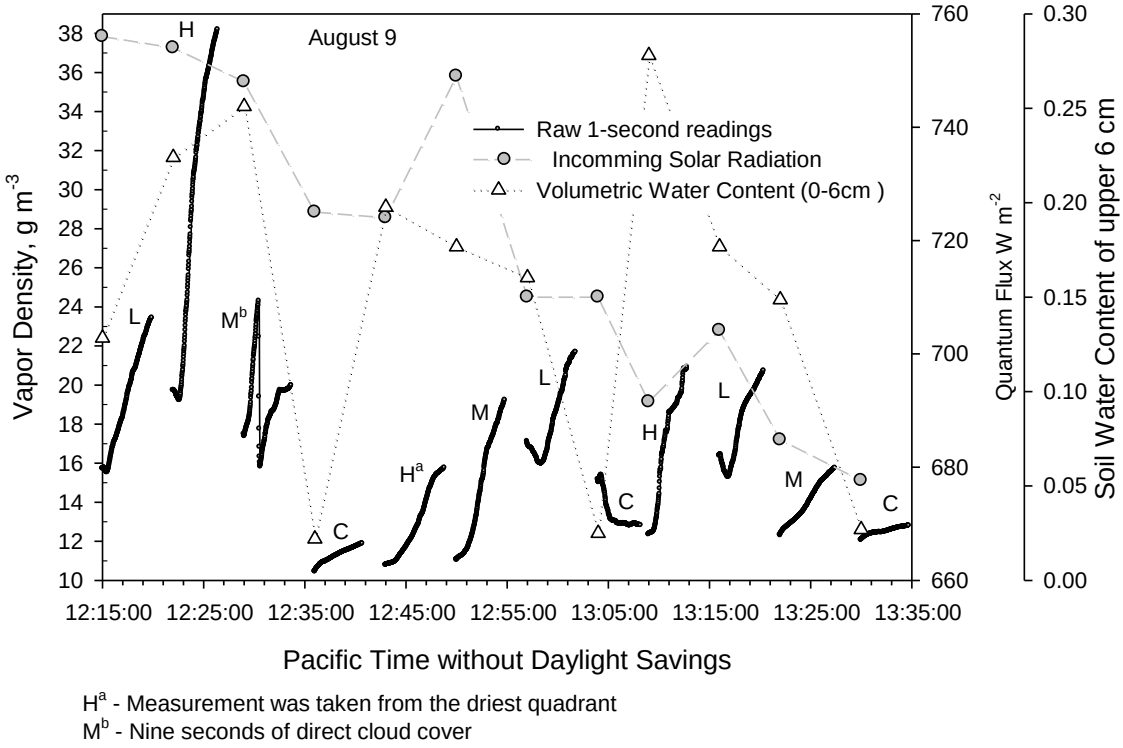

Figure 3-12 Portable dome time series of vapor density during 12 consecutive measurements of plots randomly chosen. Plots were irrigated the night before at either, 7.5cm-High, 3.75cm-Med, or 1.875cm-Low. Quantum flux and soil surface water content is also provided here.

Portable chambers have been criticized in the scientific community for changing the natural conditions of the environment of the plant-soil system being measured (Wagner and Reicosky, 1992; Dugas et al., 1997; Denmead and Reicosky, 2003; Heijmans et al., 2004). To minimize these effects, all soil evaporation measurements were conducted rapidly lasting a period of only 1 to 5 minutes. Denmead and Reicosky, 2003 and Stannard 1988, suggest that chamber measurements be made within minutes but have not stated an exact amount of minutes to avoid errors too large to use the actual measurement.

Sap Flow Measurements

Transpiration (T) measurements were obtained using stem flow gages (Dynamax TX; Devitt, et al. 1993; Smith and Allen 1996), (Figure 3-13). Sap flow from stems ranging in diameter from 10-19 mm were obtained using dynagages (Models SGA 10, SGA 13, SGB 16, and SGB 19, Dynamax) (Table 3-1). Half-hourly sap flow time series were downloaded twice weekly with a field laptop computer and a SC532A serial connector. Transpiration was later calculated as the product of sap flow and series of temperature gradient and heater power measurements using the following equation:

$$T = \frac{P - K_{st} A \left[\left(\frac{\Delta T_b + \Delta T_a}{\Delta x} \right) - K_g E_v \right]}{C \Delta T_{ba}} \qquad \text{Eq. [10]}$$

where P is the power (W) supplied to the gage, K_{st} is stem thermal conductivity (assuming 0.42 W m^{-1} K^{-1} for a woody stem), A is stem area (m^2), ΔT_a and ΔT_b are vertical temperature differences (^oK) above and below the heater, Δx is the distance (m) between two thermocouples above and below the heater, K_g is a gauge factor (W V^{-1}) for the radial loss of power per volt through a gauge when T = 0, E_v is voltage (V) of the

thermopile encircling the stem, C is the specific heat capacity (J g^{-1} K^{-1}) of the xylem sap, and ΔT_{ba} is the difference in temperature (K) across the heater.

Before attachment to a stem, the outer most layer of the stem was carefully smoothed with sand paper to remove any roughness that would prevent uniform contact with the heater and thermocouples.

Figure 3-13 Stem flow gage and leading stem wrapped in thermal resistant and solar reflective materials (circled) attached to a creosote bush stem.

Table 3-1 Canopy Mechanical Specifications for Sap Flow Gages

Model No.	Gage Height (mm)	Shield Height (mm)	Stem Diameter (mm)			TC Gap dX (mm)	Input Voltage (Volts)	Input Power (Watts)
			Min	Avg	Max			
SGA10ws	70	180	9.5	10	13	4.0	4.0	0.10
SGA13ws	70	180	12	13	16	4.0	4.0	0.15
SGA16ws	70	200	15	16	19	5.0	4.5	0.20
SGA19ws	130	250	18	19	23	5.0	4.5	0.30

After attachment to a stem, each gauge was covered above and below with a foam ring thermal sealer, moisture blocking plastic putty, tinfoil to reflect incident radiation, clear packing tape, and electrical tape for waterproofing and protection against ambient induced thermal gradients (Dugas et al., 1994).

The twelve stem flow gauges were networked together using an AM32 Relay Multiplexer (Campbell Scientific, Inc.) in the stem flow32A and flow32B logger stations. Each station was equipped with a CR10X data logger (Campbell Scientific, Inc.) and a SM8 storage module that stored 30 minute gage signals (dTa, dTb, dTc and PIN) later averaged to 60 minute periods. The zero night time variable (K_g) was estimated from the minimal flow that occurred at night from 8pm to 5 am during the first three days after gauge installation. The K_g factor was calculated for each gage and each seasonal rainfall simulation run. At the time of the last gauge removal, leaf area index (LAI) was estimated (Dugas et al., 1994; Devitt et al., 1993), such that stem flow rates could be normalized for the whole plant canopy. All LAI measurements were taken using a plant canopy analyzer (model LAI-2000; LI-COR, Lincoln, Nebraska).

Scaling Sap Flow to the Canopy Level

Sap flow was normalized to the canopy level using a normalization factor calculated by taking the ratio of fresh sub-canopy area to fresh canopy area. Because of the low leaf area indices and significant range in values (1.47 to 2.87), T was sensitive to leaf area (Ritchie, 1972). Thus, all analyses ware conducted on per leaf area basis (g day^{-1} m^{-2} leaf or g dry leaf) and not plant area basis (g day^{-1} per plant). Sub-canopy biomass associated with each stem flow gage was harvested and leaves were later separated to

calculate sub-canopy dry and fresh weight (g) and leaf area. The leaves were placed in an oven set at 70 C for 48 hours and then weighed. By taking random subsamples of (approximately 13,000 leaves) the ratio (g dry stem to g dry leaf) of sub-canopy cover, the harvested dry weight biomass (HB_{dw}) was calculated as having 5.58% of small stems by weight. All dry weight biomass was corrected using the stem reduction factor of $0.9442HB_{dw}$. Further, a portion of harvested sub-canopy fresh leaves was scanned before drying for leaf area using a PM-930 leaf area scanner (Ikegami Tsushinki Co., Utsunomiya, Japan) to estimate the percent shrinkage after oven drying. A shrinkage correction factor of ($1.3597\ HB_{dw}$) was calculated using 1-(Leaf Dry area/Leaf Wet area) in m^2 and was applied to the harvested dry weight measurements.

Table 3-2 Sap Flow Ratio Specifications used for Estimate of Transpiration

Plot	Treatment (mm)	Gauge Diameter (mm)	SDW (g)	SDA (m2)	SFA (m2)	LAI (m^2fol/ m^2 ground)	CDW (g)	CDA (m2)	CFA (m2)	Ratio
1	Control	13	12.43	0.05	0.07	1.71	128.63	0.53	0.72	10.17
2	18.75	16	19.65	0.08	0.11	1.47	79.24	0.34	0.46	4.10
3	37.5	13	25†	0.10†	0.14†	1.80	147.15	0.60	0.82	5.74
4	18.75	16	28.17	0.12	0.16	1.90	167.73	0.68	0.93	5.77
5	75	13	37.67	0.16	0.21	2.87	367.34	1.45	1.98	9.22
6	Control	13	25†	0.10†	0.14†	1.67	120.40	0.50	0.68	4.75
7	37.5	10	48.97	0.21	0.28	1.95	178.02	0.72	0.98	3.51
8	75	19	81.98	0.34	0.47	2.75	342.65	1.36	1.85	3.96
9	75	10	88.71	0.37	0.51	2.20	229.46	0.92	1.25	2.48
10	37.5	19	38.71	0.16	0.22	1.79	145.09	0.59	0.81	3.66
11	18.75	13	25†	0.10†	0.14†	1.68	122.46	0.51	0.69	4.82
12	Control	19	11.14	0.05	0.06	1.71	128.63	0.53	0.72	11.34

Where, stem dry weight (SDW), stem dry area (SDA), stem fresh area (SFA), leaf area index (LAI), canopy dry weight (CDW), canopy dry area (CDA) and canopy fresh area (CFA).
† Derived from image regressions of the leaf area pixels to dry weight.

Whole canopy and stem sub-canopy leaf dry weights were later converted to fresh weights for canopy area (CFA) and steam fresh area (SFA) (m^2) using Equations 11, 12,

and 13. The simple ratio SFA to CFA was used to normalize all sub-canopy or stem transpiration (g $stem^{-1}$) to the canopy level (g $canopy^{-1}$, Table 3-2). Canopy fresh area (CFA) estimates were calculated for all twelve creosote shrubs in the experiment by finding the CFA from the canopy leaf weight (CLW).

At the end of the experiment LAI (m^2) measurements were made for four creosote bush shrubs outside of the applied experimental area and associated whole canopies were collected and analyzed for canopy leaf weight (CLW) (g) measurements. Average LAI, based on these selected shrubs, was 2.015 within a range of 1.56 to 2.39 m^2 m^{-2} (Figure 3-14). The twelve plants within the study had an average LAI of 1.96, with a range of 1.47 to 2.87 m^2 m^{-2} (Table 3-2). A significant linear relationship was found for the CLW and LAI outside of the study area, shown in equation 11 ($r^2 = 0.9088$, $P<0.05$) and Figure 3-14.

$$CLW_{fresh}\ [g] = -223.26198(LAI) + 205.7847 \qquad \text{Eq. [11]}$$

The canopy fresh area (CFA) (m^2) was calculated by multiplying the fresh leaf weight (CLW_{fresh}, g) by a leaf weight to leaf area factor of 41.8676 (cm^2 g^{-1}) in equation 12 and then converting leaf area from cm^2 to m^2. The 41.8676 factor was estimated by taking the total leaf area (303 cm^2) measured from the PM-930 leaf area scanner divided by the total weight (7.2371 g) of 13 samples of field collected creosote bush leaves (over 1,000 leaves each) sampled before initiation of the experiment.

$$CFA\ [m^2] = ((CLW_{fresh}, g)\ 41.8676\ cm\ g^{-1})\ 0.0001\ m^2\ cm^{-2} \qquad \text{Eq. [12]}$$

Finally, the stem fresh area (SFA) (m^2) was calculated by multiplying the stem dry weight (SDW) (g) by the leaf weight to canopy leaf area factor and a fresh to dry leaf shrinkage adjustment factor shown in Equation 13.

$$SFA\ [m^2] = (((SDW\ g)\ 41.8676\ cm\ g^{-1})\ 1.3597)\ 0.0001\ m^2\ cm^{-2} \qquad \text{Eq. [13]}$$

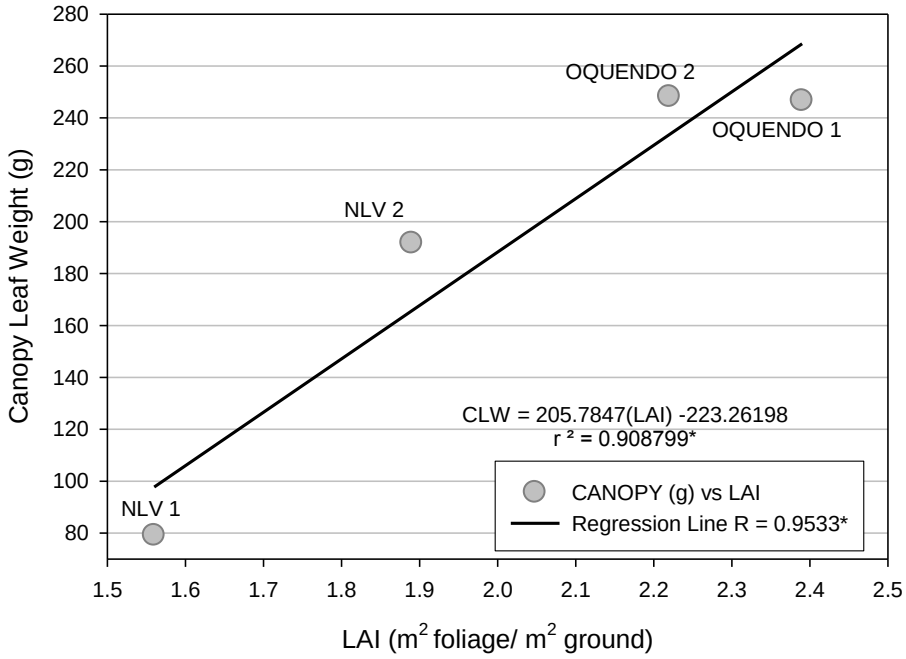

Figure 3-14 Linear regression fit between whole canopy leaf weight (g) and associated LAI (m^2 foliage m^{-2} ground) of four Creosote (*Larrea Tridentata*) shrubs sampled outside of the treatment area.

Final stem to canopy normalization ratios were high for plots 3, 6 and 11 due to abnormally low stem area estimates. The low stem area counts were due to excessive heating of stems from the stem flow gages. Stem leaf canopy areas were estimated for these plots from digital images taken just after gage installation via a pixel number to leaf biomass (g) relationship ($r^2 = 0.9891$, $P<0.001$). The pixels numbers and harvested dry

weights (g) for this relationship were comprised of only healthy green stems with installed gages. The Adobe Photoshop (version 6.0) package was used to estimate the total number of pixels (area) associated with green leafy tissue areas from stems with installed gages.

Data Validation

A ten day mini-lysimeter experiment was initiated in July 2009 to investigate day night partitioning of soil evaporation. The investigation was undertaken to validate gap filling procedures for evaporation measurements taken with the portable dome system. The lysimeters were constructed of 20.2 cm inner diameter PVC pipe, cut to a height of 25.8 cm, fitted with a plastic base with a small 1 mm diameter drainage hose inserted at the bottom. The columns were packed with soil (Las Vegas Loam) taken from the field test plot area at the North Las Vegas field research center. A total of 10.96 kg of air dried soil was packed into four lysimeters to achieve a bulk density of 1.5 g cm^{-3}. The upper 3 cm of each lysimeter was not packed with soil, allowing for water to be applied to the soil surface. Four different water treatments were imposed. Water was applied in low (1.88 cm), medium (3.18 cm) and high (7.5 cm) amounts, corresponding to 600, 1200, and 2400 mL respectively. The fourth treatment was the control, which received no water. Beginning at 20:00, tap water was applied to all soil columns in spray applications until soil saturation was observed. Additional pulses of water were applied when soils began to dry down to facilitate uniform infiltration. The mini-lysimeters were weighed on a hourly basis and weight changes were recorded. Lysimeter results revealed that soil evaporation did not drop to zero during the night period, unlike results shown in Stannard (1988), who showed a drop in evaporation rate to zero after sunset that lasted through pre-sunrise

(although data were not collected from plots recently saturated from precipitation or irrigation events).

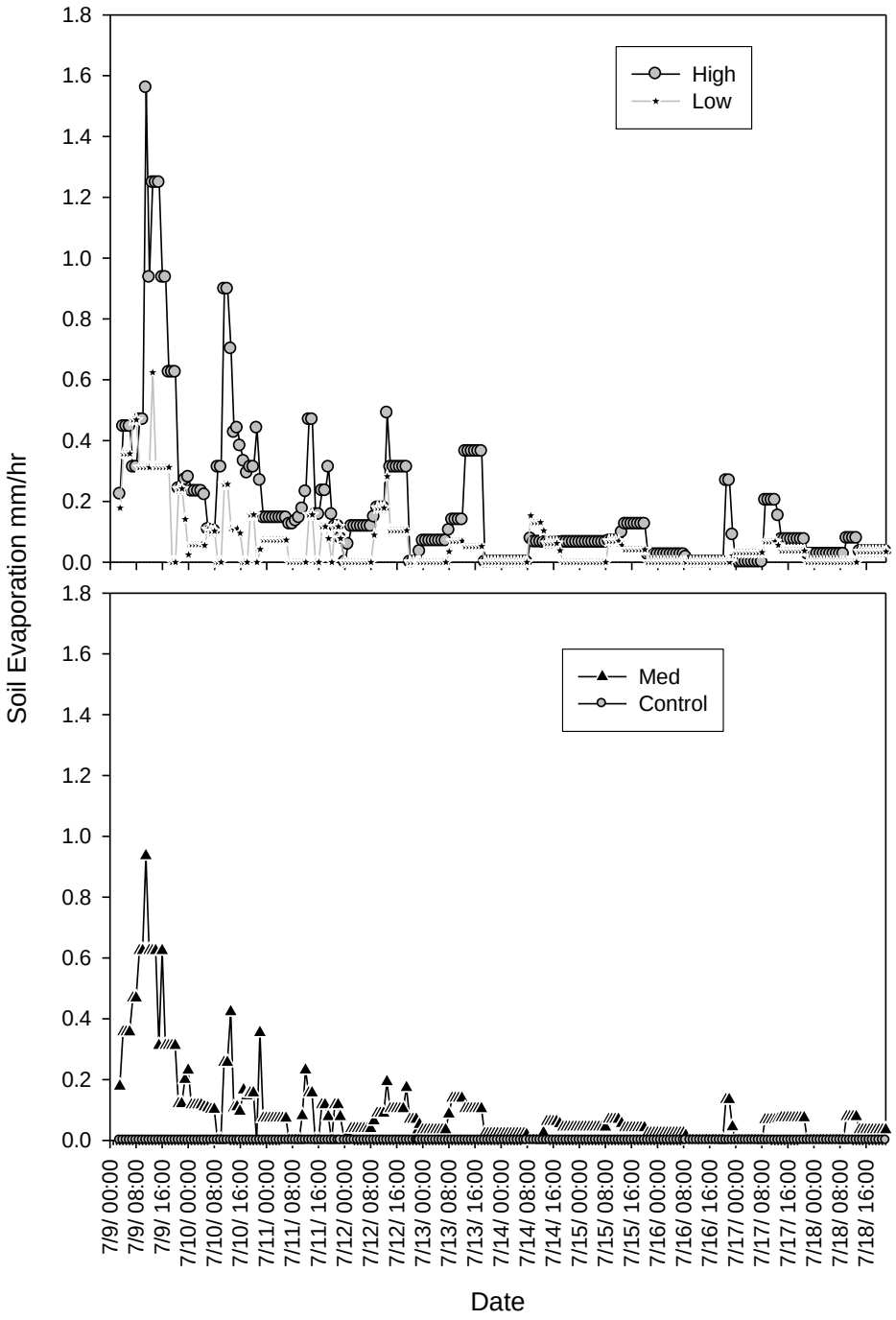

Figure 3-15 A ten day dry-down mini-lysimeter soil evaporation (mm hr^{-1}) experiment treated with water, (High-7.5, Med-3.75, Low-1.875 + Control-l 0 cm).

For the lysimeters, used in this study, the high and medium treatments showed non-zero evaporative water loss rates until the fifth night at 18:00. Whereas the low treatment continually showed evaporative water losses up to the second morning at 08:00, when evaporation rates slowed to zero for two hours before rising again, then settled to an eight day stepping down diurnal evaporation pattern resembling Stannards' (1988) published data, (Figure 3-15).

The percent of total water applied that was lost to evaporation was partitioned between night and day for every 24 hours. During the first 24 hours the low, medium, and high treatments lost a total of 20, 8, and 6% of the total water applied. The total night time water losses were 6.7 times greater for the low treatment than the high treatment, and 2.5 greater than the medium treatment. The results suggest that a greater percentage of the applied water in the low water treatment remained closer to the soil surface than in the other two treatments and thus more likely to be lost through evaporation. Soil evaporation stages (I. non-water limited, II. transition from non-limiting to vapor driven, III. completely driven by vapor transport from deeper soils), as defined by Idso et al. (1974), could be clearly identified from the percentage of total water applied loss to evaporation (Figure 3-16). The stages were found at the intersection of drawn tangent lines for the three concurrent maximal slopes containing non-intersecting data series of at least 20 data points. Night time evaporation rates for all treatments were either zero or approaching zero (entering stage III evaporation) by the fifth or sixth night, but stage II evaporation continued well into the seventh day for day time evaporation for all treatments.

The portable evaporation chamber produced similar results as the mini-lysimeter, as both methods produced bell-shaped evaporation curves for all water treatments (Figure 3-17). Additionally, by normalizing diurnal data from both methods by dividing hourly values by the daily maximum value, both data sets demonstrated temporal response (e.g., similar bell-shape curves stepping down in size over time). Regression results revealed that all diurnal normalized evaporation rates from dome measurements (all treatments) taken in July could be predicted from normalized evaporation rates from lysimeter measurements (all treatments), ($r^2 = 0.5613$, $P<0.001$, $n = 35$).

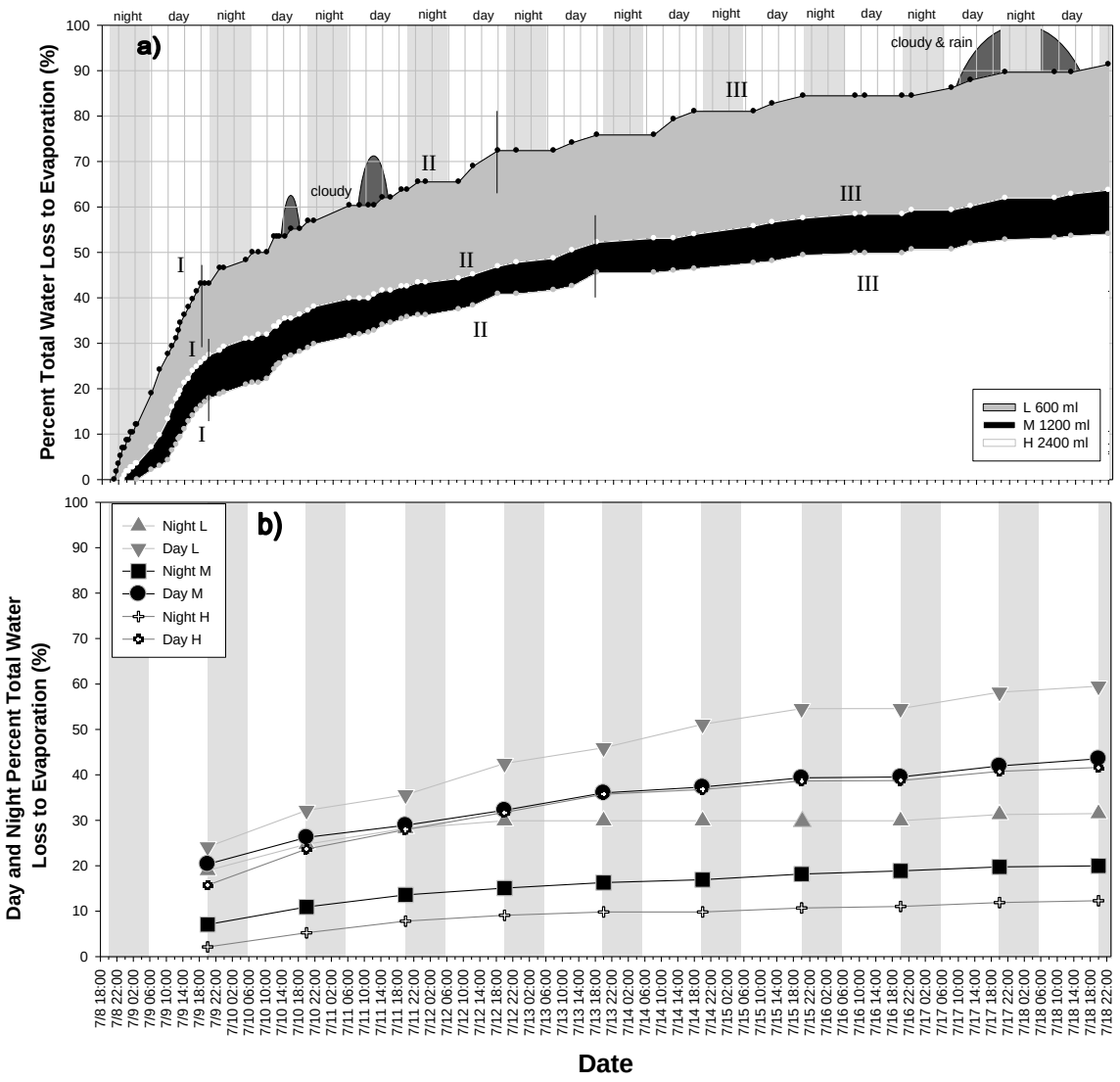

Figure 3-16 Plot of the percent total cumulative loss through evaporation of applied water (a), and totals partitioned between the day and night time (b) for all three treatments.

Linear correlations were also found ($P<0.050$) for all treatments (low, med, high) with individual normalized evaporation rates from dome measurements when compared with normalized evaporation rates from lysimeter measurements (Figure 3-17).

Total 24 hour estimates could be determined by adding estimated nighttime evaporative estimates to diurnally measured rates from 08:00 to 15:00 (Figure 3-18).

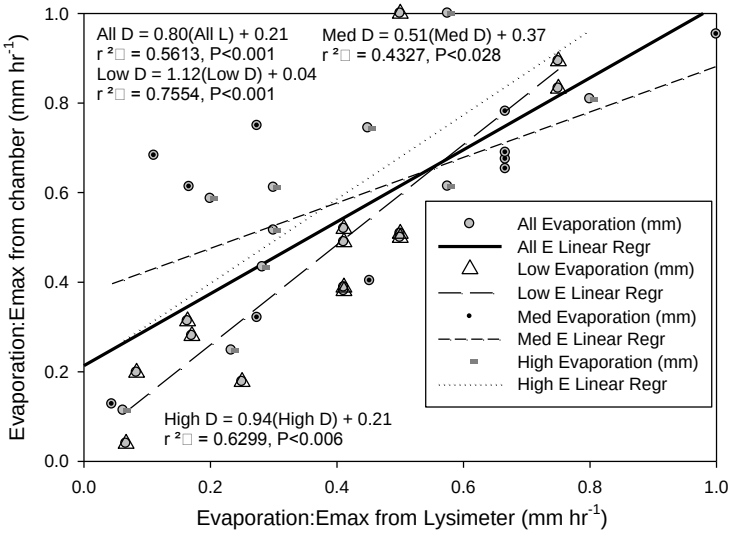

Figure 3-17 Regression correlations between the portable chamber and lysimeter evaporation measurements.

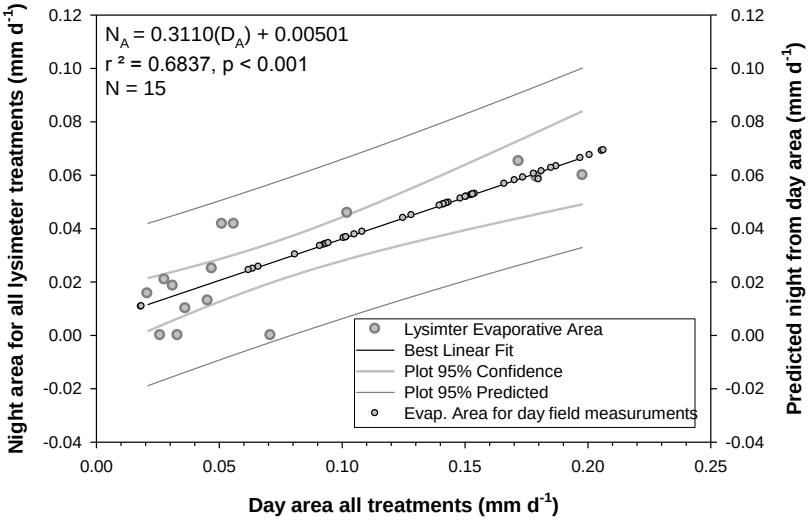

Figure 3-18 Hourly evaporative loss measurements from four mini-lysimeters partitioned into day (08:00-15:00) versus night (16:00-07:00).

Night time estimated evaporation was determined from day time measurements using equation 14. The night-to-day relationship also passed the Shapiro-Wilk test for

normality (P=0.815) and the constant variance test (P=0.705) signaling a robust sampling size was used.

$$E_{night} = 0.311(E_{day}) + 0.00501, (r^2 = 0.684, p<0.001, n = 15) \quad \text{Eq.[14]}$$

Total Soil Evaporation

Daily evaporation rates (E) (mm) for irrigated plots were later calculated by integrating the area under the curve of diurnal hourly evaporation rates from equation 15 (Excel, Microsoft Corp.)

$$\int_a^b x^n dx = \frac{1}{n+1}\left(b^{n+1} - a^{n+1}\right) \quad \text{Eq. [15]}$$

where a is the ending date, b is the starting date, $b \geq a \geq 0$, and $\{x_0, \ldots, x_n\}$ is the E (mm hr^{-1}) partition of the set of diurnal E measurements [a,b]. The total integrated E rates for both measurements made during the day (08:00 to 15:00) and measurements normalized by the daily maximum ($E_n/E_{max\ n}$) were calculated to estimate night time portion of E (mm) using equation (14), then summed to get the total 24 hour estimate of evaporation. Next, the 24 hour totals (E_d) were estimated for all mid-day measurements, allowing daily estimates to be made when only mid day measurements ware made (days 4-7). The relationship between E_d and solar noon evaporation (E_{sn}) (detailed in Figure 3-19) could be predicted from E_{sn} in Equation 16 with a coefficient of determination of ($R^2 = 0.91$, $P<0.001$).

$$E_d = 5.6187(E_{sn}) + 0.3998 \quad \text{Eq. [16]}$$

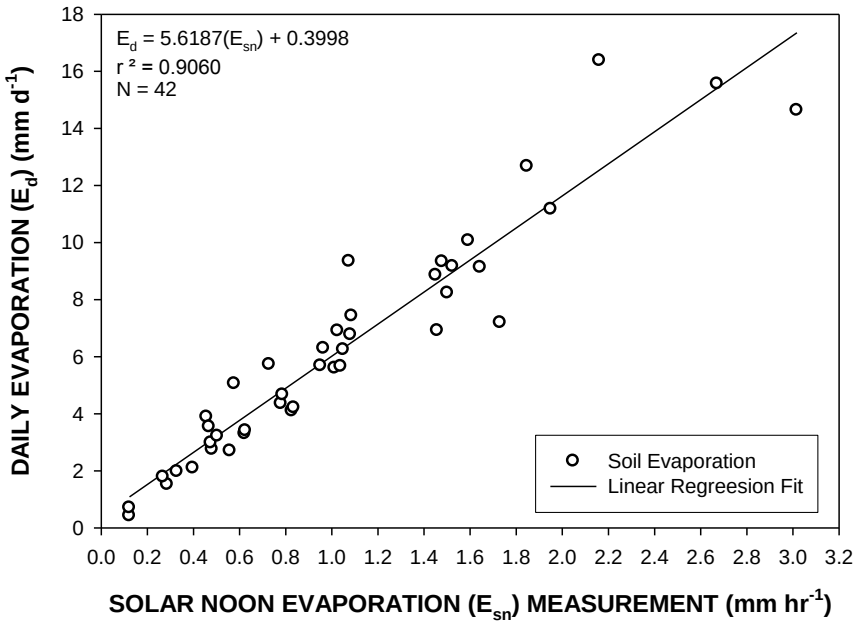

Figure 3-19 Regression of daily soil evaporation with solar noon evaporation for all treatments (Control, 15cm, 30cm, & 60cm).

Soil Physical Properties

Before initiating the experiment, soil physical and hydraulic properties were analyzed. Soil samples were collected in the field from the side wall of a 45.7 cm diameter augured hole at depths of 15, 30, 45, 60, and 75cm below the soil surface. Holes were augured approximately 180 cm north-east from the base of the shrub within each plot. Physical properties, such as the cumulative particle size distribution for sand, silt, and clay from soil samples were analyzed for each plot using a laser light scattering technique (model Saturn DigiSizer 2000, Particle & Surface Sciences Pty Ltd, Gosford NSW, Austrailia) (Table A-1). Modeled hydraulic van Genuchten (VG) (van Genuchten, 1980) properties were calculated using Neural Network Prediction module (Rosetta-Lite v. 1.1 2003, Schaap et al., 2001) contained within the HYDRUS-1D VS 4.1.4 computer

program (Simunek et al., 2006), (Table A-3). Additionally, each soil sample collected from the field was sub-sampled for a suit of ion analysis (EC, Na, K, Ca, Mg, Cl, and SO_4) performed on saturation extracts, Table A-4.

Soil Water Storage

Total soil water storage (SWS) ($cm^3\ d^{-1}$ or $g\ d^{-1}$) within each 3.66 m^2 plot was established using equation 17, which is based on all independent TDR soil water content measurements taken from the soil surface (interspace), under the canopy, and from soils outside the canopy. All measurements were taken within minutes of each other on each plot.

$$SWS\ (cm^3\ d^{-1}) = 20A_{plant}\Theta_{0\text{-}20} + 20A_{plant}\Theta_{20\text{-}40} + 12{*}A_{soil}\Theta_{0\text{-}6} + 18A_{soil}\Theta_{15} + 30A_{soil}\Theta_{45} + 20A_{plant}\Theta_{45} + 15A_{total}\Theta_{0\text{-}5} \quad \text{Eq. [17]}$$

where, $\Theta_{0\text{-}20}$ and $\Theta_{20\text{-}40}$ were water content values from TDR probes installed vertically, $\Theta_{15,\ 45,\ 75}$ are water contents from horizontally installed probes under canopy and in bare soil sites, respectively, $\Theta_{0\text{-}6}$ is water content of the top 6 cm of soil, and A_{plant}, A_{soil}, A_{total} for the area under the plant, soil interspace, and total area, respectively. All estimated areas and associated canopy measurements are shown in (Table 3-3). Water contents under canopy sites were applied to an area (A_{plant})1.4 times the measured diameter of the canopy (C_d), where nonrandom processes are known to dominate and hydraulic conductivity $K(\psi)$ is spatially correlated with the desert shrub (Caldwell et al., 2008). The area outside of the plant influence (A_{soil}) was assigned to the nested water content measurements taken from corner of the plot, (Figure 3-20). The change in SWS was later calculated as:

$$\Delta S = SWS_{t2} - SWS_{t1} \quad \text{Eq. [18]}$$

where ΔS is the change in storage, SWS is the soil water storage from Equation 17, t1 is the first day, t2 is the second day or time period, e.g. day 5.

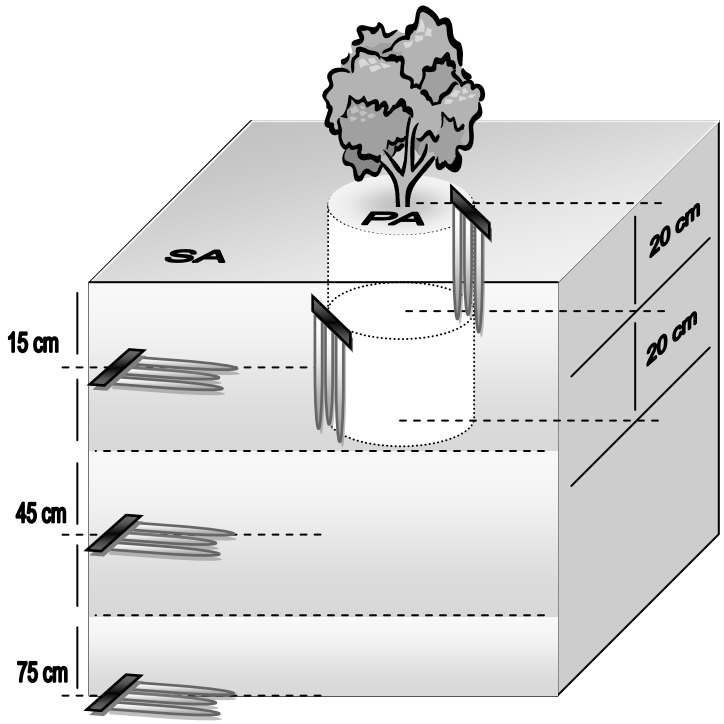

Figure 3-20 Illustration of TDR placement within soil (SA) and plant areas (PA).

Table 3-3 Canopy Diameter and Area Estimates for all 12 plots.

Canopy Shape	Plot	Canopy Area (m^2)	Plant Area[c] (m^2)	Soil Area (m^2)	Canopy height (cm)	Canopy horizontal diameter (cm)	Canopy laterals (cm)
Elliptical	1	2.51	3.51	9.87	114	228	100[a], 140 [b], 140 [b], 100 [a]
Elliptical	2	0.77	1.08	12.3	95	140	25 [a], 70, 68 [a]
Elliptical	3	1.30	1.82	11.56	95	190	70 [a], 87, 70 [a]
Oblate Oval[d]	4	1.42	1.98	11.40	140	168	157, 140
Elliptical	5	1.83	2.57	10.81	140	173	110 [a], 135, 80 [a]
Circular[d]	6	2.01	2.81	10.56	108	175	175, 145
Circular[d]	7	0.90	1.26	12.12	48	123	108, 105, 93
Elliptical	8	2.23	3.12	10.26	105	175	125 [a], 162, 103 [a]
Elliptical	9	1.64	2.30	11.08	110	182	128 [a], 115, 77 [a]
Circular[d]	10	1.70	2.38	11.00	105	174	155, 133, 126
Elliptical	11	1.09	1.53	11.85	110	148	73 [a], 94, 100 [a]
Circular[d]	12	1.58	2.22	11.16	90	160	142, 134, 132

[a,b] Measured 102 and 254 cm from the canopy edge respectively.
[c] Plant area taken by multiplying 1.4 times the estimated shrub canopy area.
[d] Observed geometric differences in canopy shape were taken into consideration when measuring and calculating canopy areas.

Water Balance

The water balance was calculated by summing all measurements of E normalized to the plot (Equation 15 and 16) and T normalized to the plant canopy (ratios from Table 3-2) and subtracting the total from the change in storage (ΔS) found from Equation 18, plus the addition of the total simulated rain applied and any natural recorded rainfall from the weather station. Daily and 5 day water balances were calculated over a 5 to 10 day window preceding treatments (Dec 16-26, Feb 22-28, April 19-24, June 7-14, July 5-12, August 9-15). The water balance equation is:

$$E + T = P + I - \Delta S \text{ (cm)} \qquad \text{Eq. [19]}$$

where E is soil evaporation, T is transpiration, P is precipitation, I is input from rainfall simulation, and ΔS is the change in storage (S_2-S_1), or the actual difference in storage between the last day of (S_2) and just before (S_1) a simulated rainfall event.

Closure was estimated by dividing the total output by total input, i.e., ((E+T / P+I-ΔS)*100 %), where 100% would be perfect closure. If the closure estimate was above 100%, more water was lost from the system (E+T) than added (P+I+ΔS).

Mid day values, such as soil/plant temperature differentials (Ts-Ta, Tc-Ta), soil temperature, soil surface water content and total SWS closest to mid day (12:00) were selected from diurnal data sets using a time selection function in Microsoft Excel (Figure 3-21) from diurnal data sets.

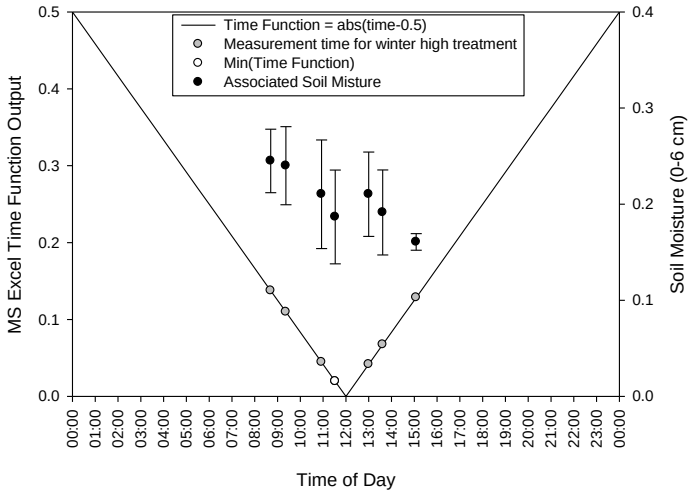

Figure 3-21 Example of a time function output used for the systematic selection of mid-day surface soil moisture measurement from a diurnal data set. The white circle shows the minimum value that would be selected for inclusion in further regression analysis.

Not all mid-day measurements (e.g., temperature, soil and plant surface temperature, air temperature, soil evaporation, wind speed, quantum flux, soil surface

water content, and water contents were made at exactly noon). However, the average mid day time selected was noon +/-75 minutes.

Statistical Methods

Two-way ANOVAs were run in SIGMAPLOT 11 (SYSTAT Software, inc., San Jose, CA) to analyze the effect of different levels of simulated rainfall treatments on each water balance component (E, T, and ΔS). Each component assessed was the weekly sum of water loss (E, T or ΔS) or gain (ΔS) after treatment, (Table A-5). A total of 72 component weekly totals were included in the ANOVA. Additionally, two-way ANOVA's were run to assess interactions between repeated measures of the daily totals of water balance components and T_c-T_a, and T_s-T_a. A total of 539 daily total values for each component were assessed in the ANOVA. The Holm-Sidak method was selected for the all pair-wise multiple comparison procedures implemented via the ANOVA. The October and September data sets could only be partly analyzed due to complications with sap flow system and/or the hemispherical chamber.

Backward Stepwise Multiple Regression Results

Five day totals for each of the following column variables was compared in 5 day backward stepwise regressions: E, T, reference evapotranspiration (ET_{ref}), SWS, I, P, VPD, LAI, basal canopy area (BC_A), plant area (P_A, P_A is 1.4 times BC_A), and soil area (S_A, area of the plot minus P_A). A total of 72, 5 day totals were included for each column variable. Correlation variables were accepted only for $P<0.050$, and only if individual variance inflation factor (VIF) < 2.00, and total VIF < 10.

Additionally, diurnal hourly measurements of soil/plant temperature differentials (Ts-Ta, Tc-Ta), soil temperature, soil surface water content and SWS closest to mid day (12:00) selected via a time selection function in Microsoft Excel (Figure 3-21) were compared. Also, daily E, T, ET_{ref}, Rain, Basal Canopy Area (BCA), LAI, Soil Area (SA), and VPD were included in the daily backward stepwise regression approach. There were 539 daily totals included for each column variable and as with the 5 day multiple regression results, VIF < 2.00 and total VIF < 10 were imposed.

CHAPTER IV

RESULTS

Environmental Demand and Actual Precipitation

The experimental test plots were located in an undisturbed area approximately 100 m north of an automated weather station. The daily grass reference evapotranspiration (ET_{ref}) and daily precipitation totals from the on-site weather station are shown in Figure 4-1 for the last three months of 2005 and the first nine months of 2006. During this 12 month period total ET_{ref} was 156.7 cm and the minimum and maximum daily ET_{ref} (0.940 and 8.70 cm) occurred on December 19th and July 15th, respectively. A total of 16 precipitation events occurred (total of 7.874 cm) during this time period, four of which occurred during some stage of a field monitoring period (0.203 cm in April, 0.178 cm in June, 0.025 cm in July, and 0.152 cm in August). The two largest recorded precipitation events (1.245 and 3.544 cm, October, 17 and 18, 2005) accounted for 60% of the total precipitation recorded. The ET_{ref} measurements were taken with irrigated Bermuda grass as fetch and not for open stand creosote bush: as such, ET_{ref} may have been over estimated due to differences in specific crop characteristics, such as canopy resistance length that control energy exchange. However, the reference evapotranspiration values were used only as a guide for relative seasonal and monthly changes in environmental demand in this study.

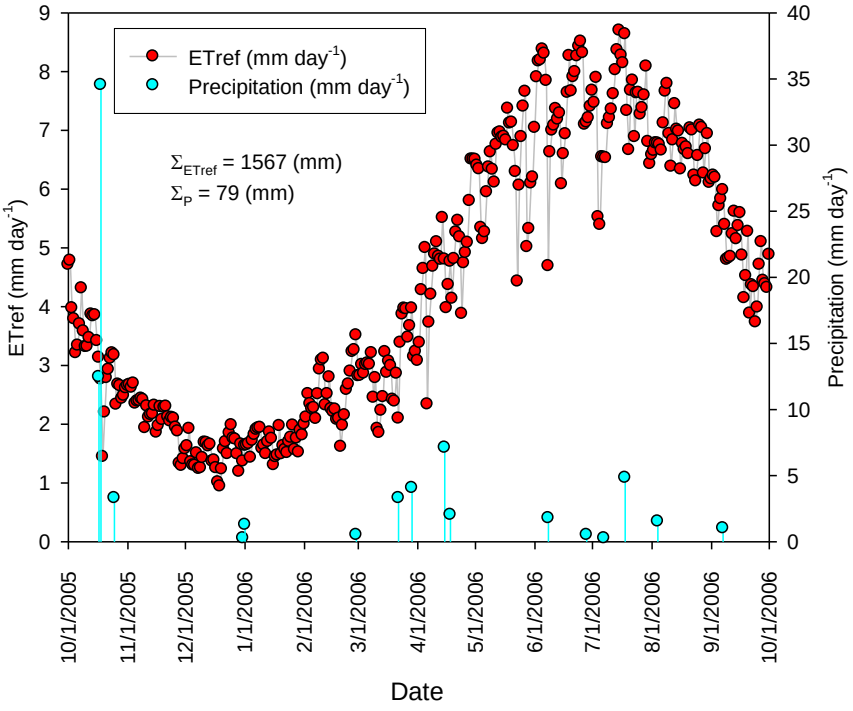

Figure 4-1 Total Daily Reference Evapotranspiration (ET_{ref}, mm) and Precipitation (mm) from an onsite weather station.

Soil Physical Properties

Soil samples taken from the field and analyzed using a laser light scattering technique (model Saturn DigiSizer 2000, Particle & Surface Sciences Pty Ltd, Gosford NSW, Australia) are shown in Table A-1. The sand separate for all treatments (control, low, medium, and high) are shown in Figure 4-2. The treatment plots; control, low and high had 30-40% more sand in the upper 15 and 30 cm of the soil surface than the medium replicate plots (Figure 4-2). For soils in all plots, with the possible exception of the medium plots, the physical hydraulic properties favored higher infiltration rates or deeper percolation from the surface evaporative dominated layers (Idso et al., 1974).

van Genuchten (VG) (1980) soil hydraulic properties are shown in Table A-3 and figure 4-3. Model results showed saturated hydraulic conductivity values near ground

surface (15 cm) as much as nine times lower for the medium plots than for other plots; hydraulic conductivity values of the other plots were outside 1 standard deviation of the medium plots until a depth of 45 cm for control and low treatment plots and 60cm depth for the high treatment plots. However some plot by plot variability was observed. The controls and high treatment plots had the two highest estimated saturated hydraulic conductivity values (86.0 and 87.9 cm d^{-1}), respectively. The model results also showed the low treatment plots had hydraulic conductivity rates as high as 65.8 cm d^{-1}, whereas the medium treatment plots revealed little variation between replicates or with depth, with an overall average estimated saturated hydraulic conductivity of 7.7 cm d^{-1} (classified as moderately rapid by the American Society of Agronomy, 1983). Even given the differences in textural components, regression results showed that the percent sand for the upper 30cm of soil was rejected as a significant factor for the dependent variables of E, T and ΔS, ($P>0.05$).

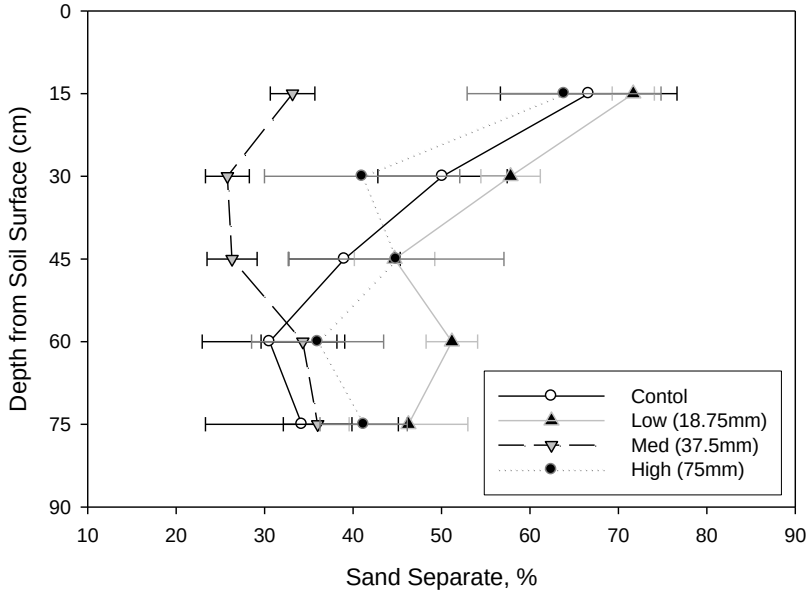

Figure 4-2 Average % sand with depth along with standard error bars for each treatment.

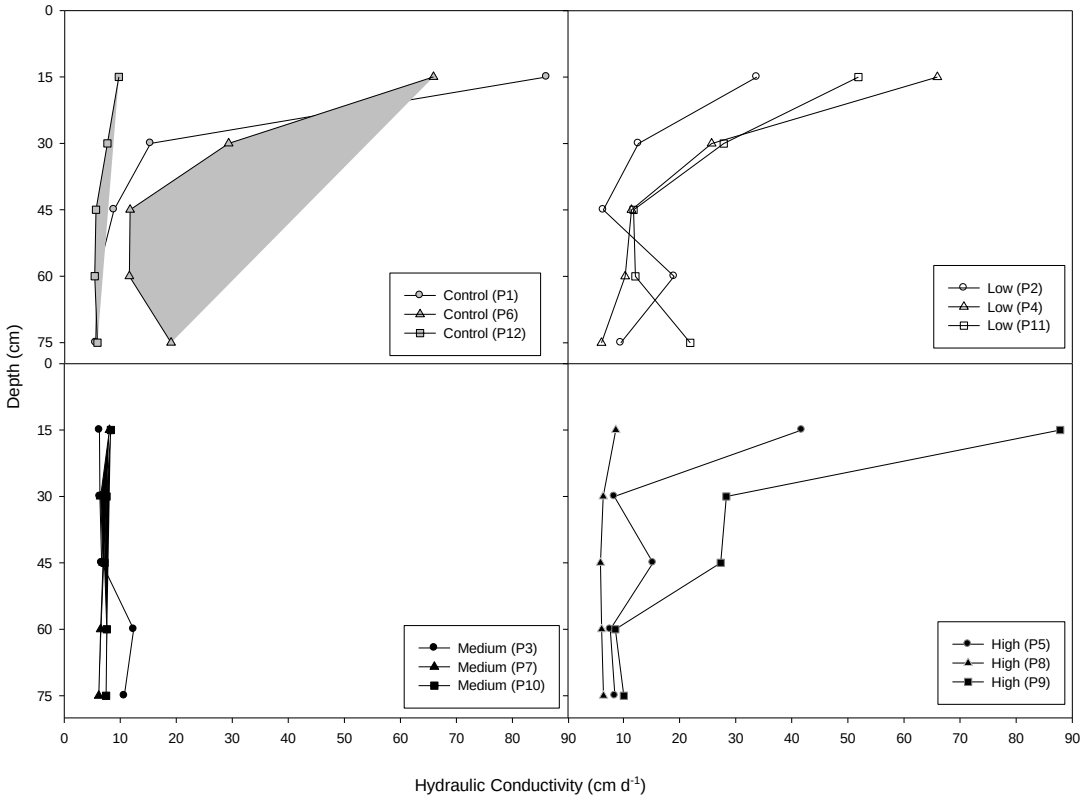

Figure 4-3 Predicted saturated hydraulic conductivity (cm d^{-1}) as a function of depth for all 12 plots based on ROSETTA.

Soil Water Content and Soil Water Storage

When comparing SWS for the three simulated rainfall treatments and controls, higher SWS occurred in high treatments, especially during winter months. Soil water storage was 23% or 3.1 cm lower on average in August than December. During the October monitoring period, SWS increased by 34% (average of controls in response to the two large rainfall events) and then returned to base line levels (approximately 5 cm) before initiation of the next monitoring campaign on February 21st (Figure 4-4).

As the environmental demand increased (ET_{ref}) (Figure 4-1), SWS decreased (Figure 4-4), leading to an increase in soil-to-air temperature differentials (T_s-T_a), (Figure 4-10). A five-fold increase in ET_{ref} was observed from winter to summer. During this time, SWS assessed on the day after rainfall simulation decreased by 9% on average; whereas, by the seventh day of monitoring, SWS decreased by 21% on average (Table 4-1). The daily SWS had a strong seasonal, treatment and season with treatment interaction effect ($P<0.001$, ANOVA). During the summer months of July and August, daily SWS at the end of 7 day monitoring periods after a rainfall simulation revealed a non significant difference between the control, low and medium treatments (Figure 4-4), indicating that only after the highest simulated rainfall treatment was input greater than the sum of E + T.

Table 4-1 The percent change in measured daily SWS between the summer and winter periods (comparing day 1, 7) for all rainfall simulation treatments.

	Control SWS[a] (cm)	**Low SWS[a] (cm)**	**Medium SWS[a] (cm)**	**High SWS[a] (cm)**
Dec day 1	7.8	9.4	11.3	16.1
July day 1	7.7	9.6	8.9	13.6
% change	-1.3%	2.1%	-21.2%	-15.5%
Dec day 7	7.4	8.5	9.6	12.8
July day 7	7.0	6.3	7.3	9.1
% change	-5.4%	-25.9%	-24.0%	-28.9%

[a] SWS values provided are the average of the three replicated plots.

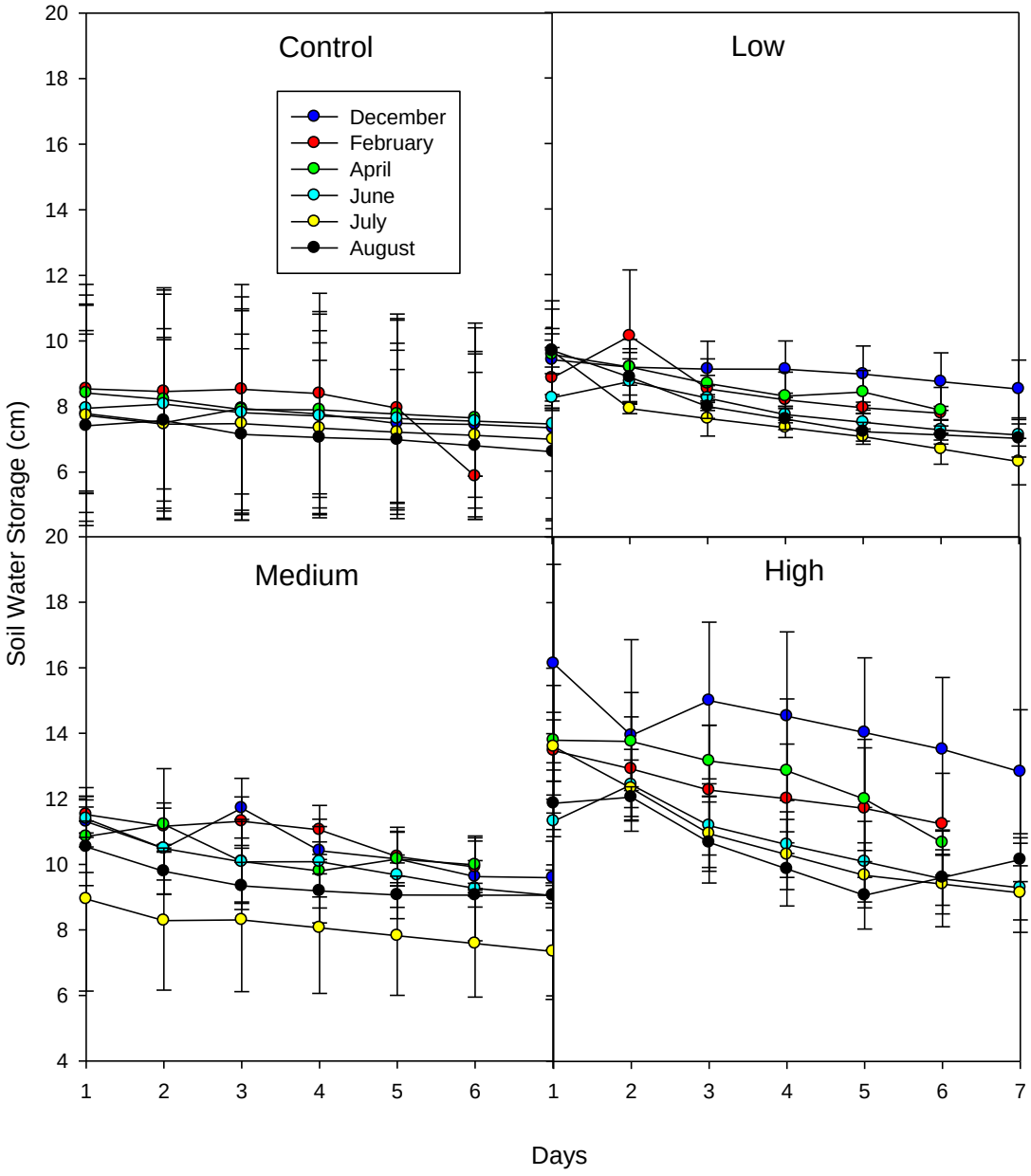

Figure 4-4 Daily SWS separated for each season and treatment for 7 day periods after rainfall simulations.

Daily Total SWS ANOVA Results

The daily total SWS results failed both the equal variance and the normality tests ($P<0.050$). The probability plot correlation coefficient (PPCC) was highly linear and

significant to accept the two-way ANOVA analysis (Cum. Freq. = 0.4028 (Residual) - 3.7589, r^2 = 0.9694, P<0.001, N = 539). A statistically significant treatment, time, and interaction between treatment and time effect occurred, (P<0.001). Treatment effect decreased as environmental demand increased. All treatments were significantly different for December, when the lowest ET_{ref} was recorded. In February and March, all treatments were significantly different, except for the low treatment and control plots. In June and August, all treatments were significantly different, except for medium versus control and low treatment; and low treatment versus control. In July (highest ET_{ref} period) only the high treatment versus control and low treatment, and medium treatment versus control were significantly different. Weekly ANOVA results for SWS were not assessed. Instead ΔS ($SWS_{last\ day}$-SWS_{day1}) results were selected for the ANOVA to add greater insight into the water partitioning dynamics.

Multiple Linear Regression Results for SWS

Daily SWS could be predicted from a linear combination of VPD, volumetric water content, SA, T and E (R^2 0.412, P<0.001, N = 539) (Table 4-3).Results showed that total SWS over five days could be predicted using I, VPD, and S_A as independent variables (R^2 0.857, P<0.001, N = 72) (Table 4-4). Backward stepwise regression results showed all other variable combinations were not significant.

ANOVA Results for Total ΔS

The ΔS ($SWS_{last\ day}$-SWS_{day1}) results passed the equal variance test, but failed normality (P<0.050). Inclusive of the extremes, the probability plot correlation coefficient (PPCC) was highly linear and significant to accept the two-way ANOVA analysis (Cum. Freq. = 0.6809(Residual) – 0.1882, r^2 = 0.9191, P<0.001, N = 72). A

statistically significant treatment and season effect occurred, (P<0.001). Also, a significant interaction between treatment and season (P = 0.008) occurred for ΔS. No significant difference occurred between the controls, the low or medium treatments for the seasons as reflected in the treatment months of Dec, Feb, Apr, Jun, Jul, and Aug. The ΔS for Dec was significantly different from all other months, (P=0.002 versus Feb versus all other months; P<0.001) due to the higher winter time ΔS associated with greater amounts of simulated rain entering storage (Figure 4-5).

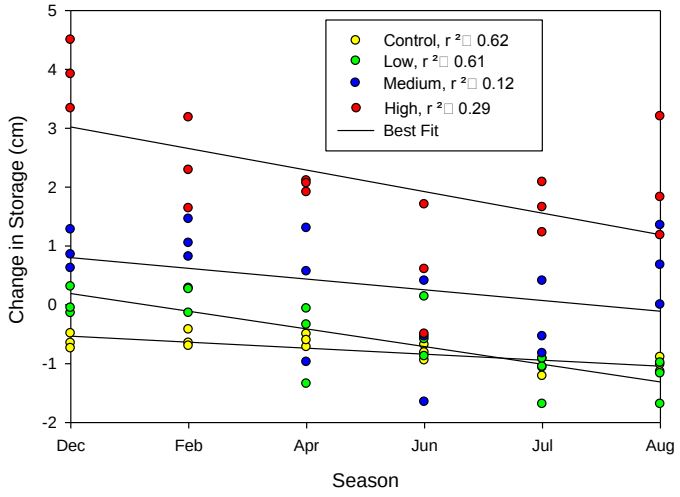

Figure 4-5 Change in soil water storage over time for all treatments.

Soil Moisture Redistribution

Baseline water content measurements were assessed before simulated rainfall events occurred and continued on a daily basis, typically for one to two weeks until water content values returned to baseline conditions (Figure 4-6). Simulated plus actual rainfall water that absorbed into upper soil layers was redistributed to lower layers and could be identified as a change in measured volumetric water content Θ_v as wetting fronts moved into the sensor domain. The soil water content was similar at all depths over time in the

control plots (CV = 0.159), with the exception of lower soil water content conditions in the 0-20 cm interval under the canopy. Soil water content and the oscillations in soil water content were higher at the 15 cm depth in all rainfall simulated plots. Separation in soil water with depth was clearest in the high rainfall simulated plots with values exceeding 0.30 m^3m^{-3} during the first day. Variability in depth of wetting was observed in the replicates with some plots (P10, P9, P4, and P3) showing water content changes (0.05, 0.09, 0.16, 0.02 m^3m^{-3}, respectively) at 45 cm depth after rainfall simulations; however, little response was noted at the 75 cm depth.

Evaporation and Ts-Ta

Evaporation totals for full 24-hour periods are shown separated by month in Figure 4-7 and separated by treatments in Figure 4-8. Evaporation during a 6-9 day dry down monitoring period is higher and extends longer for months with higher environmental demand and higher simulated rainfall amounts. However, evaporation rates were not directly proportional to treatments (i.e., high treatments did not exhibit rates two times higher than medium treatments, etc). No statistical difference was observed by day 3 when comparing days 3-7 during Jul (Figure 4-7) and no statistical difference was observed in evaporation based on treatment for days 2-7 during the winter (Figure 4-8). However, a statistical significant difference was observed ($P<0.05$) in evaporation when day 1 was compared with days 2-7, especially during the winter months, which led to a larger portion of the simulated rainfall remaining in storage during the winter than the summer period.

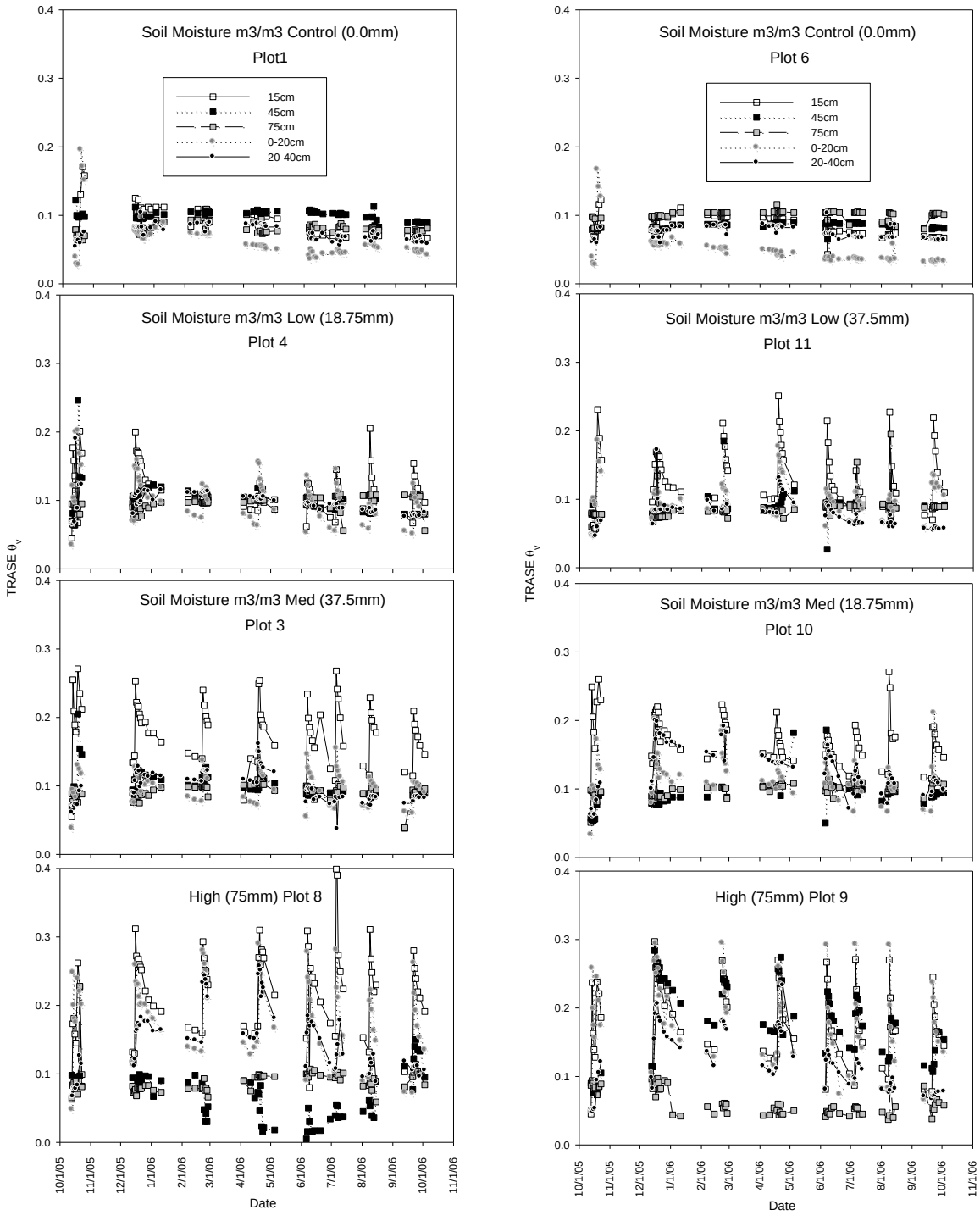

Figure 4-6 Daily TDR measurements from the TRASE unit from sensors installed under the plant canopy drip line at depths of 0-20 and 20-40 cm, and further away in the open inter-space (15, 45 and 75 cm) for all treatments.

Evaporation values in the controls were constant and lower (Figure 4-8), suggesting the three phases of evaporation appear to be best represented by day 1, day 2-5, and day 5-7. The daily evaporation (Figure 4-6) was totaled over six days following monthly rainfall simulation treatments in Table 4-2. The difference in the six day evaporation totals comparing Dec and Jul were significantly different based on rainfall simulation treatment ($P<0.05$). Also, evaporation increased with treatment for all summer months (Jun, Jul, and Aug) exceeding all other monthly evaporation totals with the exception of the low treatment in Feb.

Table 4-2 Daily Evaporation (cm) Totaled Over 6 Days Following a Rainfall Simulation Treatment.

Rain Treatment	Dec	Feb	Apr	Jun	July	Aug
Control	0.31±0.10	0.39±0.15	0.60±0.10	0.65±0.09	0.77±0.10	0.97±0.26
Low	1.84±0.16	1.58±0.22	2.73±0.59	2.25±0.36	3.17±0.26	3.16±0.96
Medium	2.22±0.12	2.32±0.20	3.29±0.92	4.13±1.34	4.12±0.53	2.94±0.73
High	2.90±0.07	3.93±0.51	5.56±0.76	6.06±0.43	6.25±0.50	5.10±1.54

Weekly Evaporation ANOVA Results

Evaporation totaled over the monitoring period passed the equal variance test ($P=0.050$), but did not pass the normality test (Shapiro-Wilk) ($P<0.050$). The Normal Probability Plot (NPP) in Figure 4-9 showed the normality test violation was not due to distributional assumptions, but instead was caused by a few extreme values typical with very large data sets (Fernandez, 2009). The Normality test was accepted ($P=0.058$) ($W=0.962$) when the extremes identified were excluded. These values included the four highest values (7.096, 7.089, 7.015 and 6.959 cm) and the seven lowest values (from 0.290 to 0.675 cm).

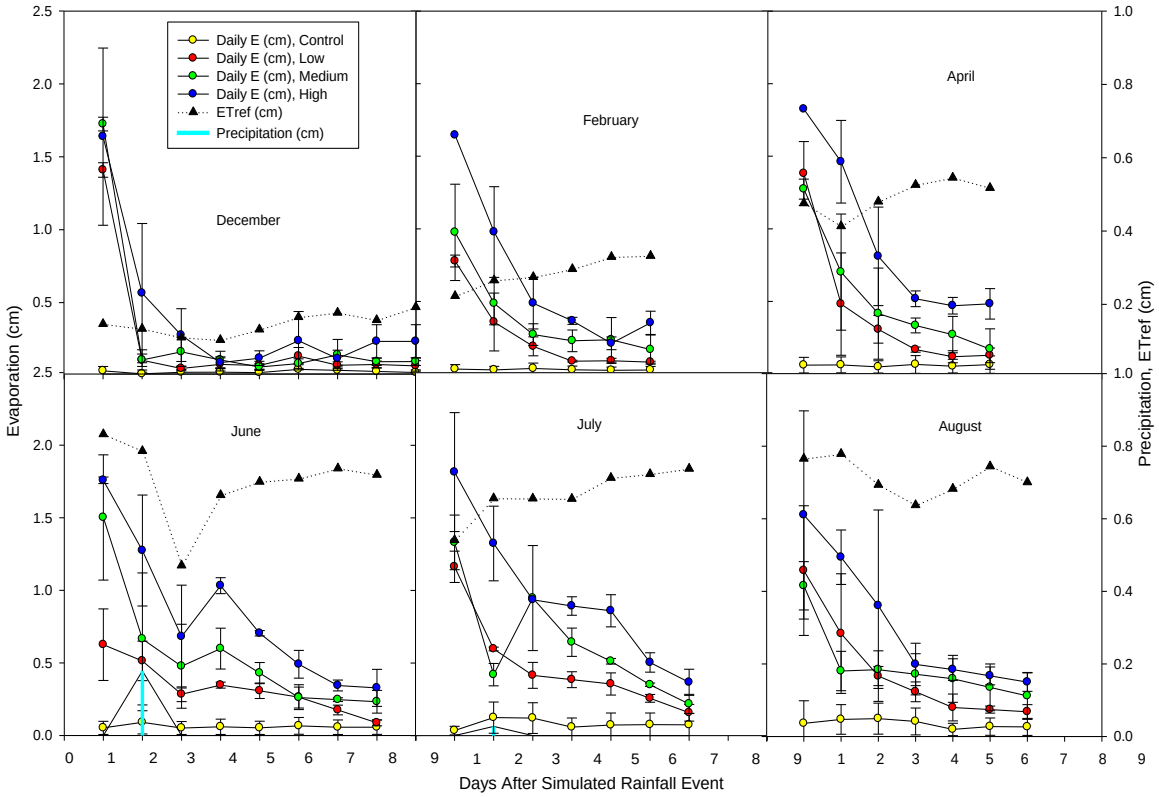

Figure 4-7 Daily evaporation (24 hour totals) scaled to the plot level after rainfall simulations, along with ET_{ref} and actual precipitation.

These exceptionally small and high weekly evaporation values were associated with either the highest treatments during summer months or winter controls. Specifically, all Dec and Feb controls, plus two controls in Apr, one high treatment in Jun and Aug, and two in Jul were problematic. Not excluding the extremes, the probability plot correlation coefficient (PPCC) showed the linearity of the probability plot, or the distribution fit of the data was significant enough ($r^2 = 0.9511$, $P<0.001$, $N = 72$) to accept the two-way ANOVA analysis without exclusion of any data (Fernandez, 2009). The lognormal PPCC was also calculated but did not improve the distribution model fit ($r^2 = 0.9230$, $P<0.001$).

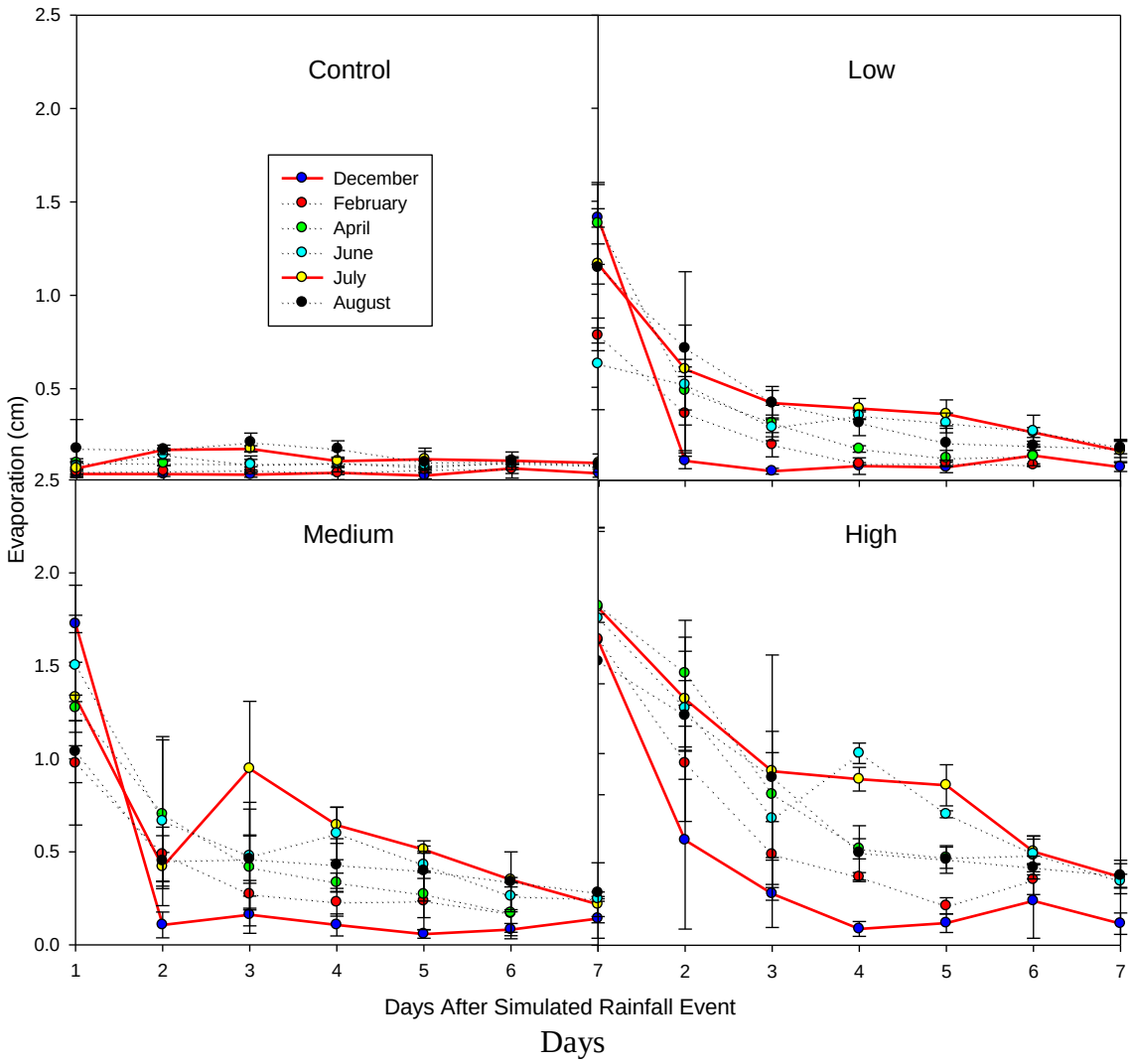

Figure 4-8 Daily evaporation scaled to the plot level by season separated by treatment (0, 15, 30, 7.5cm) for 7 day periods following rainfall simulations.

A statistically significant treatment effect occurred for all total evaporation comparisons ($P<0.001$). Additionally, a time effect occurred ($P<0.001$), but no statistically significant interaction was observed between treatment and time on total E ($P=0.100$). The effect of season on total E was significantly different for all summer months (Jun, Jul, and Aug) when compared to the winter months (Dec, Feb), ($P<0.001$),

while all other seasonal comparisons were not significant. Also, Apr was significantly different from Aug at the P<0.001 level. No significant difference in evaporation occurred between the controls over time (Dec, Feb, Aug, Jun, Jul, and Aug).

Total evaporation for the low treatments were only significantly different for one month (Jun vs Feb) (P<0.001), all other comparisons among months were not significantly different. The medium treatment was only significantly different for all inter-comparisons between Jun, Jul, Dec, and Feb. The high treatment, just as the medium treatment, had the same significant interaction results with one additional interaction (Aug vs Dec) (P =0.003). In Dec, all treatments (control, low, med, and high) were significantly different (P<0.001) from one another with two exceptions (med vs high, and med vs low). In Feb and Apr the same was true except only med vs. low were not significantly different from each other.

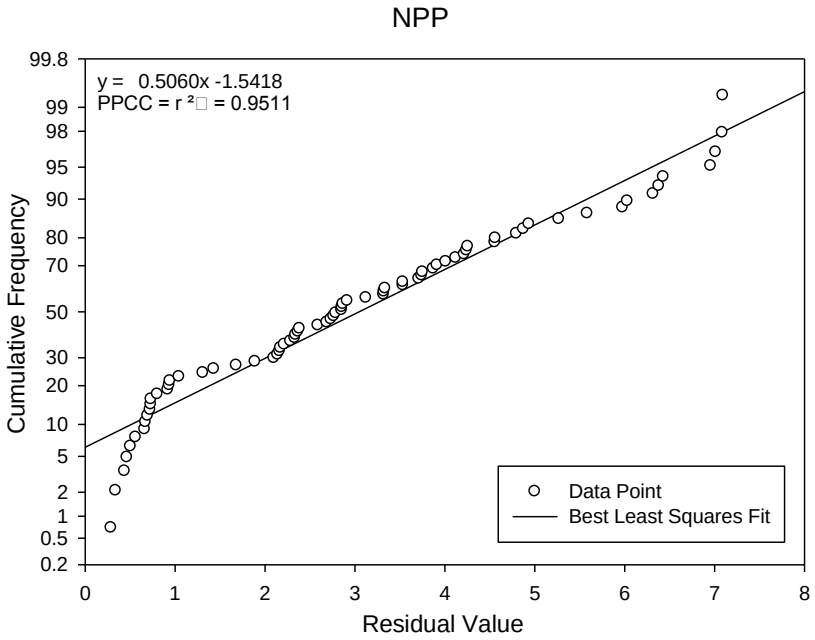

Figure 4-9 A Normal Probability Plot (NPP) for total evaporation.

In all three summer months (Jun, Jul and Aug) total E for all treatments were found to be significantly different ($P<0.001$) from each other, except for medium vs low in Aug.

ANOVA Results for Daily Total E

The daily total evaporation results failed both the equal variance and normality tests ($P<0.050$). The probability plot correlation coefficient (PPCC) was linear (Cum. Freq. = -0.7805(Residual) – 1.9396, $r^2 = 0.7641$, N = 539). A statistically significant treatment and time effect occurred ($P<0.001$); however, no significant interaction between treatment and time ($P = 0.123$) was observed.

Multiple Linear Regression Results for Daily E

Daily E could be predicted by a linear combination of daily ET_{ref}, Soil Area, Ts-Ta noon, SWS and the surface water content, ($R^2 = 0.526$, $P<0.001$). Including additional variables such as season did not improve the multi-linear relationship ($R^2 = 0.526$) to justify its addition. A relationship was found for daily E with just daily T and storage (cm) ($R^2 = 0.486$, $P<0.001$) (Table 4-3).

Multiple Linear Regression Results for Five Day Total E

A multiple linear regression model could account for 87% of the variability in the 5 day evaporation totals with only ET_{ref}, I, and the SA ($E = -6.300 + (0.560\ ET_{ref}) + (0.524I) + (0.527\ S_A)$, adjusted R^2 0.865, $P<0.001$). Without knowledge of the soil area, the model adjusted $R^2 = 0.818$ ($P<0.001$) (Table 4-4).

Table 4-3 Multiple Linear Regression Equations based on results of Daily Parameter Estimates.

Daily Parameter Multi-linear Regression Equation	R^2	P	Total VIF
E = 0.286 + (0.767ETref) – (0.0790SA) – (0.00822Ts-Ta) + (0.0348SWS) + (3.088SVWC)	0.526	<0.001	7.84
E = -0.490+ (5.104T) + (0.0848SWS)	0.486	<0.001	2.00
T = -0.0235 + (0.0372ETref) + (0.00853BCA) + (0.000213Ts-Ta) + (0.00127SWS) - (0.0105SVWC)	0.417	<0.001	7.84
SWS = 7.232 – (0.593VPD) + (13.277SVWC) + (0.103SA) + (18.923T) + (1.091E)	0.412	<0.001	8.06
ET_{ref} = 0.0692 + (1.934P) – (0.0110Tc-Ta) + (0.175VPD)	0.750	<0.001	3.04
T_s-$T_{a,noon}$ = 1.047 – (0.820TRMT)+(2.036Season)-(2.640E)+(2.367BCA)-(17.262SVWC)	0.551	<0.001	8.80

E is daily evaporation (cm), ETref is the daily reference evapotranspiration (cm), T is the daily whole plant canopy transpiration (cm), Ts-Ta is the soil to air temperature differential (^oC), Tc-Ta is the plant to air temperature differential (^oC), BCA is the plant basal canopy area (cm^2), SA is the soil area (total plot area – BCA, cm^2), P is the daily total precipitation (cm), SWS is the daily soil water storage, VPD is the total vapor pressure deficite (kPa), and SVWC is the volumetric water content at the 0-6 cm surface.

Table 4-4 Multiple Linear Regression Equations based on results of Five Day Total Parameter Estimates.

Five day period Total Parameter Multi-linear Regression Equation	R^2	P	Total VIF
E = -6.300 + (0.560ETref) + (0.524I) + (0.527SA)	0.870	<0.001	3.12
E = -0.384 + (0.560ETref) + (0.514I)	0.823	<0.001	2.00
E = -17.384 + (0.436VPD) + (3.275LAI) + (1.128SA)	0.670	<0.001	3.35
T = 0.432 + (0.0384VPD) – (0.0366PA)	0.397	<0.001	2.00
SWS = -10.837 + (3.641I) – (2.333VPD) + (4.360SA)	0.857	<0.001	3.12

E is the total evaporation (cm), ETref is the total reference evapotranspiration (cm), I is the total simulated rainfall amount (cm), VPD is the total vapor pressure deficite (kPa), LAI is the leaf area index (cm^2 cm^{-2}), T is the total whole plant canopy transpiration (cm), BCA is the plant basal canopy area (cm^2), SA is the soil area (total plot area – BCA, cm^2), PA is 1.4 times the BCA (cm^2), and SWS is the total soil water storage.

Ts-Ta Measurement Results

All measured temperature differentials between the soil surface and air temperature (T_s-T_a) after a simulated rainfall treatment are shown in Figure 4-10. As daily soil moisture in storage increased, with increasing rainfall simulation amounts, lower soil-to-air temperature differentials occurred, especially during summer months

when environmental demand was greater, (Figure 4-10). The T_s-T_a was higher for controls than treated plots (3.4, 4.0, and 7.3 ^oC for low, medium and high plots, respectively) and all plots had higher T_s-T_a differentials during summer months (5.5, 6.5, 5.8, 2.8 ^oC for control, low, medium and high plots, respectively). All control T_s-T_a differentials were above the T_s-T_a zero line after Dec and all T_s-T_a differentials for high treatment plots were below the T_s-T_a zero line for the first day after a rainfall simulation for all months except Feb.

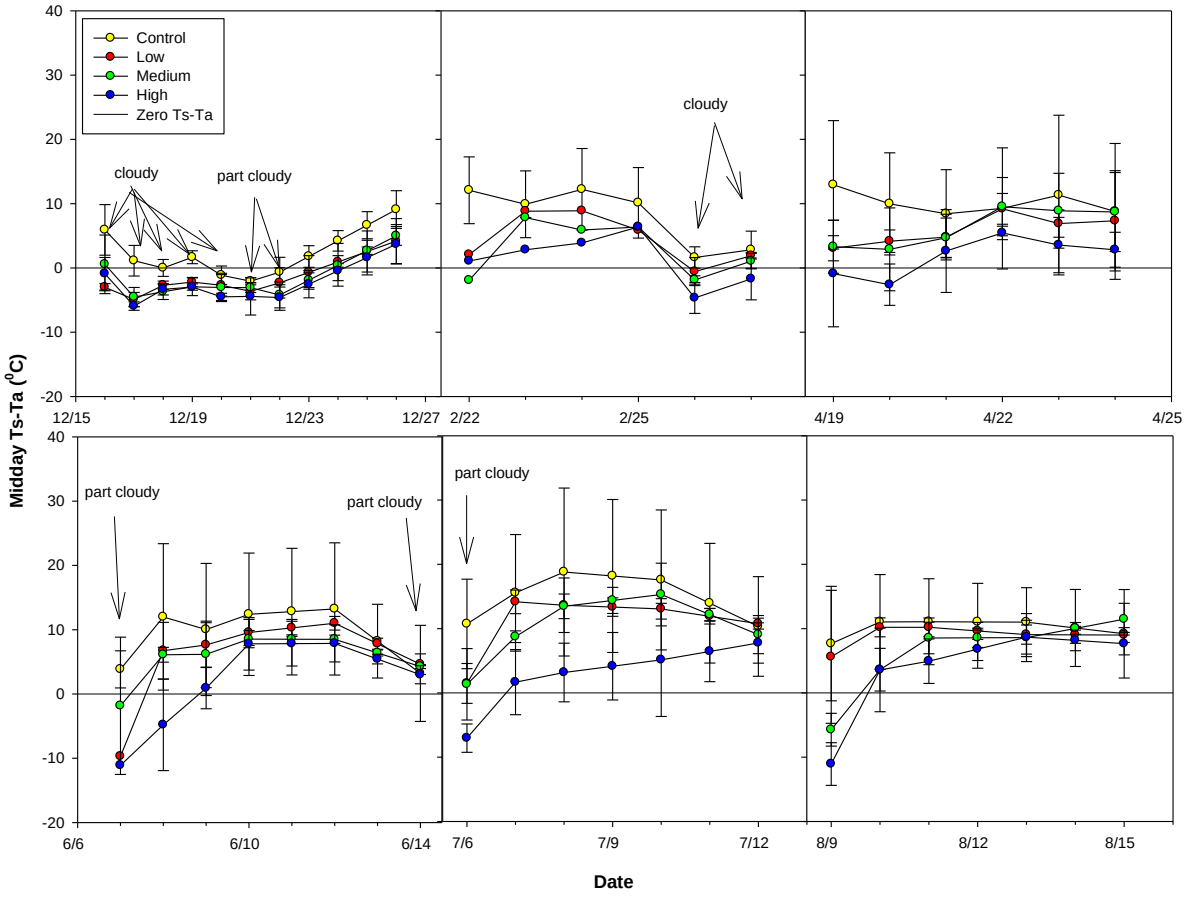

Figure 4-10 Seasonal and treatment trends of midday temperature differentials between the soil surface and ambient air temperature after simulated rainfall events.

In Feb, the measurement period ended by day 6 with a sudden drop in all T_s-T_a values that coincided with observable cloud cover and lower environmental demand.

The daily mid day T_s-T_a results failed both the equal variance test and the normality test ($P<0.050$). The probability plot correlation coefficient (PPCC) was highly linear and significant to accept the two-way ANOVA analysis (Cum. Freq. = 0.1322(Residual) -0.7734, $r^2 = 0.9945$, $P<0.001$, $N = 539$). A statistically significant treatment and season effect occurred ($P<0.001$) with the mid day soil to air differentials (T_s-T_a). Also, a statistically significant interaction between treatment and season was found, ($P<0.001$). When each month (Dec, Feb, Apr, Jun, Jul, Aug) was compared, the mid day T_s-T_a controls were significantly different (ANOVA, $P=<0.001$) than all other rainfall simulations. Specifically, the least squares means for T_s-T_a treatment were 13.053, 5.875, 5.133, and 1.698 for the control, low, medium and high plots respectively. However beginning in Apr and lasting until Aug T_s-T_a values for the highest treatment was significantly different than the medium and low treatments, with significant p-values ranging from ($P<0.001$ to 0.012).

Transpiration and Tc-Ta

Weekly transpiration totals are shown in Figure 4-13 and in Table A-5 for each treatment while daily transpiration totals are shown in Figure 4-14. Transpiration was the smallest (4.5%) component of the overall water budget. Transpiration varied little during the entire monitoring period irrespective of the simulated rainfall amounts applied; no significant differences in weekly T were observed between the controls or any treatment. ANOVA results showed Dec was significantly different from the summer values

($P<0.001$). A small increase in T_c-T_a was observed during Jul and Aug (Figure 4-11). T_c-T_a varied little over time or between treatments, oscillating near the zero line (Figure 4-11). The similarity of the canopy temperature relative to the ambient temperature observed was most likely linked to *Larrea tridentata's* ability to tightly regulate stomatal conductance, thus effectively controlling transpiration and evaporative cooling. ANOVA results of daily T showed that only during summer months was there a statistically significant ($P<0.001$) difference observed between treated and control plots.

ANOVA results for weekly T passed both the equal variance and normality tests (Shapiro-Wilk) ($P<0.050$). Although no treatment effect ($P = 0.115$) or interaction between treatment and time was observed ($P=0.488$), a statistically significant time effect occurred ($P<0.001$). Treatment means were very close to one another, with the control means closely matching the high treatment means (0.171, 0.110, 0.144, and 0.178 for control, low, medium and high plots, respectively). Weekly T results for summer months were found to be higher and significantly different than Dec ($P<0.001$). Furthermore, 38% of the variability in the weekly T estimates could be determined by a combination of VPD and PA ($R^2 = 0.38$, $P<0.001$).

ANOVA results for daily total T failed both the equal variance and normality tests ($P<0.050$). The probability plot correlation coefficient (PPCC) was highly linear and significant to accept the two-way ANOVA analysis (Cum. Freq. = -1.1698(Residual) – 59.4619, $r^2 = 0.9286$, $P<0.001$, $N = 539$). A statistically significant treatment, time, and interaction between treatment and time effect occurred ($P<0.001$). Only during the summer months was a significant ($P<0.001$) difference observed between simulated rain and control plots. Similarly with weekly T, the daily T treatment means were very close

to one another, with the control means (0.0241) closely matching the high treatment means (0.0244). Daily T totals for all three summer months were found to be significantly different than Dec ($P<0.001$).

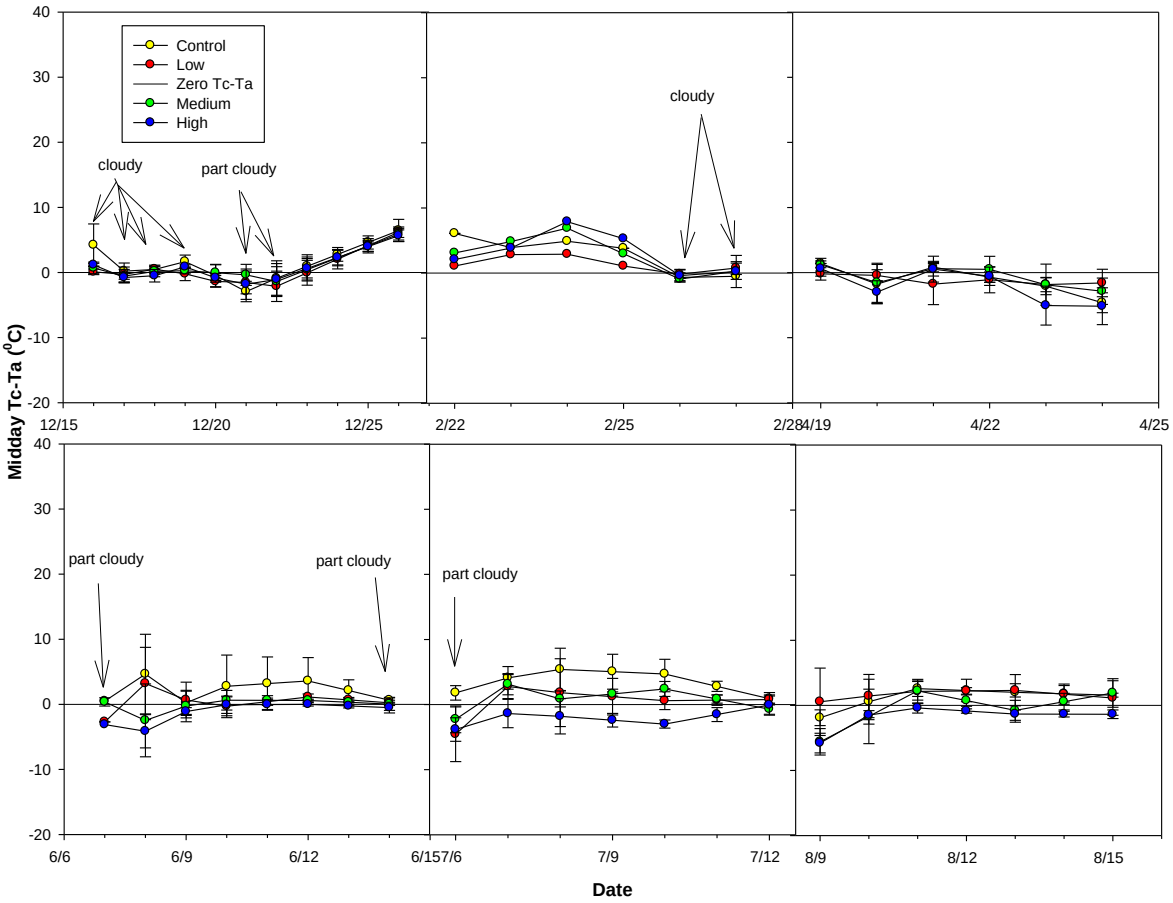

Figure 4-11 Midday temperature differentials between the canopy surface and ambient air temperature for 7 day periods after simulated rainfall events based on season and treatment.

The daily mid day T_c-T_a results passed the equal variance test but failed the normality test ($P<0.050$). The probability plot correlation coefficient (PPCC) was highly linear and significant to accept the two-way ANOVA analysis (Cum. Freq. = 0.3415(Residual) -0.2155, $r^2 = 0.9827$, $P<0.001$, $N = 539$). A statistically significant

treatment, time, and interaction between treatment and time effect occurred ($P<0.001$). Similarly to daily T ANOVA results, treated T_c-T_a plots were significantly different from non-treated plots only during the summer months. In July this significant difference occurred in all replicates $P<0.001$; however, in June and Aug only two of three controls were significantly different ($P<0.001$).

Water Balance Closure

Water balance closure was assessed by evaluating input parameters ($I+P-\Delta S$) and output parameters ($E+T$). Measured precipitation events (Table A-6) that occurred during the Apr, Jun, Jul and Aug water balance closures were included for each treatment plot. The coefficient of variation associated with the water balance was small for all treatments with a very narrow range 0.097 to 0.127 (Table 4-5).

A water balance closure of 100.8% ± 12.2% was obtained for all treatment sites and all available months (Dec, Feb, Apr, Jun, Jul, Aug) (Figure 4-12). The minimum closure estimate of 79% was found for a control treatment plot during Dec and the maximum closure estimate of 134% was found for a low treatment during the Apr rainfall simulation run. Monthly, closures averaged; 105.9%, 98.4%, 96.4%, 104.7%, 110.1%, and 103.8% (Dec, Feb, Apr, Jun, Jul, Aug) for all twelve plots whereas the annual closure for each treatment was, 99.6%, 108.9%, 99.5%, 103.1% for control, low, medium and high, respectively.

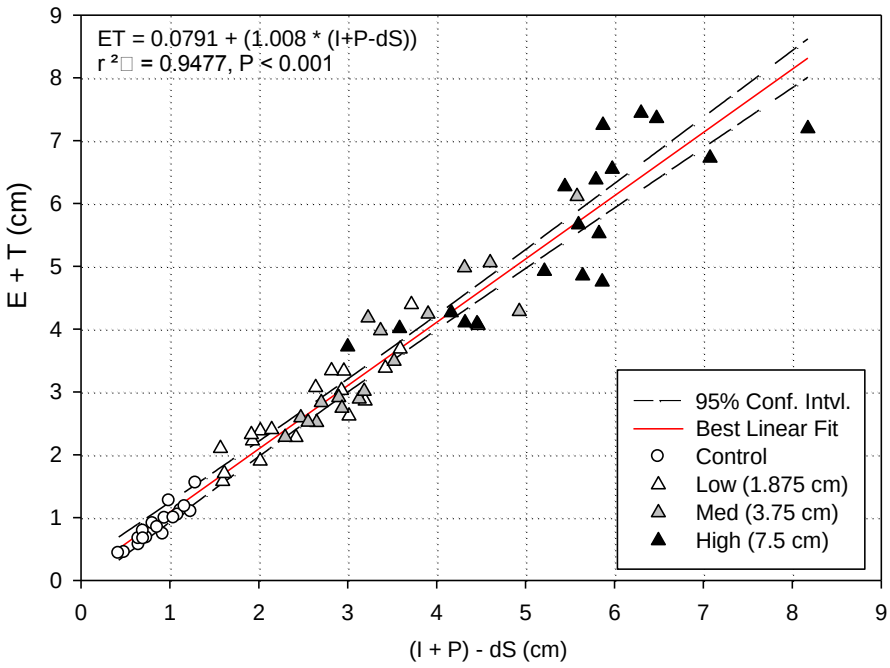

Figure 4-12 Water balance closure assessed by evaluating input (I+P-ΔS) vs output (E+T) parameters.

Table 4-5 Water Balance Closure Estimates and Statistics. A value of 1.00 would constitute perfect closure.

Treatment	Mean Closure	SD	CV	RMSE
Control	0.996	0.1201	0.1206	0.0858
Low	1.089	0.1148	0.1054	0.1001
Medium	0.995	0.0966	0.0971	0.1056
High	1.031	0.1310	0.1271	0.1207
Season				
December 16-26	1.059	0.1498	0.1414	0.0962
Feb 22-28	0.984	0.0773	0.0786	0.0990
April 19-24	0.969	0.1042	0.1075	0.1040
June 7-14	1.047	0.1226	0.1171	0.1090
July 5-12	1.101	0.1059	0.0962	0.1066
August 9-15	1.039	0.1375	0.1324	0.1048

Water Partitioning

Water balance totals for each treatment (E, T, ΔS, I, and P) for the full monitoring period are shown in Figure 4-13. For all treatments and time periods, transpiration was a minor component and evaporation dominated each system. Evaporation on average accounted for 90% of the water loss from the total input (actual + simulated rain for all plots during the entire monitoring period). Transpiration on average only accounted for 4.5% of the total input (Figure 4-13). The evaporation portion of the water balance on average was 33% lower for winter months (72%) than for summer months (105%). During the winter (Dec) 72.04% of total input was lost via E, 1.05% from T and 27% went to storage. During the summer (Jun-Aug) 104.74% of the water balance was lost through E and 6.14% to T (100% lost from input and 10.88% lost from storage) (Table 4-6). The water balance monthly totals for each treatment are shown in Table 4-7.

The evaporation results for this study, especially for the controls, were largely from SWS originating from the October monsoonal season. The two largest precipitation events (12.45 and 35.44 mm) occurred in October and accounted for 60% of the 12 month total precipitation. If the experiment had been extended to the next monsoon season, an increase in soil water recharge and SWS would be required to offset E and T losses for the controls during the subsequent spring summer period. Evaporation exceeded the simulated rainfall amounts in the low and medium treatments during the summer months, whereas in the high treatment evaporation approached the simulated rainfall amounts during Jun and Jul but never exceeded the total amounts (Figure 4-13). Storage depletion occurred in all plots except the high treatment where greater storage

occurred during winter months (Figure 4-14). Only during Dec in the high treatment did a positive change in SWS have the same magnitude as evaporation.

Table 4-6 Water Balance Component Totals by Month

Month	Total E (cm)	Total T (cm)	Total I+P (cm)	%E loss	%T loss
December	28.36	0.41	39.38	72.04	1.05
February	27.09	1.60	39.38	68.79	4.07
April	35.74	1.32	41.61	85.88	3.18
June	43.26	2.51	41.51	104.21	6.04
July	45.95	2.50	39.68	115.80	6.29
August	38.98	2.51	41.20	94.60	6.08

Where, I is the total rain simulation input, P is the total precipitation input, %E and is the percentage of Total I+P loss through evaporation, and %T is the percentage of Total I+P loss through transpiration.

Table 4-7 Water Balance Component Totals by Month for each Treatment

Treatment - Month	Total E (cm)	Total T (cm)	Total I+P (cm)	%E loss	%T loss
Control - December	1.58	0.10	0.00	0.00	0.00
Control - February	1.30	0.58	0.00	0.00	0.00
Control - April	1.77	0.53	0.61	289.87%	86.64%
Control - June	2.38	0.83	0.53	446.61%	155.80%
Control - July	2.62	0.49	0.08	3439.50%	648.79%
Control - August	3.17	0.54	0.46	692.47%	118.54%
Low - December	6.65	0.05	5.63	118.28%	0.97%
Low - February	5.01	0.17	5.63	89.07%	3.09%
Low - April	7.76	0.30	6.23	124.41%	4.84%
Low - June	7.81	0.61	6.16	126.81%	9.92%
Low - July	9.98	0.37	5.70	175.12%	6.56%
Low - August	9.40	0.47	6.08	154.50%	7.76%
Medium - December	8.32	0.07	11.25	73.95%	0.65%
Medium - February	7.60	0.25	11.25	67.56%	2.25%
Medium - April	9.51	0.30	11.66	81.56%	2.61%
Medium - June	13.23	0.43	11.78	112.31%	3.67%
Medium - July	13.26	0.76	11.33	117.06%	6.68%
Medium - August	10.18	0.76	11.71	86.95%	6.53%
High - December	11.81	0.19	22.50	52.48%	0.84%
High - February	13.18	0.60	22.50	58.58%	2.66%
High - April	16.71	0.19	23.11	72.29%	0.81%
High - June	19.83	0.64	23.03	86.10%	2.76%
High - July	20.09	0.87	22.58	88.98%	3.86%
High - August	16.24	0.73	22.96	70.72%	3.17%

Where, I is the total rain simulation input, P is the total precipitation input, %E and is the percentage of Total I+P loss through evaporation, and %T is the percentage of Total I+P loss through transpiration.

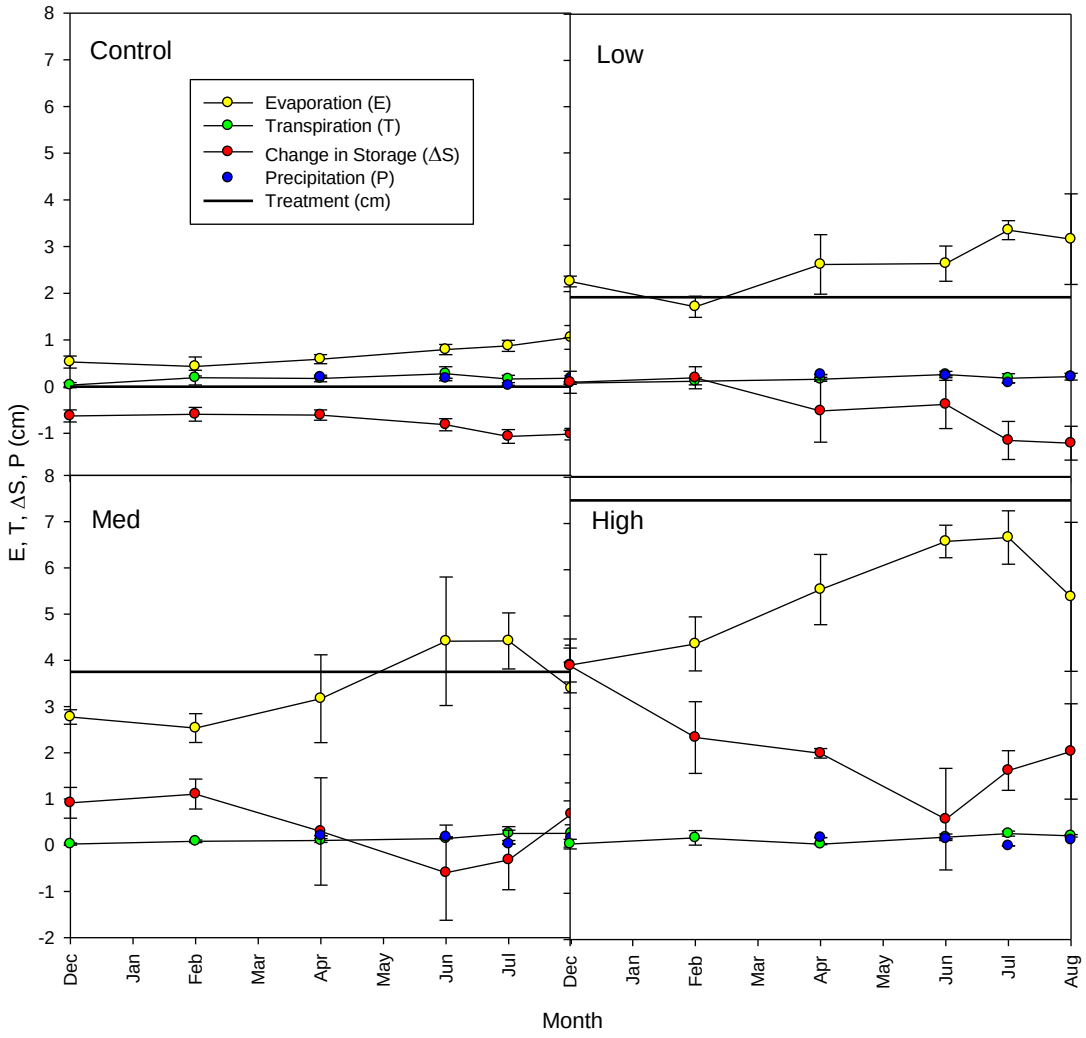

Figure 4-13 Total evaporation (E), transpiration (T), precipitation (P), input treatment (I), and change in soil water storage (ΔS) during six rainfall simulation events, separated by treatment.

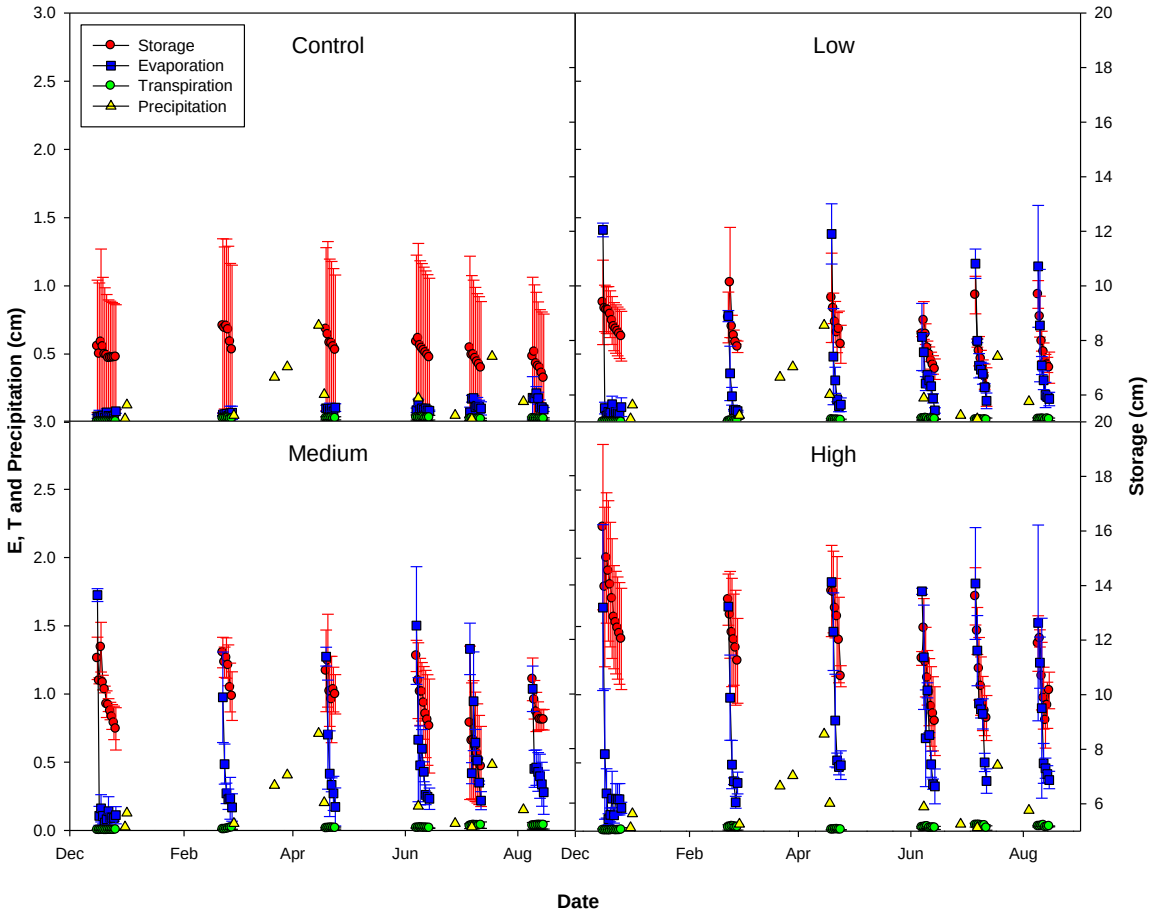

Figure 4-14 Daily evaporation (E), transpiration (T), precipitation (P) and soil water storage (SWS) during six rainfall simulation events, separated by treatment.

CHAPTER V

DISCUSSION

The safe containment and isolation of radioactive waste is of major concern in the United States, especially with recent interest in nuclear energy technology as a way of reducing carbon emissions, coal and oil usage, while boosting U.S. energy production. In the arid southwest, long term natural covers for waste containment have become attractive due to their high ET rates, deep unsaturated soils, and isolation from populated areas (Reith and Thomson, 1992). The water balance status of these hydrologic systems ultimately determines the eventual magnitude and direction of water flux after storm events.

Results from this study clearly demonstrated that evaporation dominated the water balance in rainfall simulated *larrea tridentata* plots located within the Mojave Desert. Evaporation up-scaled from chamber flux measurements to the plot level accounted for an average of 90% of water loss from total natural precipitation and simulated rainfall treatments. Transpiration measured from stem flow data and normalized by leaf area only accounted for 4.5% f water loss on average. *Larrea tridentata* is the dominant species in much of the Mojave, Sonoran, and Chihuahuan deserts of western North America and is typically found in monotypic open stands (Mabry et al. 1977; Wythers et al. 1999). The root systems of these shrubs are capable of extracting soil water to levels lower than required for most other plants to become established, and have been shown living in areas with water potentials as low as -120 bars (Mabry et al. 1977). Wythers et al. (1999) and Ben-Asher et al (1983) also showed evaporation from arid desert shrub land soils to be the largest component of the water balance behind precipitation. Nichols (1987) showed

the cumulative and mean annual actual evaporation was estimated to account for 97% of the cumulative precipitation over a 16 year period for a desert shrub land study near Beatty, NV. Sammis and Gay (1979) found a ratio of T to ET of 7.0 for *Larrea Tridentata* within the Sonora desert.

In this study, during the summer months of Jul and Aug, daily SWS at the end of 7 day monitoring periods after a rainfall simulation revealed non significant differences between the control, low and medium treatments, indicating that only after the highest simulated rainfall treatment (7.5 cm) was input greater than the sum of E + T leading to significantly higher SWS values ($P<0.001$). The water balance results also showed that evaporation exceeded the low and medium simulated rainfall amounts during the summer months. Cumulative five day totals of actual evaporation was found to be significantly dependent ($R^2 = 0.870$, $P<0.001$) and positively correlated with ET_{ref}, I, and SA, ($E = -6.300+(0.560ET_{ref})+(0.524I)+(0.527SA)$, VIF = 3.12). However, day-to-day variability in E was significantly greater and only 52.6% of the variation could be accounted for via ET_{ref}, SA, T_s-T_a, SWS, and surface volumetric water content ($P<0.001$, individual VIF < 2 and total VIF = 7.84). The multiple regression results suggest actual evaporation (five day interval) for all seasons (winter, summer, spring and fall) could be accurately predicted from coupling ET_{ref} and precipitation measured from a weather station with knowledge of the total soil area (SA) for *larrea tridentata* dominant ecosystems within the Mojave Desert. However, the relationship between plant cover and bare soil is expected to change over large biogeographic regions of the world due to global climate change (Schwinning et al. 2005a). Arid regions are most susceptible to change due to their tight coupling between soil moisture and vegetative growth and diversity

(Schwinning and Ehleringer, 2001; Knapp et al., 2002). If precipitation increases over time leading to greater soil moisture storage, an increase in existing plant canopy size could occur, increasing plant cover and productivity, and potentially increasing invasive species growth and diversity.

The results from this study suggest that both the timing and magnitude of precipitation events are critical for determining eventual water balance partitioning. ANOVA results showed a statistically significant treatment (magnitude of simulated rainfall), time, and interaction between treatment and time effect occurred ($P<0.001$) for daily T totals, mid day T_c-T_a, daily SWS and mid day T_s-T_a. Also, a statistically significant treatment and time effect occurred ($P<0.001$) for weekly total change in storage ($SWS_{day,last}$-SWS_{day1}), daily E totals, and weekly totals of E. Temporal variation in precipitation favored a 33% increase in the evaporative portion of the water balance on average for summer months (105%) than for winter months (72%) and a six fold increase in transpiration (6.1% and 1.0% for summer and winter, respectively) on average. Water in storage increased by 27% during winter and decreased by 11% during summer, on average. Such results would suggest that winter time events would have the highest capacity to increase water availability for vegetation prior to spring green up. However, *Larrea tridentada* is an evergreen shrub and the added wintertime soil moisture would probably be most helpful for shallower rooted annuals, such as grasses.

Rainfall simulations were imposed at 1.5, 3, and 6 times the local 71 year average of 10 cm (Gorelow, 2008) between October 2005 and 2006 monsoon seasons. As the magnitude of precipitation increased, evaporation changed from exceeding precipitation for all months (control), to exceeding precipitation only during summer months (low and

medium), to finally only approaching precipitation amounts during the summer (high). Storage depletion occurred in all plots except for the high treatment plots where greater storage occurred during winter months. However had the experiment continued through the next monsoon season, soil moisture recharge would have increased, balancing or exceeding E for the controls. Only during Dec in the high treatment did a positive change in storage have the same magnitude as evaporation. However, if future regional precipitation patterns follow predicted cycles (Figure 2-1) (IPCC, 2007; Karl et al., 2008), such as longer droughts followed by a larger occurrence of heavy precipitation events, the timing and magnitude of these events will be key for assessing the performance of soil vegetative covers. The timing and magnitude of precipitation pulses drives key ecological processes, associated with plants and soil microbiota (Loik, et al. 2004), differential utilization by herbaceous perennial species out competing woody perennials (Ehleringer et al., 1991), and phenological development and timing of new root growth (Devitt et al., 1997). Schwinning et al. (2005b) investigated the effects of winter and summer time drought using rainout shelters found that the longer occurrence of summer time drought favored deep rooted woody species in the ecosystem, and the shallower rooted species either died or were forced into dormancy.

At each simulated rainfall level, the amount of soil moisture redistribution was greater under lower environmental demand, creating a seasonal change in water storage. For the highest rainfall treatment, soil water storage by Aug was 23% lower on average than the previous Dec and ANOVA results revealed a strong treatment and seasonal effect on soil water storage ($P<0.001$). From Dec to Jul a fivefold increase in ET_{ref} was associated with a 5%, 26%, 24% and 29% average decrease in SWS for the control, low,

medium, and high treatments, respectively. With weekly total SWS, 87% of the variability could be predicted by a linear combination of the simulated rainfall treatment amount (I), the vapor pressure deficit (VPD), and the soil area SA. Where SA is the area outside of the influence of the plant (1.4 times plant canopy), where nonrandom processes are known to dominate and hydraulic conductivity $K(\psi)$ is spatially correlated with the desert shrub (Caldwell et al., 2008). Daily total SWS was shown to be significantly correlated with VPD, SVWC, SA, T and E ($R^2 = 0.412$, $P<0.001$, $N = 539$).

Although transpiration was only a minor component in the simulated rainfall treatments, spatial patterns of soil moisture emerged with greater redistribution occurring at distances farther from the plant, suggesting a region of lower plant water extraction. This region was equipped with TDR probes placed 189 ± 23 cm away from the plant base (Figure 3-5a) and 101.5 ± 49.5 cm outside the canopy drip lines. Also, all probes were outside the region influenced by the plant, varying from 14 to 155cm based on the size of the shrub canopy. The soil water content was similar at all depths over time in the control plots (Mean = 0.090, CV = 0.159), with the exception of the 0-20 cm interval under the canopy (Mean = 0.062, CV = 0.456). The lowest water content values measured with the TDR were found at the 0-20 cm interval closest to the plant during summer months for the control, low, and medium treatment plots. Whereas, with the exception of TDR measurements at the 15 cm interval at plot 8 (high treatment) in July with two values approaching 0.40 $cm^3\ cm^{-3}$, the highest values (0.30 $cm^3\ cm^{-3}$) were associated with the high treatment during winter at 15 cm depth, at the furthest location from the plant. Soil water content and oscillations in soil water content were highest at the 15 cm depth in all rain simulation plots, especially for day 1 in the high treatment plots. Plots with the

highest treatments also had the sharpest decline in SWS and the highest rates of measured evaporation flux.

Transpiration was the smallest component of the budget overall. Irrespective of the rainfall simulation treatments imposed, no significant difference was found between the controls and or any treatment plot ($P>0.05$). Treatment means were very similar (0.171, 0.110, 0,144 and 0.178 for control, low, medium and high treatments, respectively). However, a statistically significant time effect occurred ($P<0.001$). Daily T was positively correlated with greater ET_{ref}, larger canopies (BCA), higher Ts-Ta, greater SWS and lower soil moisture in the upper 6 cm of the soil ($R^2 = 0.42$, $P<0.001$). Seasonally, surface volumetric water content was lower when ET_{ref} was higher, due to greater surface soil water evaporation. ANOVA results for weekly T showed Dec was significantly different from the summer months ($P<0.001$). Additionally, a small increase in T_c-T_a was observed during the summer months of Jul and Aug. All plots had higher average T_s-T_a differentials during summer months than winter months (5.5, 6.5, 5.8, and 2.8 ^oC for control, low, medium, and high treatments, respectively). Additionally, T_s-T_a was positively correlated with season, larger canopies (BCA), and negatively correlated with rain simulation treatment, actual bare soil evaporation, and greater surface soil moisture. For weekly total T, only 39.7% of the variability could be described by a VPD and PA combination ($P<0.001$). However, this study was only conducted over twelve months. At the end of the study, treated plants were observed to have increased greenness and leaves were observed to be more succulent than non treated plants, suggesting that over multiple years of increased precipitation, growth in the form of new leaves would increase with transpiration possibly becoming a larger component of the water balance.

The canopy coverage of the site was very sparse (approximately 10-15%) typical for arid environments where plant cover less than 50% is the norm (Wythers et al., 1999). Individually, shrub canopy leaf and stem structures were open and tenuous. LAI measurements from all twelve plants averaged 1.96 and ranged between 1.47 to 2.87 m^2 m^{-2}. A linear relationship was found between the canopy leaf weight and LAI (r^2 = 0.9088, $P<0.05$). Similar to daily T ANOVA results, treated T_c-T_a of plots were significantly different from non-treated plots during the summer ($P<0.001$).

During the data validation study conducted in July 2009, lysimeter results revealed that E did not drop down to zero during the night period, unlike results shown in Stannard (1988). Such an assumption could result in greatly under estimated E especially for chamber measurements close to a rainfall event (i.e., within 6 days). The high and medium treatments had evaporative rates that did not slow to zero until the fifth night after treatment and then they settled to diurnal E patterns resembling Stannard's (1988) published data. Normalized diurnal data from the chamber and lysimeter (hourly totals divided by daily max) had a significant linear relationship ($r^2 = 0.56$, $P<0.001$, $n = 35$) with all treatments over 15 days after simulated rainfall events. Normalizing the hourly chamber and lysimeter E totals via hourly ET_{ref} did not improve the linear relationship ($P>0.05$). Pickering et al. (1993) compared lysimeters measuring instantaneous ET with a portable chamber and showed both methods were highly linear under clear skies for both wet and dry soils. Similar results were found by Reicosky et al. (1983). Also, Wagner and Reicosky (1992) reported an agreement within 5% between measured ET with a closed chamber system and lysimeter values during a drying period. The 24 hour total chamber derived E values in this study were estimated using night time predictions from day time

chamber measurements taken diurnally from 08:00 to 15:00. Without accounting for nighttime evaporation, daily total evaporation estimates could be under estimated by 31% on average (r^2 = 0.684, P<0.001) after a rainfall event (data based on L, M and H simulated rainfall events in July, Figure 3-21). A limited number of research studies have examined nighttime ET contributions to the 24 hour totals. However, Tolk et al, (2006) estimated nighttime ET could account up to 12% of the 24 hour total ET for irrigated alfalfa (*Medicago sativa L.)* grown in a semiarid environment, and Rosenberg (1969) showed ET night could vary from 7 to 21% in spring, to 0 to 15% in summer for irrigated alfalfa in the central great plains. Also, 24 hour chamber E measurements could be predicted from mid day chamber E measurements with a coefficient of determination of (r^2) 0.91. Results from the lysimeter study showed clear evaporation stages as defined by Idso et al. (1974). One limitation of the experimental design was the treatment plots may have been subject to advective forcing due to untreated surrounding fetch areas. As such, observations of E and T reported may have been elevated relative to non advective conditions, especially during summer months.

Water balance closure was assessed from the evaluation of input parameters (I+P-dS) to output parameters (E+T). The spatial and temporal boundaries were strictly set to five day totals and all input/output components were scaled to the plot level. A water balance closure of 100.8% was obtained for all treatments sites and available months. The closure estimate on average was high; however, plot closure ranged from a minimum of 79% for a Dec control to a maximum of 134% for a low treatment in Apr. Lack of water balance closure can reduce confidence of measurements and forcing closure can create measurement bias as large as the closure offset. However, the results in this study

indicated closure was underestimated for the controls, mediums, and all winter time treatments and was over estimated during the summer months, and for the low and high treatment plots. Because simulated rainfall amounts were measured by an attached water meter and actual precipitation and transpiration were minimal components of the water balance, closure error would have been driven to a larger extent by E or ΔS. However it should be noted that, great care was taken in forcing spatial and temporal boundaries. Including cutting roots, constructing berms, and using evening periods for irrigation to reduce evaporation. Future research might employ mini lysimeters in plots, multiple soil moisture monitoring locations within the plot and outside the plot, vertical barriers below ground around each plot, implement portable domes to assess the entire plot evapotranspirative rates, and conduct the study over multiple years.

The research study results supported the first hypothesis, but not completely:

"As rainfall amounts increase, transpiration and evaporation will also increase but the amount of soil moisture redistribution will be greater under lower environmental demand, creating a seasonal dependency of threshold water holding capacity."

Evaporation responded to the treatment effect ($P<0.001$) and the highest soil moisture redistribution occurred in Dec. However, to our surprise, transpiration did not increase with treatment, the backward stepwise regression results showed no treatment effect. Only summer transpiration was significantly different ($P<0.001$) from other months.

The research study results supported the second hypothesis:

"Spatial patterns of soil moisture redistribution will be driven by a plant water extraction pattern, such that greater redistribution will occur farther from the plant (fertile island effect)." TDR results showed greater redistribution farther from the plant, with the

greatest decreases in soil moisture occurring closest to the plant at the 0-20 cm depth interval.

Although, evaporation dominated the water balance in this study, if larger precipitation amounts occur as predicted by current global circulation models, a greater amount of soil water will be available to support vegetation canopy covers greater than used in this study. Increased precipitation would also lead to greater species diversity, allowing for higher transpiration rates than reported in this study. Soil covers with greater canopy coverage of creosote or creosote-bur sage associations (or perhaps even invasive species) would be favored under such increased rainfall scenarios, leading to a greater amount of water moving upward from storage, reducing deep infiltration to a greater extent than obtained with bare soil covers, such as demonstrated by Gee et al. (1993). Based on the water holding capacity of these soils, the plant water uptake and environmental demand, recurrence interval for deep infiltration could be predicted and used for long-term performance assessment studies of soil covers.

APPENDIX

DATA

Table A-1 Soil Textural Results from Saturn DigiSizer Laser Light Scattering.

	Values for < 63 um portion only								
			Cum. Partical Diam (um) % finer			Laser Results			
Field ID: Plot + depth (cm)	Mean	Median	90%	50%	10%	% Sand	% Silt	% Clay	Sum
1015	12.300	129.400	129.372	129.372	1.947	78.4	11.5	10.1	100.0
1030	11.050	69.560	115.303	69.557	0.721	51.9	28.7	19.4	100.0
1045	9.251	21.510	117.580	21.505	0.480	44.3	30.7	25.1	100.1
1060	6.345	4.412	129.372	4.412	0.382	29.8	35.2	35	100.0
1075	7.175	4.516	122.135	4.516	0.412	26.3	40.3	33.4	100.0
2015	7..994	145.200	145.157	145.157	0.804	67.5	14.8	17.7	100.0
2030	7.244	80.730	126.959	80.730	0.428	51.3	21.4	27.3	100.0
2045	6.121	6.010	129.372	6.010	0.346	35.7	28.7	35.6	100.0
2060	9.310	124.500	124.547	124.547	0.613	56.8	23	20.2	100.0
2075	8.499	22.100	117.580	22.105	0.502	45.3	30.3	24.4	100.0
3015	11.440	9.841	113.153	9.841	0.455	31.6	41.2	27.1	99.9
3030	12.270	7.812	111.003	7.812	0.489	24.0	49.2	26.7	99.9
3045	12.320	9.350	117.580	9.350	0.566	28.6	46.2	25.2	100.0
3060	18.980	35.020	117.580	35.024	0.907	43.1	40.6	16.4	100.1
3075	16.570	26.060	117.580	26.056	0.819	40.6	41.8	17.6	100.0
4015	11.150	134.500	134.482	134.482	1.428	75.8	12.2	12	100.0
4030	11.960	115.300	115.303	115.303	0.987	59.8	24.5	15.7	100.0
4045	9.998	39.640	119.857	39.635	0.535	48.4	28.3	23.3	100.0
4060	9.050	30.910	129.372	30.909	0.473	47.2	27.5	25.3	100.0
4075	7.192	6.511	139.744	6.511	0.415	35.1	33.4	31.5	100.0
5015	8.572	176.300	176.320	176.320	0.830	71.3	11.8	16.9	100.0
5030	13.600	20.540	119.857	20.537	0.650	40.1	38.3	21.6	100.0
5045	12.940	52.480	115.303	52.479	0.774	50.5	31.5	18	100.0
5060	9.035	15.990	131.927	15.993	0.427	42.5	28.5	29	100.0
5075	9.370	21.700	129.372	21.697	0.434	44.5	27.5	28.1	100.1
6015	15.340	145.300	145.318	145.318	1.811	74.8	14.6	10.6	100.0
6030	14.550	127.000	126.959	126.959	1.085	61.8	23.6	14.6	100.0
6045	11.730	32.770	119.857	32.765	0.727	46.3	34	19.7	100.0
6060	13.790	29.930	124.682	29.931	0.821	44.1	37.8	18.1	100.0
6075	11.610	127.100	127.102	127.102	0.742	55.8	25.6	18.7	100.1
7015	11.640	10.240	113.153	10.237	0.673	29.8	48.6	21.6	100.0
7030	9.651	6.702	113.153	6.702	0.517	22.7	50.8	26.5	100.0
7045	9.921	6.903	113.153	6.903	0.550	20.7	53.7	25.6	100.0
7060	9.792	7.483	117.580	7.483	0.541	26.9	47.3	25.9	100.1
7075	8.997	7.068	115.303	7.068	0.505	28.3	44.4	27.3	100.0
8015	8.722	15.220	117.580	15.221	0.614	42.3	34.9	22.7	99.9
8030	8.499	6.039	108.853	6.039	0.526	22.4	50.6	26.9	99.9
8045	7.957	5.410	113.153	5.410	0.465	21.5	49.1	29.4	100.0

8060	8.439	5.614	102.764	5.614	0.502	21.1	50.5	28.5	100.1
8075	8.828	7.905	100.847	7.905	0.522	31.5	41.9	26.6	100.0
9015	15.140	119.900	119.857	119.857	2.519	78.0	13	9	100.0
9030	13.810	108.900	108.853	108.853	1.098	60.6	25.2	14.2	100.0
9045	11.720	111.000	111.003	111.003	0.766	62.6	20.2	17.2	100.0
9060	7.632	19.730	124.717	19.730	0.377	44.4	23.4	32.2	100.0
9075	8.802	32.520	145.157	32.522	0.411	47.6	23.8	28.7	100.1
10015	11.900	15.640	115.303	15.642	0.659	38.1	40.9	21	100.0
10030	11.280	9.796	115.430	9.796	0.592	30.7	46.6	22.7	100.0
10045	11.470	9.840	108.853	9.840	0.573	29.7	46.7	23.6	100.0
10060	12.730	12.990	115.303	12.988	0.564	33.0	44.4	22.7	100.1
10075	11.180	15.540	117.580	15.542	0.564	39.1	37.4	23.5	100.0
11015	12.940	134.500	134.482	134.482	1.419	71.8	16.1	12.1	100.0
11030	10.990	124.500	124.547	124.547	0.840	62.4	21.1	16.5	100.0
11045	7.573	49.840	137.189	49.840	0.473	50.0	23.3	26.7	100.0
11060	9.671	46.630	117.580	46.625	0.526	49.5	27.3	23.2	100.0
11075	10.480	119.900	119.857	119.857	0.705	58.4	23.4	18.2	100.0
12015	8.178	28.070	124.102	28.070	0.459	46.8	25.4	27.8	100.0
12030	12.280	18.200	102.762	18.200	0.488	36.7	40.8	22.5	100.0
12045	8.896	6.148	117.580	6.148	0.339	26.5	41.5	32	100.0
12060	8.360	4.628	102.764	4.628	0.345	17.8	48.3	33.9	100.0
12075	9.787	5.604	115.303	5.605	0.449	20.6	49.6	29.9	100.1

Table A-2 Daily Potential Evapotranspiration (ET_o) (mm) from the North Las Vegas Weather Station.

	2005			2006								
Day	**Oct**	**Nov**	**Dec**	**Jan**	**Feb**	**Mar**	**Apr**	**May**	**Jun**	**Jul**	**Aug**	**Sep**
1	4.71	2.65	1.57	1.63	2.00	2.82	3.08	6.50	7.04	7.67	6.58	6.17
2	4.78	2.67	1.62	1.64	2.11	2.82	3.38	6.40	7.90	7.47	6.65	6.23
3	3.97	2.62	1.92	1.66	2.51	3.01	4.28	6.34	8.17	7.89	6.78	6.19
4	3.79	2.69	1.35	1.43	2.34	2.86	4.64	5.34	8.19	5.52	6.78	5.27
5	3.21	2.35	1.30	1.72	2.26	3.01	5.00	5.15	8.38	5.39	6.75	5.71
6	3.34	2.39	1.29	1.82	2.28	3.03	2.34	5.26	8.30	6.54	6.66	5.83
7	3.70	2.40	1.50	1.91	2.09	3.01	3.73	5.95	7.84	6.53	7.12	5.98
8	4.31	2.43	1.24	1.93	2.51	3.21	4.20	6.37	4.69	6.53	7.66	5.39
9	3.58	2.41	1.25	1.94	2.93	2.45	4.68	6.63	6.63	7.11	7.79	4.80
10	3.31	1.93	1.42	1.58	3.08	2.78	4.89	6.33	7.00	7.21	6.94	4.82
11	3.32	2.30	1.68	1.64	3.11	1.92	5.09	6.11	7.08	7.36	6.38	4.85
12	3.46	2.11	1.68	1.49	2.32	1.85	4.85	6.75	7.36	7.62	6.83	5.23
13	3.87	2.16	1.62	1.70	2.51	2.23	4.80	6.95	7.19	8.02	7.45	5.62
14	3.84	2.17	1.65	1.86	2.80	2.46	5.51	6.96	7.29	8.36	7.01	5.15
15	3.85	2.31	1.36	1.75	2.26	3.23	4.80	6.87	6.08	8.70	6.98	5.37
16	3.41	1.86	1.38	1.30	2.21	2.87	3.98	6.89	6.59	8.27	6.33	5.59
17	3.13	1.97	1.25	1.44	2.25	3.07	4.37	6.83	6.93	8.14	6.77	4.87
18	2.76	2.29	1.01	1.47	2.07	2.99	4.76	7.37	7.64	8.64	6.67	4.14
19	1.44	2.07	0.94	1.97	2.09	2.42	4.13	7.12	8.26	7.33	6.71	4.52
20	2.20	2.28	1.23	1.49	1.61	2.38	4.81	7.13	7.67	6.66	6.60	5.27

21	2.78	2.30	1.57	1.63	1.97	2.86	5.26	6.73	7.91	7.68	7.04	3.88
22	2.93	2.12	1.69	1.56	2.15	2.09	5.46	6.29	7.99	7.85	7.00	4.36
23	3.11	2.05	1.49	1.51	2.58	3.39	5.18	4.43	8.26	6.88	6.23	4.33
24	3.20	2.11	1.85	1.70	2.67	3.87	3.88	6.06	8.42	7.63	6.13	3.73
25	3.17	2.09	1.98	1.77	2.89	3.97	4.74	6.89	8.51	7.64	6.56	3.99
26	2.33	1.94	1.75	1.98	3.23	3.96	4.91	7.41	8.31	7.27	7.08	4.71
27	2.67	1.88	1.74	1.56	3.26	3.47	5.09	7.66	7.10	7.38	7.04	5.10
28	2.65	1.33	1.49	1.75	3.51	3.67	5.80	5.01	7.14	7.59	6.27	4.44
29	2.43	1.29	1.19	1.52	---	3.97	6.51	5.32	7.21	8.09	6.68	4.38
30	2.48	1.40	1.65	1.89	---	3.14	6.50	6.10	7.40	6.80	6.94	4.32
31	2.61	---	1.36	1.81	---	3.23	---	6.20	---	6.43	6.11	---
Total mm	100.36	64.56	46.06	52.02	69.62	92.03	140.64	197.34	224.49	228.21	210.49	150.23
Total in	3.95	2.54	1.81	2.05	2.74	3.62	5.54	7.77	8.84	8.98	8.29	5.91

Table A-3 Van Genuchten Network Predicted (Rosta Lite v 1.1 2003).

Field ID: Plot + depth (cm)	theta r (cm^3/cm^3)	theta s (cm^3/cm^3)	alpha (1/cm)	n (-)	Ks (cm/d)	BD (gr/cm^3)
1015	0.049	0.393	0.03	1.67	86.01	1.5
1030	0.057	0.389	0.02	1.42	15.34	1.5
1045	0.067	0.398	0.01	1.42	8.82	1.5
1060	0.081	0.417	0.01	1.39	5.8	1.5
1075	0.081	0.415	0.01	1.43	5.54	1.5
2015	0.057	0.399	0.03	1.43	33.71	1.5
2030	0.070	0.408	0.02	1.36	12.58	1.5
2045	0.081	0.418	0.01	1.35	6.33	1.5
2060	0.059	0.396	0.02	1.40	18.95	1.5
2075	0.066	0.397	0.01	1.42	9.45	1.5
3015	0.072	0.400	0.01	1.48	6.3	1.5
3030	0.073	0.401	0.01	1.52	6.37	1.5
3045	0.070	0.395	0.01	1.52	6.68	1.5
3060	0.052	0.371	0.01	1.49	12.41	1.5
3075	0.055	0.373	0.01	1.50	10.73	1.5
4015	0.051	0.395	0.03	1.58	65.92	1.5
4030	0.051	0.387	0.02	1.42	25.64	1.5
4045	0.064	0.397	0.02	1.41	11.35	1.5
4060	0.067	0.401	0.02	1.40	10.22	1.5
4075	0.077	0.410	0.01	1.40	5.99	1.5
5015	0.058	0.400	0.03	1.47	41.79	1.5
5030	0.062	0.386	0.01	1.48	8.37	1.5
5045	0.055	0.384	0.02	1.43	15.26	1.5
5060	0.072	0.407	0.01	1.39	7.65	1.5
5075	0.071	0.405	0.02	1.39	8.48	1.5
6015	0.048	0.391	0.03	1.57	65.82	1.5
6030	0.050	0.387	0.02	1.43	29.28	1.5
6045	0.058	0.385	0.01	1.45	11.68	1.5
6060	0.055	0.378	0.01	1.47	11.56	1.5

6075	0.056	0.391	0.02	1.41	19	1.5
7015	0.064	0.384	0.01	1.55	8.07	1.5
7030	0.073	0.401	0.01	1.54	6.51	1.5
7045	0.073	0.401	0.01	1.55	6.93	1.5
7060	0.071	0.397	0.01	1.52	6.51	1.5
7075	0.073	0.401	0.01	1.50	6.17	1.5
8015	0.064	0.391	0.01	1.45	8.64	1.5
8030	0.074	0.402	0.01	1.53	6.4	1.5
8045	0.077	0.409	0.01	1.50	5.91	1.5
8060	0.076	0.407	0.01	1.52	6.11	1.5
8075	0.071	0.398	0.01	1.48	6.45	1.5
9015	0.047	0.391	0.04	1.66	87.85	1.5
9030	0.049	0.384	0.02	1.43	28.35	1.5
9045	0.055	0.394	0.02	1.42	27.34	1.5
9060	0.076	0.414	0.02	1.34	8.56	1.5
9075	0.071	0.408	0.02	1.36	10.06	1.5
10015	0.061	0.383	0.01	1.49	8.34	1.5
10030	0.065	0.387	0.01	1.53	7.56	1.5
10045	0.067	0.390	0.01	1.53	7.2	1.5
10060	0.065	0.387	0.01	1.52	7.61	1.5
10075	0.065	0.391	0.01	1.47	7.48	1.5
11015	0.049	0.392	0.03	1.51	51.84	1.5
11030	0.053	0.392	0.02	1.42	27.81	1.5
11045	0.069	0.406	0.02	1.37	11.71	1.5
11060	0.064	0.397	0.02	1.40	12.04	1.5
11075	0.056	0.392	0.02	1.41	21.82	1.5
12015	0.070	0.406	0.02	1.38	9.67	1.5
12030	0.064	0.387	0.01	1.49	7.64	1.5
12045	0.079	0.412	0.01	1.45	5.59	1.5
12060	0.083	0.421	0.01	1.46	5.37	1.5
12075	0.411	0.008	0.01	1.50	5.86	1.5

Table A-4 Ion Balance of Soil Samples Taken Before Experiment Initiation

Plot, depth bgs (cm)	EC ($dS\ m^{-1}$)	Na ($meq\ L^{-1}$)	K ($meq\ L^{-1}$)	Ca ($meq\ L^{-1}$)	Mg ($meq\ L^{-1}$)	Cl ($meq\ L^{-1}$)	SO_4 ($meq\ L^{-1}$)
1, 15	0.3592	1.014	0.267	2.204	5.510	0.286	0.538
1, 30	0.7818	3.639	0.967	2.204	3.306	0.697	2.558
1, 45	1.832	11.920	1.432	4.408	7.714	2.486	11.857
1, 60	10.891	53.426	5.116	57.304	83.752	29.577	93.033
1, 75	5.305	26.893	2.236	22.040	36.366	9.270	47.552
2, 15	0.5256	1.553	0.095	4.408	4.408	0.656	1.369
2, 30	0.4605	1.570	0.068	3.306	5.510	0.422	1.568
2, 45	0.6593	1.748	0.145	3.306	3.306	0.788	3.100
2, 60	0.7522	3.589	0.118	2.204	3.306	0.642	3.198
2, 75	0.4343	1.330	0.122	2.204	1.102	0.228	0.915
3, 15	10.286	45.861	7.819	53.998	87.058	30.518	79.901
3, 30	0.45	0.896	0.667	2.204	4.408	0.307	1.341
3, 45	1.0297	4.007	1.804	2.204	4.408	0.953	4.751
3, 60	6.696	30.942	7.106	38.570	48.488	8.329	73.836

3, 75	9.784	34.816	7.057	50.692	76.038	25.253	82.809
4, 15	13.93	89.421	12.954	57.304	100.282	53.825	107.190
4, 30	0.5855	0.523	0.824	1.102	5.510	0.898	1.485
4, 45	1.115	5.836	2.090	3.306	3.306	1.732	4.383
4, 60	4.504	27.418	5.558	6.612	20.938	15.446	24.252
4, 75	0.7783	1.385	0.439	6.612	6.612	1.045	2.814
5, 15	0.3388	0.862	0.162	3.306	5.510	0.280	0.672
5, 30	0.4487	1.638	0.462	1.102	3.306	0.302	0.998
5, 45	1.438	9.812	0.820	2.204	4.408	1.792	8.550
5, 60	6.682	34.070	2.051	16.530	55.100	28.751	31.644
5, 75	9.08	35.157	2.364	50.692	83.752	34.305	75.060
6, 15	0.4325	0.595	1.335	2.204	2.204	0.319	0.527
6, 30	0.5168	1.693	1.625	1.102	2.204	0.301	0.923
6, 45	1.187	7.753	1.263	1.102	3.306	1.333	3.646
6, 60	3.989	34.076	4.231	2.204	8.816	1.207	1.400
6, 75	7.569	58.152	6.762	9.918	33.060	29.900	27.126
7, 15	0.4257	0.997	0.547	1.102	5.510	0.330	0.853
7, 30	1.662	11.308	2.316	1.102	5.510	2.196	8.865
7, 45	9.523	60.485	7.475	45.182	57.304	23.455	75.933
7, 60	23.67	156.160	11.676	83.752	168.606	130.821	97.350
7, 75	16.97	90.547	9.096	68.324	115.710	75.510	88.075
8, 15	0.9098	1.456	1.247	4.408	5.510	1.233	3.421
8, 30	1.166	7.621	2.216	2.204	2.204	0.925	3.119
8, 45	5.18	38.788	8.027	3.306	5.510	10.749	23.251
8, 60	25	127.895	20.486	67.222	88.160	79.182	97.630
8, 75	23.97	194.897	17.663	65.018	111.302	130.470	135.184
9, 15	0.5387	1.377	0.866	2.204	3.747	0.287	1.179
9, 30	0.5502	0.856	1.322	1.763	2.204	0.249	0.432
9, 45	5.87	25.373	8.465	40.113	31.517	3.910	65.994
9, 60	13.06	95.022	11.264	48.488	77.801	33.498	95.396
9, 75	15.42	117.890	10.947	52.896	103.588	55.172	95.051
10, 15	0.4422	2.293	1.107	1.543	1.763	0.199	0.737
10, 30	0.9405	3.884	2.696	1.102	1.102	0.442	2.564
10, 45	2.804	19.764	5.789	2.204	4.408	1.749	19.384
10, 60	7.4	37.197	10.874	40.333	33.942	6.456	82.222
10, 75	14.85	108.556	13.527	53.998	85.956	52.830	98.282
11, 15	0.3033	1.064	0.309	2.204	2.204	0.180	0.490
11, 30	0.39	1.505	0.928	2.204	2.204	0.152	0.829
11, 45	9.601	4.332	1.682	1.102	3.306	0.930	4.473
11, 60	10.098	41.817	7.589	46.284	67.222	23.634	87.089
11, 75	16.7	93.622	11.264	48.488	120.118	56.317	126.179
12, 15	0.365	1.458	0.006	3.306	2.204	0.276	0.574
12, 30	0.4605	1.678	0.029	2.204	7.714	0.497	1.133
12, 45	0.5974	1.087	0.155	3.306	3.306	0.605	2.517
12, 60	0.9423	6.349	0.327	2.204	2.204	1.467	3.198
12, 75	5.42	35.289	1.722	15.428	30.856	16.220	48.365

Table A-5 Water Balance Calculation Weekly Totals.

Water Balance Date	E (cm)	T (cm)	I+P (cm)	ΔS (cm)	P (cm)	Date of Precip.	Treatment (cm)	Plot #
December 16-26	0.47	0.10	0	-0.652	0	…	0	1
	0.44	0.00	0	-0.489	0	…	0	6
	0.67	0.00	0	-0.741	0	…	0	12
	2.33	0.05	1.875	-0.142	0	…	1.875	2
	2.10	0.00	1.875	0.306	0	…	1.875	4
	2.22	0.01	1.875	-0.054	0	…	1.875	11
	2.86	0.03	3.75	0.621	0	…	3.75	3
	2.87	0.04	3.75	0.851	0	…	3.75	7
	2.59	0.00	3.75	1.277	0	…	3.75	10
	3.54	0.18	7.5	4.500	0	…	7.5	5
	4.26	0.01	7.5	3.335	0	…	7.5	8
	4.01	0.00	7.5	3.917	0	…	7.5	9
February 22-28	0.29	0.37	0	-0.651	0	…	0	1
	0.34	0.09	0	-0.424	0	…	0	6
	0.66	0.12	0	-0.701	0	…	0	12
	1.89	0.01	1.875	-0.141	0	…	1.875	2
	1.43	0.14	1.875	0.280	0	…	1.875	4
	1.68	0.02	1.875	0.263	0	…	1.875	11
	2.18	0.10	3.75	1.454	0	…	3.75	3
	2.74	0.10	3.75	1.047	0	…	3.75	7
	2.69	0.05	3.75	0.815	0	…	3.75	10
	3.74	0.36	7.5	3.180	0	…	7.5	5
	4.56	0.19	7.5	1.638	0	…	7.5	8
	4.88	0.05	7.5	2.288	0	…	7.5	9
April 19-24	0.51	0.23	0.203	-0.720	0.203	April 18	0	1
	0.56	0.10	0.203	-0.501	0.203	…	0	6
	0.70	0.20	0.203	-0.605	0.203	…	0	12
	3.33	0.05	2.078	-1.345	0.203	…	1.875	2
	2.14	0.13	2.078	-0.341	0.203	…	1.875	4
	2.29	0.12	2.078	-0.066	0.203	…	1.875	11
	2.37	0.15	3.953	1.302	0.203	…	3.75	3
	4.22	0.06	3.953	-0.976	0.203	…	3.75	7
	2.92	0.09	3.75	0.566	0.203	…	3.75	10
	5.59	0.08	7.703	2.108	0.203	…	7.5	5
	4.80	0.05	7.703	2.061	0.203	…	7.5	8
	6.32	0.06	7.703	1.912	0.203	…	7.5	9
June 7-14	0.73	0.38	0.178	-0.946	0.178	June 7	0	1
	0.73	0.11	0.178	-0.684	0.178	…	0	6
	0.92	0.34	0.178	-0.815	0.178	…	0	12
	2.86	0.17	2.053	-0.877	0.178	…	1.875	2
	2.79	0.28	2.053	-0.587	0.178	…	1.875	4
	2.17	0.16	2.053	0.136	0.178	…	1.875	11
	3.34	0.15	3.928	0.406	0.178	…	3.75	3
	5.98	0.13	3.928	-1.652	0.178	…	3.75	7
	3.92	0.15	3.928	-0.538	0.178	…	3.75	10
	7.01	0.18	7.678	-0.497	0.178	…	7.5	5
	6.38	0.16	7.678	1.702	0.178	…	7.5	8

	6.43	0.29	7.678	0.603	0.178	…	7.5	9
July 5-12	0.74	0.25	0.025	-0.920	0.025	July 7	0	1
	0.94	0.10	0.025	-1.066	0.025	…	0	6
	0.95	0.15	0.025	-1.213	0.025	…	0	12
	3.54	0.15	1.9	-1.689	0.025	…	1.875	2
	3.13	0.21	1.9	-1.055	0.025	…	1.875	4
	3.32	0.02	1.9	-0.917	0.025	…	1.875	11
	3.75	0.22	3.775	0.406	0.025	…	3.75	3
	4.94	0.12	3.775	-0.826	0.025	…	3.75	7
	4.56	0.41	3.775	-0.538	0.025	…	3.75	10
	7.10	0.34	7.525	1.226	0.025	…	7.5	5
	6.03	0.24	7.525	2.084	0.025	…	7.5	8
	6.96	0.29	7.525	1.655	0.025	…	7.5	9
August 9-15	0.80	0.19	0.152	-0.893	0.152	August 8	0	1
	1.05	0.12	0.152	-1.016	0.152	…	0	6
	1.31	0.23	0.152	-1.140	0.152	…	0	12
	4.24	0.15	2.027	-1.689	0.152	…	1.875	2
	2.39	0.23	2.027	-0.986	0.152	…	1.875	4
	2.77	0.09	2.027	-1.169	0.152	…	1.875	11
	2.34	0.18	3.902	1.348	0.152	…	3.75	3
	4.12	0.12	3.902	0.000	0.152	…	3.75	7
	3.71	0.47	3.902	0.674	0.152	…	3.75	10
	5.27	0.25	7.652	1.827	0.152	…	7.5	5
	3.88	0.21	7.652	3.198	0.152	…	7.5	8
	7.09	0.27	7.652	1.178	0.152	…	7.5	9

Table A-6 Daily Precipitation (mm) from the North Las Vegas Weather Station.

	2005			2006								
Day	**Oct**	**Nov**	**Dec**	**Jan**	**Feb**	**Mar**	**Apr**	**May**	**Jun**	**Jul**	**Aug**	**Sep**
1	0	0	0	1.27	0	0	0	0	0	0	0	0
2	0	0	0	0	0	0	0	0	0	0	0	0
3	0	0	0	0	0	0	0	0	0	0	0	0
4	0	0	0	0	0	0	0	0	0	0	1.524	0
5	0	0	0	0	0	0	0	0	0	0	0	0
6	0	0	0	0	0	0	0	0	0	0	0	0
7	0	0	0	0	0	0	0	0	0	0.254	0	1.016
8	0	0	0	0	0	0	0	0	1.778	0	0	0
9	0	0	0	0	0	0	0	0	0	0	0	0
10	0	0	0	0	0	0	0	0	0	0	0	0
11	0	0	0	0	0	0	0	0	0	0	0	0
12	0	0	0	0	0	0	0	0	0	0	0	0
13	0	0	0	0	0	0	0	0	0	0	0	0
14	0	0	0	0	0	0	0	0	0	0	0	0
15	0	0	0	0	0	0	7.112	0	0	0	0	0
16	0	0	0	0	0	0	0	0	0	0	0	0
17	12.446	0	0	0	0	0	0	0	0	0	0	0

18	34.544	0	0	0	0	0	2.032	0	0	4.826	0	0
19	0	0	0	0	0	0	0	0	0	0	0	0
20	0	0	0	0	0	0	0	0	0	0	0	0
21	0	0	0	0	0	0	0	0	0	0	0	0
22	0	0	0	0	0	3.302	0	0	0	0	0	0
23	0	0	0	0	0	0	0	0	0	0	0	0
24	0	0	0	0	0	0	0	0	0	0	0	0
25	3.302	0	0	0	0	0	0	0	0	0	0	0
26	0	0	0	0	0	0	0	0	0	0	0	0
27	0	0	0	0	0	0	0	0	0	0	0	0
28	0	0	0	0	0.508	0	0	0	0.508	0	0	0
29	0	0	0	0	---	4.064	0	0	0	0	0	0
30	0	0	0	0	---	0	0	0	0	0	0	0
31	0	---	0.254	0	---	0	---	0	---	0	0	---
Total mm	50.292	0	0.254	1.27	0.508	7.366	9.144	0	2.286	5.08	1.524	1.016
Total in	1.98	0	0.01	0.05	0.02	0.29	0.36	0	0.09	0.20	0.60	0.40

BIBLIOGRAPHY

ASCE. 2005. The ASCE standardized reference evapotranspiration equation. ASCE-EWRI Task Committee Final Report January 2005.

Ben-Asher, J., A.D. Matthias, A.W. Warrick. 1983. Assessment of evaporation from bare soil by infrared thermometry. Soil Sci. Soc. Am. J. 47:185-191

Blanquies, J., Scharff, M., Hallock, B. 2003. The design and construction of a rainfall simulator. International Erosion Control Association (IECA), 34th Annual Conference and Expo., Las Vegas, NV.

Brohan, P., Kennedy, J.J., Harris, I., Tett, S.F.B., and Jones, P.D. 2005. Uncertainty estimates in regional and global observed temperature changes: A new data set from 1850. J. Geophys. Res., 111, D12106, doi:10.1029/2005JD006548.

Bubenzer, G. D.. 1979. Inventory of rainfall simulators. Pages 120-130. In Proceedings of the Rainfall Simulator Workshop, Tucson Arizona, March 7-9, 1979. U.S. Department of Agriculture Science and Education Administration Agricultural Reviews and Manuals. ARM-W-10/July 1979.

Caldwell, T.G., M.H. Young, J. Zhu, E.V. McDonald. 2008. Spatial structure of hydraulic properties from canopy to interspace in the Mojave Desert. Geophys. Res. L. 35:1-6.

Christiansen, J.E. 1942. Irrigation by sprinkling. California Ag Expt Sta Bulletin 670, University of California, Berkeley, CA. 1-124

Conaway, J., C.H.M. Van Bavel, 1967. Evaporation from a Wet Soil Surface Calculated from Radiometrically Determined Surface Temperatures. Journal of Applied Meteorology. 6:650-655

Denmead, O.T. and D.C. Reicosky. 2003. Tillage-Induced Gas Fluxes: Comparison of Meteorological and Large Chamber Techniques. In: Proc. International Soil Tillage Research Organization 16th Triennial Conf. Brisbane, Australia. 14-18 July, 2003. p. 357-363.

Devitt D.A., A. Sala, S.D. Smith, J. Cleverly, L.K. Shaulis and R. Hammett. 1997. Bowen Ratio Estimates of Evapotranspiration for *Tamarix ramosissima* Stands on the Virgin River in Southern Nevada**.** Water Resour. Res. 34: 2407–2414

Devitt, D.A., M. Berkowitz, P.J. Schulte, and R.L. Morris. 1993. Estimating Transpiration for Three Woody Ornamental Tree Species using Stem-flow Gauges and Lysimetry. Hort Sci. 28:320-322

Dugas, W.A., D.C. Reicosky, J.R. Kiniry. 1997. Chamber and micrometeorological measurements of CO_2 and H_2O fluxes for three C_4 grasses. Agricultural and Forest Meteorology. 83:113-133

Dugas, W.A., M.L. Heuer, D. Hunsaker, B.A. Kimball, K.F. Lewin, J. Nagy, M. Johnson. 1994. Sap flow measurements of transpiration from cotton grown under ambient and enriched CO2 concentrations. Agricultural and Forest Meteorology. 70:231-245

Ehleringer J.R., S.L. Philips, W.S.F. Schuster and D.R. Sandquist. 1991. Differential utilization of summer rains by desert plants. Oecologia 88:430-434.

Fernandez, G. 2009. Personal communication of December 16 to Dale Devitt and Brian Bird regarding the distributional assumptions associated with ANOVA analysis.

Gee, G.W., P.J. Wierenga, B. J. Andraski, M. H. Young, M. J. Fayer and M.L. Rockhold. 1994. Variations in water balance and recharge at three western desert sites. Soil Sci. Soc. Am. J., 58:63-72.

Gorelow, Andrew S. 2008. Climate of Las Vegas, Nevada. Technical Memorandum. National Weather Service Western Region. Las Vegas, NV.

Grau, A. 1995. A closed chamber technique for field measurements of gas exchange of forage canopies. N. Z. J. Agric. Res., 38, 71-77

Granier A 1985 Une nouvelle methode pour la mesure du flux de seve brute dans le tronc des arbres. Annales Sciences Forestieres 42, 193–200.

Griffin, R.H., B.J. Ott and J.F. Stone. 1966. Effect of water management and surface applied barriers on yield and moisture utilization of grain soroghum in the southern Great Plains. Agron. J. 58:449-452

Gunn, R., and G. D. Kinzer, 1949. The terminal velocity of fall for water droplets. Journal of Meteorology 6:243-248.

Ham J. M., J.L. Heilman and R.J. Lascano. 1990. Determination of soil water evaporation and transpiration from energy balance and stem flow measurements. Agriculture Forest Met. 52:287-301.

Hart, W. E., and W. N. Reynolds. 1965. Analytical design of sprinkler systems. Trans. Am. Soc. Agri. Eng. 8:83-89

Heijmans, M.M.P.D., W.J. Arp, and F.S. Chapin III. 2004. Carbon dioxide and water vapor exchange from understory species in boreal forest. Agric. For. Meterol. 123, 135-147

Herkelrath, W.N., S.P. Hamburg, and F. Murphy. 1991. Automatic, real-time Monitoring of soil moisture in a remote field with time-domain reflectometry. Water Resources Research, 27:857-864

Huxman, T.E., B.P. Wilcox, D.D. Breshears, R.L. Scott, K.A. Snyder, E.E. Small, K. Hultine, W.T. Pockman, R.B. Jackson. 2005. Ecohydrological implications of woody plant encroachment. Ecology 86: 308-319.

Idso, S.B., R.D. Jackson. 1968. Comparison of Two Methods for Determining Infrared Emittances of Bare Soils. Journal of Applied Meteorology. 8:168-169

Idso, S.B., R.J. Reginato, R.D. Jackson, B.A. Kimbal, and F.S. Nakayama. 1974. The three stages of drying of a field soil. Soil Sci. Soc. Am. 38:831-837.

IPCC, 2007. Climate Change 2007: The Physical Science Basis. Contribution of Working Group I to the Fourth Assessment Report of the Intergovernmental Panel on Climate Change. Cambridge University Press, Cambridge, p. 996.

Jackson, R.D., B.A. Kimball, R.J. Reginato, F.S. Nakayama. 1973. Diurnal Soil-Water Evaporation: Time-Depth-Flux Patterns. Soil Sci. Soc. Am. J. 37:505-509

Karl, T.R., Meehl, G.A., Miller, C.D., Hassol, S.J., Waple, A.M., Murray, W.L. Weather and Climate Extremes in a Changing Climate. Regions of Focus: North America, Hawaii, Caribbean, and U.S. Pacific Islands. A Report by the U.S. Climate Change Science Program and the Subcommittee on Global Change Research (Washington, D.C.: Department of Commerce, National Oceanic and Atmospheric Administration, National Climate Data Center, June 2008), p. 2.

Keeling, C.D. and T.P. Whorf. 2005. Atmospheric CO2 records from sites in the SIO air sampling network. In Trends: A Compendium of Data on Global Change. Carbon Dioxide Information Analysis Center, Oak Ridge National Laboratory, U.S. Department of Energy, Oak Ridge, Tenn., U.S.A.

Knapp, A.K., Fay, P.A., Blair, J.M., Collins, S.L., Smith, M.D., Carlisle, J.D., Harper, C.W., Danner, B.T., Lett, M.S., McCarron, J.K., 2002. Rainfall variability, carbon cycling, and plant species diversity in a mesic grassland. Science 298, 2202–2205.

Lascano, R.J., C.H.M. van Bavel, J.L. Hatfield, D.R. Upchurch. 1987. Energy and water balances of a sparse crop: Simulated and measured soil and crop evaporation. Soil Sci. Soc. Am. J. 51:1113-1121

Laws, J. O., 1941. Measurements of fall velocity of water drops and raindrops. Transactions of American Geophysics Union 22:709-721.

Laws, J. O., and D. A. Parsons. 1943. The relationship of raindrop-size to intensity. Transaction of American Geophysics Union 24:452-459

Lee, X., W. Massman, B.E. Law. 2004. Handbook of Micrometeorologu. A Guide for Surface Flux Measurements and Analysis. Kluwer Academic Publishers, Boston, 250 pp.

Liu, B. L., F. Phillips, S. Hoines, A. R. Campbell, and P. Sharma. 1995. Water movement in desert soil traced by hydrogen and oxygen isotopes, chloride, and chlorine-36, southen Arizona. Journal of Hydrology 168:92–110.

Loik, M.E., D.D. Breshears, W.K. Lauenroth, J. Belnap. 2004. A multi-scale perspective of water pulses in dryland ecosystems: climatology and ecohydrology of the western USA. Oceologia 141: 269-281.

Mabry, T.J., J.H. Hunziker, and D.R. DeFeo. 1977. Creosote Bush: Biology and Chemistry of *Larrea* in New World Deserts. United States/International Biological Program Synthesis Series 6. Dowden, Hutchinson, and Ross, Inc., Stroudsburg, PA. 284 p.

Massman, W.J. 2000. A simple method for estimating frequency response corrections for eddy covariance systems. Agric. For. Meteorol. 104, 185-198.

Massman, W.J. 2001. Reply to comment by Rannik on "A simple method for estimating frequency response corrections for eddy covariance systems", Agric. For. Meteorol. 107, 247-251.

Monteith, J. L. and M. H. Unsworth. 1990. Principals of Environmental Physics, 2nd Ed., Edward Arnold, London. 289 p

Moore, C.J., 1986. Frequency response corrections for eddy correlation systems. Bound. –Layer Meteor, 37, 17-35.

Moore, Ian D., Michael C. Hirschi, and Billy J Barfield. 1983. Kentucky rainfall simulator. Transactions of the American Society of Agricultural Engineers 23:1085-1089.

Nichols, W.D., 1987, Geohydrology of the unsaturated zone at the burial site for low-level radioactive waste near Beatty, Nye County, Nevada: U.S. Geological Survey Water-Supply Paper 2312, 57 p. Washington, D.C.: U.S. Department of the Interior.

Pickering, N.B., J.W. Jones and K.J. Boote. 1993. Evaluation of the portable chamber technique for measuring canopy gas exchange by crops. Agricultural and Forest Meterology. 63:239-254

Reicosky, D.C. Canopy gas exchange in the field: Closed chambers. Remote Sensing. 5:163-177.

Reicosky, D.C., B.S.Sharratt, J.E. Ljungkull, and D.G. Baker. 1983. Comparison alfalfa evapotranspiration measured by a weighing lysimeter and a portable chamber. Agric. Meteor. 28:205-211

Reith, C., and B. M. Thomson. 1992. Deserts as Dumps: The Disposal of Hazardous Materials in Arid Ecosystems. University of New Mexico Press, Albuquerque.

Ritchie, J.T., 1972. Model for predicting evaporation from a row crop with incomplete cover. Water Resour. Res., 8:1204-1213

Rosenberg, N.J. 1969. Seasonal patterns in evapotranspiration by irrigated alfalfa in the central Great Plains. Agron. J. 61:879–886.

Sammis, T. W., and L. Y. Gay. 1979. Evapotranspiration from an arid zone plant community. Journal of Arid Environments 2:313–321.

Schaap, M.G., Leij, F.J. and van Genuchten, M.Th., 2001. Rosetta: A computer program for estimating soil hydraulic parameters with hierarchical pedotransfer functions. J. Hydrol. 251: 163-176.

Schlesinger, W. H., P. J. Fonteyn, and G. M. Marion. 1987. Soil moisture content and plant transpiration in the Chihuahuan Desert of New Mexico. Journal of Arid Environments 12:119–126.

Schuepp, P.H., Leclerc, M.Y., MacPherson, J.I., and Desjardins, R.L. 1990. Footprint Prediction of Scalar Fluxes from Analytical Solutions of the Diffusion Equation. Bound. Lay. Met. 50, 355-373.

Schwinning, S., J.R. Ehleringer, 2001. Water use trade-offs and optimal adaptations to pulse-driven arid ecosystems. Journal of Ecology 89, 464–480.

Schwinning, S., B.I. Starr and J.R. Ehleringer. 2005a. Summer and winter drought in a cold desert ecosystem (Colorado Plateau). Part I: effects on soil water and plant water uptake, Journal of Arid Environments 60, pp. 547-566.

Schwinning, S., B.I. Starr and J.R. Ehleringer. 2005b. Summer and winter drought in a cold desert ecosystem (Colorado Plateau). Part II: effects on plant carbon assimilation and growth, Journal of Arid Environments 6, pp. 61–78.

Sellers, W.D. 1965. Physical climatology. The university of Chicago Press, Chicago.

Šimůnek, J., Jacques, D., van Genuchten, M.Th. and Mallants, D. 2006. Multicomponent geochemical transport modeling using the HYDRUS computer software packages. J. Am. Water Resour. Assoc.

Smith, S.D., S.J. Allen. 1996. Measurement of sap flow in plant stems. Journal of Experimental Botany. 47:1833-1844

Stannard, D.I. 1988. Use of a hemispherical chamber for the measurement of evapotranspiration. OF 88-0452.

Stannard, D.I., and M.A. Weltz. 2006. Partitioning evapotranspiration in sparsely vegetated rangeland using a portable chamber. Water Resour. Res. 42:1-13

Suleiman, A., R. Crago. 2004. Hourly and Daytime Evapotranspiration from Grassland Using Radiometric Surface Temperatures. 96:384-390

Tanner, B.D., J.P. Green. 1989. Measurement of sensible heat and water vapor fluxes using eddy correlation methods, final report for U.S. Army Dugway Proving Grounds, 17pp., U.S. Army, Washington, D.C., 1989.

Tolk, J.A., T.A. Howell, and S.R. Evett. 2006. Nighttime evapotranspiration from alfalfa and cotton in a semiarid climate.

Topp, GC, Davis, JL, Annan, AP, 1980. Electromagnetic Determination of Soil Water Content: Measurements in Coaxial Transmission Lines. Water Resources Res, 16(3), 574-582.

U.S.NRC. 2007. Radioactive Waste. BACKGROUNDER. Office of Public Affairs NRC. http://www.nrc.gov/reading-rm/doc-collections/fact-sheets/radwaste.pdf

U.S. Nuclear Waste Technical Review Board. 2004. Report to The U.S. Congress and The Secretary of Energy. Arlington, VA 22201-3367.

Van der Laan, S., R.E.M. Neubert, and A.J. Meijer. 2009. A single gas chromatograph for accurate atmospheric mixing ratio measurements of CO2, CH4, N2O, SF6 and CO. Atmos. Meas. Tech. 2, 549-559.

van Genuchten, 1980. A closed form equation for predicting the hydraulic conductivity of unsaturated soils. Soil Sci. Soc. Am. J. 44:892-898.

Wagner, S.W., and D.C. Reicosky. 1992. Closed-Chamber Effects on Leaf Temperature, Canopy Photosynthesis, and Evapotranspiration. Agron. J. 84:731-738

Webb, E.K.. G.I. Pearman, and R. Leuning, 1980. Correction of flux measuremnts for density effects due to heat and water vapour transfer. Quart. J. Roy. Meteor. Soc. 106. 85-100.

Wythers, K.R., W.K. Lauenroth, and J.M. Paruelo. 1999. Bare-Soil Evaporation Under Semiarid Field Conditions. Soil Sci. Soc. Am. J. 63:1341-1349.

VITA

Graduate College
University of Nevada, Las Vegas

Brian Michael Bird

Degree:

Bachelor of Science, Computer Science, 2004
University of Nevada, Las Vegas

Special Honors and Awards:

Deans List 2004
2nd place award for outstanding poster presentation at NWRA 2007.

Publications:

Devitt, D.A. Fenstermaker, M.H. Young, B. Conrad, M. Baghzouz and **B.M. Bird.** 2010. Evapotranspiration of mixed shrub communities in phreatophytic zones of the Great Basin. Ecohydrology 2010, in review.

Devitt, D.A., L. Fenstermaker, M.H. Young, B. Conrad, M. Baghzouz and **B.M. Bird.** 2008. Evapotranspiration Estimates in North Eastern Nevada Basins. Report to the Southern Nevada Water Authority.

Bird, B.M. 2008. Eddie Covariance System Data Processing Techniques. Report to the Southern Nevada Water Authority. Doc No. HAM-ED-0009

Bird, B.M., Shanahan, R., Habtea, A. 2008. Evapotranspiration Program Annual Report. SNWA Hydrologic Analysis and Modeling. Doc No. HAM-ED-0003

Devitt, D.A., M. Lockett, R.L. Morris and **B.M. Bird.** 2007. Spatial and Temporal Distribution of salts in Surface Soils of Fairways and Greens Irrigated with Reuse Water. J. Agronomy. 99:692-700.

Devitt, D.A., M.H. Young, M. Baghzouz and **B.M. Bird.** 2007. Surface Temperature, Heat Loading, and Spectral Reflectance of Artificial Turfgrass. J. Turfgrass and Sports Surface Science. 83. 68-82.

Thesis Title: Temporal and Spatial Assessment of Evaporation, Transpiration, and Soil Moisture Redistribution.

Thesis Committee:

Chairperson, Dale Devitt, Ph. D.
Committee Member, Michael Young, Ph. D.

Committee Member, David Kreamer, Ph. D.
Graduate Faculty Representative, Paul Schulte, Ph. D.